Newcastle University

Investigation of polyphenylene oxide-based membranes for anion exchange water electrolyser

School of Engineering

Thesis Submitted By

Zhiming Feng

For the Degree of Philosophy

Newcastle University

January 2022

Abstract

The energy crisis and resources shortage of conventional fossil fuels such as coal, natural gas and oil are becoming severe with the rapid development of society and industrialisation. Renewables hold the key to the increasing energy demand and environmental issues. Green hydrogen (H_2) is considered one of the most promising energy carriers for the future due to its high energy density and CO_2-free emission. Anion exchange membrane water electrolyser (AEMWE) is a promising technology for producing hydrogen. AEMWE could offer significant cost reduction by enabling earth-abundant catalyst materials while providing pure hydrogen due to good H_2 and O_2 separation. Anion exchange membrane (AEM) is a significant component in AEMWE. AEM acts as an electrolyte to conduct the negative ions, e.g., OH^- and the separator between the anode and cathode compartments where the O_2 and H_2 are produced. However, the performance of AEMs still needs to be improved to meet the requirement of the long-term operation of water electrolysis.

This project aims to prepare a stable AEM and investigate its degradation mechanism under pH 7-14, relevant to AEMWE fed with deionised water to 1M KOH supporting electrolyte. Cross-linked quaternised poly(2,6-dimethyl-1,4-phenylene oxide) (QPPO)-based membranes were prepared via Friedel-Crafts reactions using $SnCl_4$ catalyst and environmentally-friendly chloromethylating reagents. New equations to calculate the degree of chloromethylation and cross-linking degree were proposed. The ionic conductivity can reach 133 mS cm^{-1} at 80 °C. Ex situ stability testing after 500 h in 1 M KOH showed membranes retained up to 94 % of their original Ion Exchange Capacity (IEC). QPPO was employed as both membranes and ionomers in electrolyser tests and compared with previously prepared polystyrene-b-poly(ethylene-co-butylene)-b-polystyrene (SEBS) and low-density polyethylene (LDPE)-based membbrane. QPPO membranes exhibited area-specific resistance of 104 mΩ cm^{-2} and electrolyser current density of 814 mA cm^{-2} at 2.0 V when 0.1 M NaOH supporting electrolyte feed at 40 °C. The oxidative stability of QPPO and LDPE-based membranes was studied. Compared with LDPE-based membrane, QPPO-based membrane shows better oxidative stability. The degradation mechanism of PPO-based membrane under DI water conditions was studied. The residual degradation solution and extracted sample after the degradation test were characterised by NMR. The possible degradation mechanism is that oxygen or OH radicals attack the methyl group on the rearranged ylide, forming aldehyde or carboxyl attached to the CH_2 group.

To increase their mechanical strength, reduce thier water swelling and improve thier dimension stability, QPPO membranes were reinforced using the pore filling technique inside porous fluoropolymer of tetrafluoroethylene (PTFE) to prepare the PPO/PTFE-based composite membranes. Reinforced membranes significantly increased tensile strength, 31 MPa from 14 MPa for unreinforced membranes. This increased membrane lifetime in working electrolyser to >200 h compared with otherwise identical electrolyser assembled with PPO-based membrane (50 h). The water uptake of the composite membrane is 77.5 %, lower than that of the PPO-based membrane (430 %). However, the PPO/PTFE conductivity was 6.25 mS cm^{-1} lower than 30 mS cm^{-1} of PPO-based membrane at 20 °C. This is caused by lower water uptake of PPO/PTFE composite membranes and lower volume fraction of QPPO in the composite membrane. At 40 % RH, the net change mass of composite membrane is 1.59 %, much lower than that of PPO-based membrane (10.98 %) at 40 °C.

Acknowledgement

Firstly, I would like to express my sincere appreciation to my supervisor, Dr Mohamed Mamlouk, Dr David A Fulton and Prof. Keith Scott for their support of my PhD study. Dr Mohamed Mamlouk led me to the electrochemical world and insightfully guided me throughout my PhD. He spends his time generously helping me solve the changeling problems I encounter. It would have been impossible for me to achieve without his consistent support.

I appreciate all group members who helped me during my journey to the end, Dr Gaurav Gupta, Prof. Pilar Ocón Esteban, Dr Ravikumar Thimmappa, Mr Hosni Ahmed Elwan, Mr Jian Huang. I also extend my appreciation to all the staff and technicians, especially Rob Dixon, Ms Ashley Craig, Mr Kevin Brown, and Mr Neville Dickman. Besides, I express my special gratitude to my family. Their love, support and encouragement are significant power sources for me.

This doctoral research project has trained me professionally and expanded my horizon. I appreciate Newcastle University, which provides me with the opportunity and platform Newcastle University for my study. I will continue to devote myself to being an academic researcher.

List of Publication

1. Feng Z, Esteban P O, Gupta G, et al. Highly conductive partially cross-linked poly (2, 6-dimethyl-1, 4-phenylene oxide) as anion exchange membrane and ionomer for water electrolysis[J]. International Journal of Hydrogen Energy, 2021, 46(75): 37137-37151.
2. A review of anion exchange membranes prepared via Friedel-Crafts alkylation route: preparation, characterisation, and degradation, Underwritten.

Presentation

1. Feng Z, SCI Electrochemistry Postgraduate Conference 2019, Newcastle upon Tyne, UK, 2019.
2. Feng Z, Butler meeting 2020, Newcastle upon Tyne, UK, 2020.
3. Feng Z, SAgE PGR Conference, Newcastle University, Newcastle upon Tyne, UK, 2017.

Poster

1. Feng Z, SAgE PGR Conference, Newcastle University, Newcastle upon Tyne, UK, 2018.
2. Feng Z, the 8th De Nora R&D Symposium, Milano, Italy, 2019.

Table of content

List of Figure

List of Table

Abbreviations

AEM	Anion exchange membrane
AeIm	1-Aminoethyl-2,3dimethylimidazolium
ATRP	Atom transfer radical polymerisation
AFM	Atomic force microscopy
AEMFC	Anion exchange membrane fuel cell
AEMWE	Anion exchange membrane water electrolyser
AC	Aromatic copolymers
AeImOH	Long-spacer-chain imidazolium
AEI	Anion exchange ionomer
BTA	Bromoalkylated tertiary alcohols
BIm	Benzimidazolium
BuIm	1-butylimidazole
BuIm	1-butylimidazole
BZM	1-benzylimidazole
BDMIm	1-butyl- 2, 3-dimethylimidazole
BP	Bipolar
CMEE	Chloromethyl ethyl ether
CMME	Chloromethyl methyl ether
CM	Chloromethylated
CDPC	3-chloro-2,2dimethylpropionyl chloride
CBC	4-chlorobutanoyl chloride
CRQGO	Chloromethylated reduced graphene oxide
CR	Chloromethylation reagent
CLD	Cross-linking degree
CL	Catalyst layer
CCM	Catalyst coated membrane method
DMD	Direct membrane deposition method
DP	Direct polymerisation
DC	Degree of chloromethylation
DF	Degree of functionalization
DH	Degree of halomethylation
DMEA	Dimethylethylamine
DMIPA	Propylamine

DMM	Dimethoxymethane
DMH	N, N- dimethylhexylammmonium
DmIm	1,2-dimethylimidazole
DMH	N, N- dimethylhexylammmonium
DABCO	Bifunctional 1,4-diazabicyclo [2,2,2]octane
DMA	Dynamic mechanical analysis
DOG	Degree of grafting
EtIm	1-ethylimidazole
ECMR	Electrochemical methanol reformation
F-C	Friedel-Crafts
FS-b-PS	Poly(2,3,4,5,6-pentafluorostyrene)-b-poly(styrene)
F-PE	Fluorinated hydrophobic moiety
FBG	Fluorenylidene biphenylene groups
FEBG	Fluorenylidene ether biphenylene groups
GQD	Graphene quantum dots
GO	Graphene oxide
GDL	Gas diffusion layer
GDE	Gas diffusion electrode
HER	Hydrogen evolution reaction
IEC	Ion exchange capacity
Im	Imidazolium
LDPE	Low-density polyethylene
MEA	Membrane electrode assembly
MPL	Microporous layers
Mm	Morpholinium
MeIm	1-methylimidazole
NMP	1-Methyl-2-pyrrolidone
OER	Oxygen evolution reaction
PO	Polyolefins
PSU-g-POx	Polysulfone-g-poly(2-alkyl-2-oxazoline)s
PFAEs	Fluorinated poly(aryl ethers)
PFEKS	Poly(fluorenyl ether ketone sulfone)
PGM	Platinum group metal
PPF	Post-polymerisation functionalization
PPP	Poly(phenylene)

PSU	Polysulfone
PS	Polystyrene
PPO	Poly(2,6-dimethyl-1,4-phenylene oxide)
PESK	Poly(phthalazinon ether sulfone ketone
PEI	Polyetherimide
PPESK	Poly(phthalazinon ether sulfone ketone)
PTPEDBP	Poly(tetraphenylethylene)-co-(dibenzoylphenylene)
PEN	Poly(ether nitrile)
PVDF	Polyvinylidene fluoride
PFEKS	Poly(fluorenyl ether ketone sulfone)
PTPES	Poly(tetraphenyl phthalazine ether sulfone)
PEM	Proton exchange membrane
QGO	Qraphene oxide particles
QA	Quaternary ammonium
SEBS	Polystyrene-b-poly(ethylene-co-butylene)-b-polystyrene
T	Temperature
TMCS	Chlorotrimethysilane
TCE	1,1,2,2-Tetrachloroethane
TMA	Trimethylamine
TEA	Triethylamine
TMEDA	N,N,N’,N’-Tetramethylethylenediamine
TMHDA	N,N,N’,N’-tetramethyl-1,6-hexanediamine
TPMG	Triphenyl methane group
TMHDA	N, N, N′,N′-tetramethyl-1, 6-hexanediamine
TSH	Tertiary sulfonium hydroxide
TEMED	N,N,N’,N’ - tetramethylethylenediamine
WU	Water uptake
t	Time
σ	Ionic conductivity

Chapter 1. Introduction

1.1 Background

The energy crisis and resources shortage of conventional fossil fuels such as coal, natural gas and oil are becoming severe with the rapid development of society and industrialisation. The irreversible environmental effects, including global warming, climate change, air pollution, etc., caused by the combustion of conventional fossil fuels have threatened the survival of humans [1, 2]. For instance, extreme weather has happened more frequently in the last few years. Renewables hold the key to the increasing energy demand and environmental issues. The global energy demand is predicted to increase by 58 % by 2040 [3]. In recent years the installed capacity of renewable energy sources has experienced rapid growth-based on limited remaining oil reserves. Green hydrogen (H_2) refers to hydrogen produced using renewable energy, such as electrolytic hydrogen from water splitting. Hydrogen is considered one of the most promising energy carriers for the future [4] due to its high energy density and CO_2-free emission [5]. There are several resources for hydrogen, such as steam reforming of methanol [6], gasification of coal and petroleum coke, photoproduction [7] and water electrolysis [8].

The water electrolyser can produce hydrogen by converting electrical and thermal energy into chemical energy, functioning as an electrochemical device. According to the electrolyte utilised in the electrolysis cell at high temperatures >500 °C, solid oxide water electrolysis (HT-SOWE) is promising technology due to the low cell voltages required (electrical energy) and the ability to use heat from other exothermic industrial processes [9]. At low temperatures <100 °C, there are two main water electrolysis technologies, namely, alkaline water electrolysis (AWE) and polymer electrolyte membrane water electrolysis (PEMWE).

AWE is a mature and well-established technology. AWE uses a porous membrane separator (diaphragm) with a high alkaline concentration of >7 M. Due to the high pH, non-noble catalysts, e.g., Ni-based, can be utilised, achieving a relatively low cost. However, there are still some issues, such as the low current density, poor gas separation/crossover (using diaphragm) and corrosive electrolyte (usually ca. 30 wt% KOH). PEMWE uses a solid electrolyte membrane to improve gas separation and narrower separation between the anode and cathode (zero gaps), allowing for lower ionic resistance losses. PEMWE provides high current density, high gas purity, and rapid system responses compared with AWE. Polymer membranes are used as the

solid electrolyte to allow ion conduction instead of liquid electrolytes. Table 1.1 compares the main characteristic of alkaline, PEM, AEM and HT-SOWE water electrolysis.

Table 1.1 Comparison of the main characteristic of alkaline, PEM, AEM and HT-SOWE water electrolysis

	AWE	PEMWE	AEMWE	HT-SOWE
Electrolyte	KOH solution	PEM	AEM	Ceramic
Charge Carrier	OH^-	H^+	OH^-	O^{2-}
Cathode	Ni, Ni-Mo alloys	Pt, Pt-Pd	Ni and Ni alloys	Ni-doped Yttria-stabilized zirconia (YSZ)
Anode	Ni, Ni-Co alloys	RuO_2, IrO_2	Ni, Fe, Co oxides	Lanthanum strontium manganate (LSM))
Operating Temperature	60-90 ^oC	20-100 ^oC	20-100 ^oC	700-1000 ^oC
Technology status	Mature	Commercial	R&D	R&D

According to the different ions conducted, the polymer electrolyte membranes (PEMs) can be divided into proton exchange membranes, also use the same acronym of (PEMs) and anion exchange membranes (AEMs). Due to the corrosive acidic cell operation environment, the materials utilised in proton exchange membrane water electrolysis (PEMWE), such as the catalysts, current collector and separator plates, should be resistant to the corrosive low pH conditions and sustain the high applied overvoltage at the anode during long-term operation > 60, 000 h. Limited materials can meet the crucial demand, for instance, the noble metal catalysts, Pt, Ir and Ru, which are expensive. PEMWEs utilise IrO_2 and Pt at the anode and cathode [10]. Cost remains a significant hindrance to PEMWEs commercialisation. Compared with PEMWEs, AEMWEs provide an environment for faster oxygen evolution reaction kinetics and utilise non-precious metals catalysts, such as nickel alloys and transition metal oxides for cathode and anode. Using a non-precious metal catalyst can significantly decrease the cost of the device.

1.2 Membrane electrode assembly

The research on AEMWE is still in its early stage. Very few reports exist on AEM performance in electrolyser cells [9]. For AEMWE, cheap and abundant materials are reported, which benefits cost reduction and commercialisation [11]. Besides, the solid electrolyte enables the generation of high-purity hydrogen. The structure of a typical AEMWE is shown in Figure 1.1.

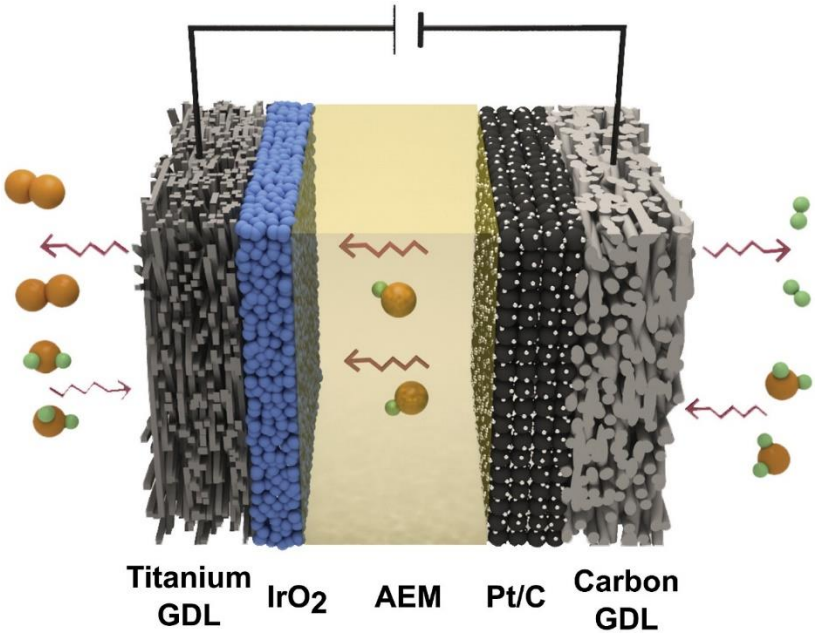

Figure 1.1 The typical structure of AEMWE. Reproduced with permission from [11]. Copyright (2019), American Chemical Society.

The membrane electrode assembly (MEA) is the most critical component in AEMW as it largely determines the cell's performance. In the middle of an MEA is the anion exchange membrane (AEM), sandwiched by the catalyst layer (CL) and gas diffusion layer (GDL) on both the anode and cathode sides. AEM can not only conduct the anions, for instance, hydroxide (OH^-), but also work as the barrier between the oxygen and hydrogen generated by the cell to avoid their mixing. CL is where the electrocatalyst is distributed evenly, and the electrochemical reactions occur. BP, located on the outermost layer of the single cell, can support the MEA, and provide the place for the flow channel. The plate is bipolar because it contains an anode flow channel for one MEA and a cathode flow channel for another MEA on one side in an electrolyser stack. The water and gas flow channels are porous electrically conductive layers known as porous transport layers (PTL). PTL can contact GDL or CL directly. There are three main methods to prepare the MEA, namely, the gas diffusion electrode (GDE) method, the catalyst coated membrane (CCM) method, and the direct membrane deposition (DMD) method. For the GDE method, the catalysts are applied on the GDL first and then get pressed on the membrane. For the CCM method, the catalyst is directly coated on both sides of the polymer membrane [12]. DMD deposits the membrane directly on the top of the GDE of the cathode and/or anode instead of casting the membrane as an independent film.

The hydrogen evolution reaction (HER) occurs at the cathode, while the oxygen evolution reaction (OER) occurs at the anode. The reactions are shown below. The

standard potential at the anode in an alkaline environment is 0.83 V lower than that in acidic environments (0.4 V vs SHE vs 1.23 V vs SHE), enabling to use of the non-platinum group metal (PGM) as a catalyst, such as Ni-, Co-, and Cu-based materials,

Anode $2OH^- \rightarrow H_2O + \frac{1}{2} O_2 + 2e^-$ $E^0 = 0.4$ V (1.1)

Cathode $2H_2O + 2e^- \rightarrow H_2 + 2OH^-$ $E^0 = -0.83$ V (1.2)

Overall $H_2O \rightarrow H_2 + \frac{1}{2}O_2$ $E^0 = 1.23$ V (1.3)

In water electrolysis, electric current flows between the two electrodes to split water generating high-purity hydrogen 97-99.5 % (and oxygen). In an anode only fed AEMWE, water moves through MEA from the anode to the cathode, where it is split into hydrogen and hydroxide (OH^-) in the presence of electrons via HER at the cathode. Then hydrotreated OH^- moves back to the anode and produces oxygen, water, and electrons via OER.

As is known, HER kinetics is sluggish under alkaline conditions, especially when using PGM-free metals as a catalyst. It is two or three orders of magnitude slower than under low pH conditions. In alkaline media, HER begins with the dissociation of water and the formation of the hydrogen intermediates (H_{ad}) shown below,

$H_2O + e^- \rightarrow H_{ad} + OH^-$ (1.4)

Then followed by the Heyrovsky step (1.5) or Tafel recombination step (1.6):

$H_2O + H_{ad} + e^- \rightarrow H_2 + OH^-$ (1.5)

$2H_{ad} \rightarrow H_2$ (1.6)

The water dissociation (1.4) on Platinum is the rate-determining step (slowest step).

Four electrons are required for O2, twice that of HER for OER, increasing the sluggish OER kinetics. However, it is much faster in alkaline than in acidic media.

$4OH^- \rightarrow 2H_2O + O_2 + 4e^-$ (1.7)

1.3 Anion exchange membrane

Anion exchange membrane (AEMs) is a significant component in AEMWEs. AEM acts as the ion conductor and the separator between hydrogen and oxygen. There have been several types of AEMs investigated for water electrolysers in literature.

AEM need to meet several physical (structural/mechanical), thermal, chemical and ion conductivity properties. AEM should have high hydroxide (OH^-) conductivity, durable mechanical properties, low gas permeability, and superior chemical stability towards oxidation and nucleophilic attacks to ensure efficient water electrolysis and long-term operation. Additionally, it should be low-cost and easy to scale up.

There are several commercial AEMs, including Fumasep® FAA3 from Fumatech (Germany), A201 from Tokuyama (Japan), AEMION™ from Ionomer (Canada), SUSTAINION® from Dioxide Materials (USA) and Orion TM1 from Orion Polymer (USA). Morgane® ADP from Solvay (Belgium). According to US DOE, the current target for the power density of AEM fuel cells is ≥1.0 W cm^{-2} at 0.76 V at 80 ^{o}C (rated power), P ≤250 kPa; platinum group metal (PGM) -free, under H_2/air conditions. Few existing AEMs can meet all the requirements simultaneously [13]. For AEM, electrolyser current density >1 A cm^{-2} is desired at cell voltage below 1.8 V with a lifetime >40,000h [14].

1.4 Characterisation of Anion exchange membrane

As one of the core materials in AEMWE, the AEM significantly affects the cell's performance. Table 1.2 shows the essential properties and corresponding characterisation techniques/equipment. Membrane characteristics are primarily dictated by the synergistic effect of the backbone and the tethered functional group.

Table 1.2 Important AEM properties and the characterisation techniques/equipment.

Properties		Techniques/equipment
Physical/chemical properties	Ion exchange capacity (IEC)	Back Titration
	Water uptake (WU)	Gravimetry
	Swelling ratio (SR)	Dimension measurement
Thermal properties	Glass transition temperature	Differential scanning calorimetry (DSC)
	Thermal stability	Thermal gravimetric analysis (TGA)
Mechanical properties	Tensile strength	Universal testing machine
	Elongation (%)	
Chemical stability	Alkaline stability	NMR, FTIR and gravimetry
	Oxidative stability	

1.4.1 Ion exchange capacity

The ion exchange capacity (IEC) is the parameter characterising the ability of the ion exchange membrane to preferentially displace the initial counterion on the tethered functional group with another ion existing in the solution [15]. Thus, it represents the number of available exchange sites within a certain membrane weight, often expressed in millimoles equivalent to the ion exchange groups in a gram of the dry membrane (mmol g^{-1}). Several methods can be used to determine the IEC. The most widely used one is titration. Typically, higher IEC resulted in higher ionic conductivity due to increased ion concertation and increased water uptake/swelling of the membrane. This is because of the hydrophilic nature of the charged groups. However, IEC only

provides an average measure of bulk ion concentration and does not provide information about the distribution of the ions.

1.4.2 Water uptake, swell ratio and hydration number

The cationic counterion is attached to AEM backbones. The mobile ion (OH^-) dissociates upon membrane hydration. A significant number of water molecules gather around the hydrophilic cationic head group, which significantly influences the membrane weight and dimension. Additionally, the OH^- ion inside the membrane is hydrated and drags water molecules as it diffuses inside the membrane. The electroosmotic drag number is the number of water moles per mole of OH^- ions. Importantly, hydroxide ion diffusion occurs through the water channels inside the membrane by hoping from one cationic group to another, and their diffusion coefficient (conductivity) is dependent on water content. Therefore, it is meaningful to characterise the water content in the membrane. Water uptake (UP), swell ratio (SR) and hydration number (λ) are used to characterise AEMs' water content. WU is determined by the mass of the fully hydrated (or equilibrium water content at given water activity/relative humidity and temperature) and dry membrane. SR is the dimension change of the membrane before and after full hydration by immersion in liquid water. λ is the number of water molecules per unit of the functional group [16]. Appropriate water content is beneficial for ionic conductivity. At the same time, high swelling of AEM may cause delamination of the catalyst layer and result in a limited lifetime from failure due to mechanical stresses associated with dry and wetting cycles.

1.4.3 Mechanical properties

Mechanical properties are physical properties that a material exhibits upon applying forces, including strength, toughness, and hardness. During the electrolyser's operation, the membrane needs to withstand forces associated with operation under high-pressure hydrogen and compression forces to ensure low contact resistance and a good gas seal. Poor mechanical properties may cause structural defects, such as pinholes and crack propagation. Hence, AEM is expected to exhibit good mechanical stability, especially tensile strength and elongation.

The polymer backbone plays a primary role in mechanical strength and stability. A rigid structure like aromatic rings and perfluorinated design provides the membrane mechanical solid stability, while poor dimension stability decreases the mechanical strength. Furthermore, long-term operation and elevated working temperature may cause the membrane to creep as continuous compaction works on the hydrated AEM.

A universal testing machine (UTM) is usually utilised to measure tensile strength and elongation. Besides, dynamic mechanical analysis (DMA) can also be used to measure the deformation of a material in resonance with vibrational forces. DMA provides information regarding the dynamic modulus, the loss modulus and mechanical damping.

1.4.4 Thermal properties

Thermal stability is the ability of the materials to resist damage under heat stress. It suggested the maximum application temperature of the membrane. Differential scanning calorimetry (DSC) and thermogravimetric analysis (TGA) are usually utilised to characterise the thermal properties of AEMs. DSC has a wide application in characterising the thermal properties, such as melting and degradation temperatures, glass transition temperature (T_g), melt and crystallization enthalpy, polymorphism, and purity of the materials, etc. TGA can be used to characterise the thermal stability and composite of the materials [17]. The TGA onset temperature can be used as reference for DSC measurements [18].

1.4.5 Ionic conductivity

Ionic conductivity is one of the most critical properties of AEM. Higher conductivity usually can translate to higher performance of electrolyser. Compared with H^+ ions, OH^- ions move inherently much slower, which makes the ionic conductivity of AEM for a given thickness and IEC much lower than that of PEM. Hydrated OH^- ion has mobility >1.6 times slower than a hydrated proton in diluted solutions at 25 °C. Thus, AEMs require higher IEC than PEMs to achieve similar conductivity. The mechanistic description of the transport processes of ions in AEM is still under debate. As is shown in Figure 1.2, there are different proposed mechanisms to explain the transportation of ions at the molecular level, namely, the Grotthuss transport mechanism (also called ion hopping mechanism), diffusion or vehicular mechanism, and convection mechanism [19]. Grotthuss transport route is the most accepted mechanism in PEM and AEM, using head groups to facilitate ion movements. In this theory, the OH^- ions cross the membrane by hopping from one hydrolysed exchange site to another, also observed for protons (H_3O^+) [10]. Water works as OH^- ion transport vehicles powered by the electrochemical potential gradient between the electrodes in the diffusion or vehicular mechanism. This mechanism is more dominant in an aqueous KOH solution where K^+ and OH^- ion diffusion carries a charge. The convection mechanism is the electro-osmotic drag or convection that drags the OH^-. It is impossible to measure ionic

conductivity directly via experimental methods. However, the conductivity is conversely derived from the resistance or impedance obtained experimentally. According to the different measurement methods, conductivity can be divided into in-plane conductivity and through-plane conductivity. The former measure the conductivity within the plane of the membrane (in-plane direction), while the latter is done through the thickness of the membrane (through-plane direction). The through-plain conductivity is closer to the practical operation situation.

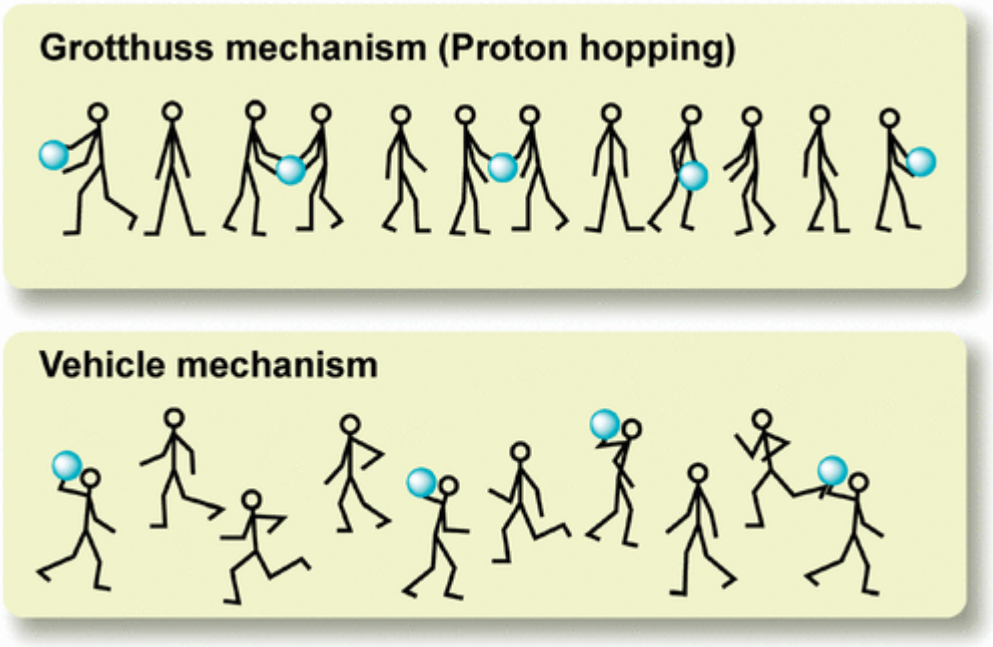

Figure 1.2 Possible transport mechanisms for ion exchange membrane. Reproduced with permission from [19]. Copyright (2008), American Chemical Society.

Ionic conductivity is determined by several factors: the IEC, membrane thickness, water content, and temperature. It is significant to balance ionic conductivity with other properties, as high conductivity may cause poor chemical stability and mechanical strength.

1.4.6 Chemical stability

Chemical stability refers to the resistance of the AEM to attacks from chemical side reactions, such as alkaline stability (hydroxide attack) and oxidative stability (reactive oxygen radical attacks). Chemical stability is a vital factor in the durability of AEMs in an electrolyser environment. The chemical resistance of AEMs in the literature mainly focused on alkaline stability tests in N_2 saturated high temperature/high alkaline environment, which is not directly relevant to water electrolysers. It is vital to have good chemical stability for the AEM as poor chemical stability leads to insufficient durability

of the AEMWE. According to the literature [20-22], there are several ways to evaluate the chemical stability of polymers, such as IEC loss, weight loss, and ionic conductivity loss before and after accelerated stability tests. Different methods can be utilised to determine the mechanisms of the degradation process, for example, NMR.

1.4.7 Electrochemical impedance spectroscopy

Electrochemical impedance spectroscopy (EIS) is an electrochemical technique to measure the impedance of a system by applying a perturbation voltage (or current). The frequency response to the perturbation voltage represents the electrochemical impedance of the electrolyser system. With the EIS, ionic conductivity can be calculated. Figure 1.3 shows the typical EIS spectra [23]. The impedance (Z) is the ratio of the sinusoidal voltage to the current at a particular frequency, consisting mathematically of the real part ($Z^{'}$) and the imaginary part ($Z^{''}$). The equations are as below, where θ is the phase angle.

$$Z^{'} = |Z|\cos\theta \qquad (1.8)$$

$$Z^{''} = |Z|\sin\theta \qquad (1.9)$$

$$\theta = \tan^{-1}\left(\frac{Z^{'}}{Z^{''}}\right) \qquad (1.10)$$

There are two typical graphs used to present EIS data. One is using the Nyquist plot, i.e., the rectangular coordinate form of $Z^{'}+jZ^{''}$. The other is the bode plot, i.e., the ratio between the logarithm of the absolute magnitude of the total impedance |Z| and the angular frequency's logarithm (log ω) [24].

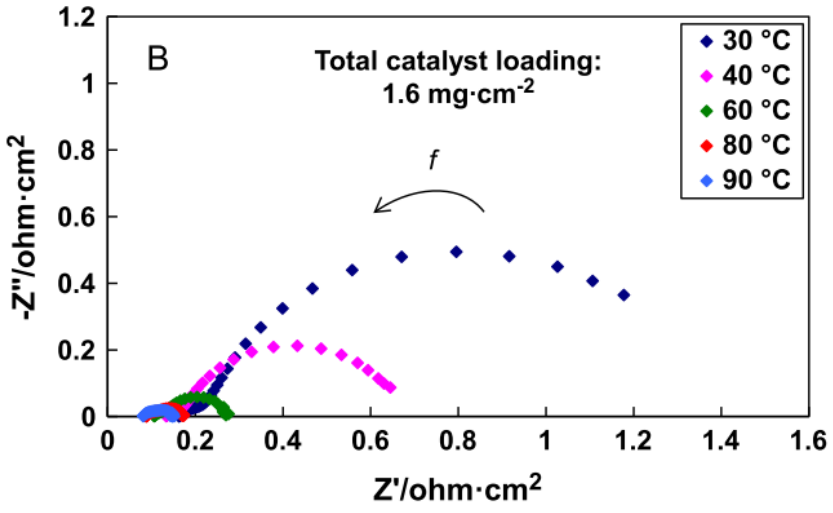

Figure 1.3 The typical AC-impedance spectra at different temperatures. Reproduced with permission from [23]. Copyright (2017), Elsevier.

.

1.4.8 Single-cell performance

To evaluate the electrochemical efficiency of the AEMWE, polarisation curve data are usually plotted to describe the relationship between the current through a device and its corresponding voltage (or potential difference across it). The performance of the AEMWE is mainly affected by the temperature, catalyst loading and the ionomer, and the alkaline concentration of the supporting electrolyte. Typically, the higher the current density at a given cell voltage, the better the cell's performance. The other significant criterion is the durability of the cell [23]. To test the durability, aside from the absolute value of the performance decay, the degradation rate of the initial cell current at a constant voltage is also used (or the degradation rate of the initial cell voltage at the constant current). Figure 1.4 shows the typical polarisation curves and the durability tests [25].

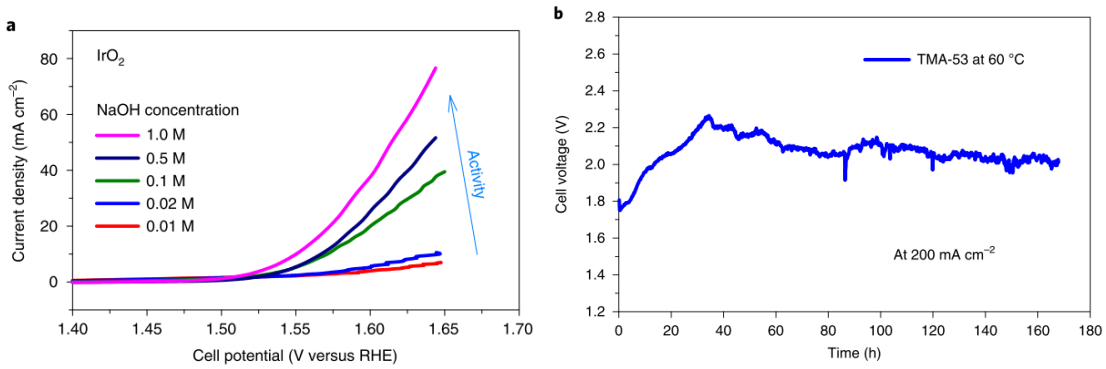

Figure 1.4 The typical polarisation curves (a) and the durability tests (b). Reproduced with permission from [25]. Copyright (2020), Springer Nature Limited.

Chapter 2. A review of anion exchange membranes prepared via Friedel-Crafts alkylation route: preparation, characterisation, and degradation

Anion exchange membrane (AEM) is one of the significant components in AEMFC and AEMWE [26-30]. A schematic representation of AEMFC and AWMWE is shown in Figure 2.1. AEMFC and AEMWE have similar structures. Taking AEMFC as an example, it comprises membrane electrode assembly (MEA), gas diffusion layers (GDL) and flow field plates. As one of the vital components, MEA is where the electrochemical reactions occur, consisting of anion exchange membranes (AEMs) and catalyst layers (CL).

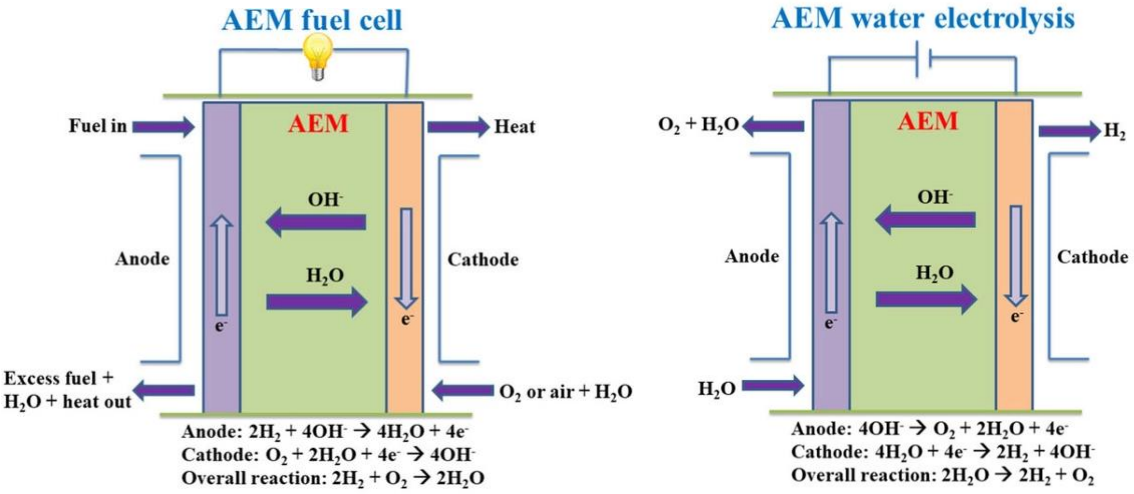

Figure 2.1 The structure of AEMFC (left) and AEMWE (right). Reproduced with permission from [30]. Copyright (2020), Wiley.

AEMs typically contain a backbone and the positive ionic group known as the headgroup or functional groups associated with anions such as OH^- ions allowing for conduction in the presence of water. The backbone is the scaffold of AEMs, which should possess good mechanical properties and chemical resistance but still have active locations to add functional groups. Head groups are the functional moiety that can be converted to a cation.

The structure of AEMs primarily determines their performance. Therefore, the backbone and the charged moiety should be designed carefully. The synthetic routes to prepare AEMs are diverse. Typically, there are two main strategies [31]. One is direct polymerisation (DF), in which the quaternised monomer can be directly incorporated into another polymer chain. The other one is post-polymerisation functionalisation (PPF). In this case, halobenzyl groups are introduced to a polymer matrix via

halomethylation of an aromatic ring or halogenation of methylbenzyl moieties [32]. PPF offers several advantages over DF [28]. Firstly, the raw materials of the backbone polymers are available to access, most of which are commercial or easy to synthesise. Secondly, the types of cationic groups are more diverse and possess more activation sites for modification as synthesis conditions will limit monomer species. Lastly, PPF has a broader range of applications as it allows for both functionalisation of monomers and polymerisation. For instance, to prepare the diblock copolymers-based AEMs, PPF is more suitable [33]. Then, quaternisation is conducted to convert the halobenzyl groups to functional groups, such as the Menshutkin reaction. The Menshutkin reaction is a catalyst-free reaction with 100% atom utilization, which could coverts the tertiary amine into a quaternary ammonium salt by reaction with an alkyl halide [34].

According to the polymer morphology, there are two methods for the amination process: homogenous phase and heterogeneous phase quaternisation. The former dissolves the polymer into solvent, and shows better results since the homogenous approach shows wider exposure between the amine and chloromethyl groups [35]. However, the heterogeneous process has no requirement for solubility and thus offers a broader range of applications. The halomethylated polymers typically have good solubility in a solvent such as THF, chloroform, or toluene. After the amination process, the halomethyl groups were converted to the ammonium groups, and the polymer's solubility changed. For example, after halomethylation, the polystyrene (PS) block of SEBS was alkylated, and the bromoalkylated polymer was soluble in CH_2Cl_2. However, after quaternisation, the TMA-functionalised SEBS was insoluble in any solvent due to polarity differences between the nonpolar and ionic end blocks [36].

The Friedel-Crafts reaction has been one of the most extensively investigated PPF methods to efficiently attach the desired halo-methyl group to the aromatic ring via electrophilic aromatic substitution under mild experimental conditions. This review focuses on AEMs prepared via the Friedel-Crafts chloromethylation route.

2.2 Backbone and cationic groups

A typical AEM comprises a polymer backbone with tethered cationic groups. The polymer backbone plays a primary role in mechanical strength and stability. A rigid structure provides the membrane mechanical solid stability like aromatic rings or perfluorinated structures. However, poor dimension stability decreases mechanical strength. Different materials have been used as backbones, including oxidation resistance fluorinated polymers, hydrocarbon-based aromatic polymers, condensation polymers and block polymers. Backbone dictates polymer rigidity and tensile strength

affecting water uptake, OH^- conductivity, and chemical stability of AEMs. There are cost and sustainability drives to move away from fluorinated polymers. Aromatic polymers are usually rigid structures and have good thermal stability. However, it was shown that benzylic carbon in polymers is vulnerable to reactive oxygen radicals' attacks. Besides, the crosslinking structure can protect the polymer chains or head groups from radical's attacks. The crosslinking structure will covalently bind the macromolecular chains, improving mechanical, chemical and solvent stability [37, 38]. Besides, crosslinking can also restrict the swell ratio of the membrane and increases the dimensional stability duo to the limited movement of the range of the polymer chains [39]. So, measures of removing vulnerable protons of benzylic carbons and cross-linking should be taken to improve the stability of AEMs [40].

This review focused on the common backbones and cationic groups prepared via F-C reactions. As is shown in Figure 2.2, the backbone contains aromatic hydrocarbons and polymeric analogues as a scaffold for chloromethylation [41], including polysulfone (PSU), Poly(arylene ether) (PAE), poly(phthalazinon ether sulfone ketone) (PESK), poly(ether ether ketone) (PEEK), poly(2 6-dimethyl-1 4-phenylene oxides)(PPO), polybenzimidazole (PBI), polyetherimide (PEI), and polyolefins (POs) [42]. Those membranes can be with multi-cation side chains and chemical/physical crosslinked.

Other than homopolymer backbones, different types of backbones, including block copolymers, composite membranes, etc., may result in phase separation. The phase separation is beneficial for the strength of the membrane, especially its dimensional stability. For instance, the backbone of the block copolymer can contain both hydrophobic and hydrophilic blocks, resulting in phase separation. The hydrophilic section provides ionic conductivity but is more vulnerable to alkaline degradation, while the hydrophobic session can decrease water uptake, maintaining good mechanical properties [43]. The size of the hydrophobic/hydrophilic blocks has an essential influence on the morphology and properties of the membrane [44, 45].

Cationic groups, known as headgroups, are tethered to AEM via covalent bonds to facilitate the movement of accessible OH^- ions. They have a significant effect on the performance of the AEMs. As is shown in Figure 2.2, several cationic groups are employed to support OH^- ions conduction, including quaternary ammonium (QA) cations, phosphonium, imidazolium cations guanidinium, and piperazinium cations and their derivatives and modifications. The chloromethyl groups can be converted to diverse cationic groups through amination, phosphonation and other processes. Ion conductivity and chemical stability are the most significant properties affected by the

cationic group. To increase the ion conductivity, one of the approaches is to increase the basicity of the functional groups. High basicity commonly results in more water molecules around cationic groups due to the strong affinity, facilitating ion conductivity under the same humidified conditions. It also results in better dissociation of OH^- from the head group. Trimethylamine (TMA) is frequently used with chloromethyl styrene to form benzytrimethylamounium functional groups due to their reasonable stability in alkaline environment due to the lack of β hydrogens that leads to Hofmann elimination upon nucleophilic attack from OH^-.

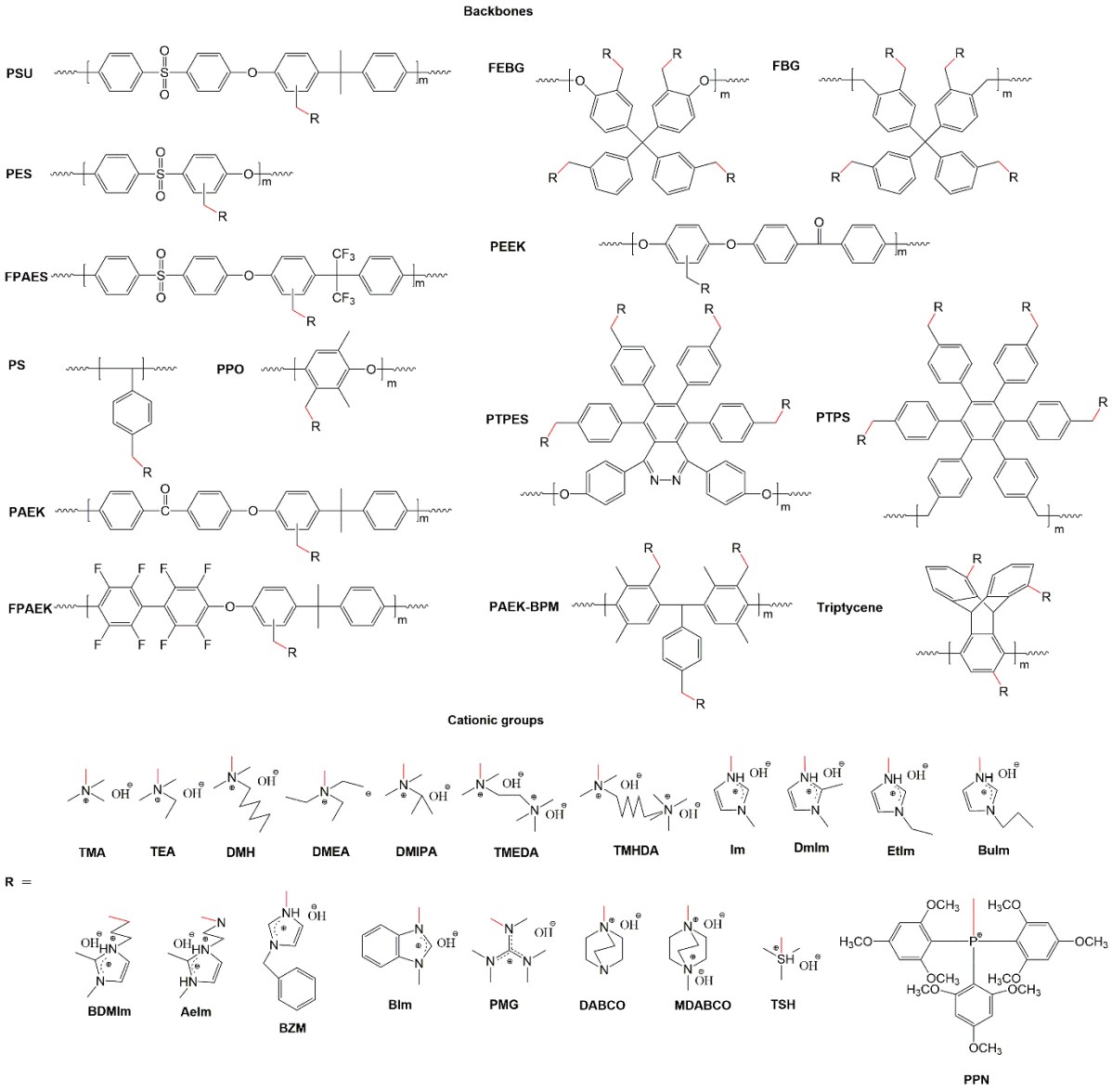

Figure 2.2 The commonly used backbones and cationic groups in AEMs via F-C reaction.

Among the various cation groups, quaternary ammonium (QA) cations are the most frequently used headgroup in AEMs as it highly offers ion-conducting properties [17], no catalyst adsorption, and good alkaline stability [46, 47]. Headgroups are usually more vulnerable than backbone towards chemical stability. This is because of their

close proximity to strong OH^- nucleophiles. QA generally possesses better alkaline stability than other cationic groups, such as quaternary phosphonium and tertiary sulfonium ions [18, 19].

To overcome those issues, considerable studies have been directed to developing the functional groups that retain their ion conductivity in extreme conditions, including quaternary phosphonium, imidazolium cations, guanidinium, piperazinium cations, tertiary sulfonium and their derivatives and modifications [48, 49]. 1,1,2,3,3-Pentamethylguanidine (PMG) is also a strong organic superbase. In addition, PMG demonstrates good thermal and essential stability as the positive charge is delocalised over the carbon and nitrogen atoms [47].

2.3 Fundamentals of Friedel-Crafts route

2.31 Category and mechanism

The Friedel-Crafts (F-C) reactions, developed by Charles Friedel and James Crafts, are a set of aromatic electrophilic substitution reactions that efficiently introduce halomethylation to the polymer backbone.

F-C reactions include two major categories, namely alkylation and acylation. Compared with the alkylation reaction, the acylation reaction is not widely applied practically in AEM preparation as the ketone groups (C=O) are easily attacked by the hydroxide ions, resulting in the poor alkaline stability of the AEMs. Otherwise, the extra reduction step to convert C=O to CH_2 is required, increasing the cost and reducing efficiency [50]. Thus, F-C alkylation is an invaluable and facile modification route to form the benzylic halogen on the aromatic side chain or its copolymers, i.e., halomethylation. In the experimental preparation process of AEMs, chloromethylation was utilised most widely due to its high efficiency. Thus, unless otherwise specified, chloromethylation was introduced mainly in this review. Typically, chloromethylation involves two main steps: the formation of electrophile and the electrophilic substitution on active phenyl rings. Alkyl carbocation by haloalkanes is prepared by using catalysts.

2.32 Catalyst and chloromethylating agent

The catalyst is one of the most significant factors in chloromethylation. Various catalysts can be used in F-C reactions, including protic organic and Lewis acids [36, 51]. Lewis acids are the most widely used catalysts for the chloromethylation process in the AEM preparation process due to their high catalytic efficiencies, such as $AlCl_3$, $SnCl_4$, and $ZnCl_2$. It is essential to control the total amount of the catalyst used and the addition/dosing rate. When adding the catalyst at a fast dosing rate, such as a one-

time injection, the formation rate of the alkyl carbon ion in the solution will be accelerated suddenly because of the promoted electrophilic substitution, which may easily cause the gelation of the solution. As a result, the catalyst is usually added dropwise into the reactants mixture or injected slowly [52]. In addition to catalysts, activating agents such as thionyl chloride can further promote the reaction [53].

Besides, the chloromethylation agent was the critical factor [54]. Chloromethyl ether (CME) and chloromethyl ethyl ether (CMME) are widely employed as chloromethylating reagents in the conventional chloromethylation process [55]. However, those agents are toxic and carcinogenic to human health and are being banned gradually [52]. The approach toward utilising more eco-friendly, non-carcinogenic chloromethylating reagents has been adopted [55], such as chlorotrimethylsilane (TMCS) and 1, 4-bis (chloromethoxy) butane (BCMB) [56-58].

2.33 Functionalization and crosslinking

Chloromethylation, a critical step in synthesising AEMs, achieves the desired alkylation of the phenyl group. The degree of chloromethylation (DC) was utilised to indicate the degree of substituting the chloromethyl groups.

Typically, DC is calculated from the NMR signal integration ratio of the chloromethyl group and the unsubstituted aromatic ring. DC has a significant effect on the final intrinsic properties of the membrane [52, 59]. Higher DC implies more functional groups attached to the main chain after amination and alkalisation. However, too high DC results in high wettability, which leads to excessive water uptake. The water molecules can act as the plasticizer in the polymer chains softening the rigid structure of AEMs, especially those with aromatic backbones. While moderate water content (10-20 moles of water per cationic head group) adds flexibility to AEMs, excessive water content (> 40 moles of water per cationic head group), results in poor dimensional stability and mechanical strength. Therefore, a trade-off between the DC and membrane performance needs to be made [36]. DC can be controlled by changing the reaction condition parameters. Such as temperature, catalyst amount, reaction time and concentration of the reactants, etc. [55].

Significant efforts have been devoted to understanding the effect of reaction parameters on the chloromethylation of various polymers [60-64], including the amount of catalyst, chloromethylating agent, reaction time, and temperature. Adjusting the amount of the chloromethylating agent or the reaction time is the most used procedures to control the chloromethylation reaction [65, 66]. Adding more chloromethylating agents can increase the contact probability of reactants. Jeon et al. changed the ratio

between the tert-alcohol reagent and the aromatic ring to obtain different DF. When the molar ratio of the tert-alcohol reagent to the aromatic ring of the PS block changed from 0.5 equiv to 1 equiv, the corresponding degree of functionalisation increased from 50 % to 80 % [36]. Gopi et al. increased the ratio between CMEE:PPO from 2:1 to 5:1, and the DF rose from 10 % to 60 % [67]. Besides, activating agents of the Lewis acid catalyst, such as thionyl chloride, can also improve the catalytic efficiency [68].

The remaining electron-rich phenyl groups can easily cause crosslinking side reactions in addition to the target chloromethylation reaction [59]. The newly formed chloromethyl groups are expected to convert to cationic groups. However, they may also react with the unsubstituted electrophilic phenyl rings in the backbone to create an intra-polymer crosslinked structure [69]. Therefore, the overall yield of chloromethylating products will be reduced due to crosslinking design.

2.4 Performance of AEMs

Different polymers were investigated as backbones for AEMs. This review will focus on AEMs prepared via F-C reaction according to the chloromethylatied positions on the backbone. The most investigated polymer backbones and their derivatives are polysulfones (PSUs), poly(arylene ether)s (PAEs), and poly(ether ether ketones) (PEEKs). Besides, other polymers containing aromatic groups are also explored, such as polyetherimide (PEI), polystyrene-b-poly(ethylene-co-butylene)-b-polystyrene (SEBS), triptycene groups, and poly(2,6- dimethyl-1,4-phenylene oxide) (PPO). Most of the studies focused on the optimization of experimental conditions. The existing challenges facing the AEMs were addressed, and recommendations for promising research ideas that help achieve decent progress in this area were provided.

2.41 PSUs

Polysulfones (PSUs) are significant thermoplastics with excellent toughness and stability at high temperatures. There are three main types, namely, polysulfone (PSU), polyethersulfone (PES) and polyphenylene sulfone (PPSU) [47, 62, 65, 70]. They are widely investigated as the backbone of the AEM preparation field due to their excellent thermal properties, chemical resistance, and mechanical strength [71]. Backbone stability forms a good starting point for the selection process. Still, it should be highlighted that the chemical and thermal properties of the polymer will be altered on functionalisation and the introduction of a tethered functional group. The performance of PSUs-based AEMs is summarised in table 2.1 below. The distinctive diphenylene sulfone groups, aryl sulfonyl groups and ether groups in the PSUs structure improve the polymer's rigidness and oxidative resistance. The commercial membrane, Udel

from Solvay and FAA from FuMA-Tech GmbH are PSU-based membranes [72, 73]. There are two activated positions for substituting the chloromethyl group, i.e., in the ortho position to the ether linkage or the ortho position to the carbon dimethyl groups. As shown in Figure 2.3(a), Mulliken population analysis shows that the priority position for introducing the chloromethyl group is the ortho position concerning the ether linkage, as the atomic charge is lower in comparison to the ortho position for the carbon dimethyl groups [74].

Reaction conditions play a crucial role in the DC of AEMs. Therefore, it is critical to optimise the chloromethylation conditions, including reaction time and temperature, solvent type and volume, and catalyst feeding mode and volume. Liu et al. prepared PSU-based AEM [74]. The membrane with IEC 1.65 mmol g^{-1} showed conductivity of 25 mS cm^{-2}. As is shown in Figure 2.3(a)&(b), they analysed the carbon atomic charges and XPS to verify the presence of $–CH_2Cl$ groups. Several cationic groups were attached to the backbone, including trimethylamine (TMA), triethylamine (TEA), dimethylethylamine (DMEA), dimethylisopropylamine (DMIPA) and tetramethylethylenediamine (TMEDA), among which TMA-AEM showed the highest the conductivity [52, 72, 75-77]. Abuin et al. prepared TMA-tethered AEMs. They tested the conductivity under a high alkaline solution (0.083 Scm^{-1} in 2 M KOH) [72]. They also measured the water sorption isotherm and found that PSU-based AEM showed higher water sorption isotherms at 20 ^oC, as is shown in Figure 2.3(c). The preparation processes, such as extruding and cast methods, and the effect of the membrane on the water sorption area are still unclear [78]. Increasing the functional groups' basicity is also beneficial for ionic conductivity, such as using 1,1,2,3,3-pentamethylguanidine (PMG) as a functional group [47].

Hydration has a significant effect on the properties of the AEM, such as ionic conductivity, mechanical properties, and dimension stability. Different cationic groups have different hydrophilicity. Wang et al. prepared the PSU-based membrane using the chloromethylation process to compare the performance of different cationic groups. They changed the pendant groups with five other tertiary amine groups, TMA, TEA, DMEA, DMIPA and TMEDA, via three quaternisation approaches to improve ionic conductivity [35, 79]. As is shown in Figure 2.3(d), PSU-based membranes with five cationic groups were prepared with two different approaches. Quaternisation was conducted on the pre-formed membranes directly with five tertiary amines in the first approach. In contrast, the second approach added a bifunctional crosslinker, TMEDA, to the reaction solution before the quaternisation process. TMEDA can act as the

crosslinker and as the chemical for quaternisation. Compared with the membrane prepared via the first approach, the crosslinked membranes prepared via the second approach showed higher ionic conductivity duo to the ion-conducting crosslinker (up to 1.2×10^{-2} S cm^{-1} in de-ionized water at 24 °C).

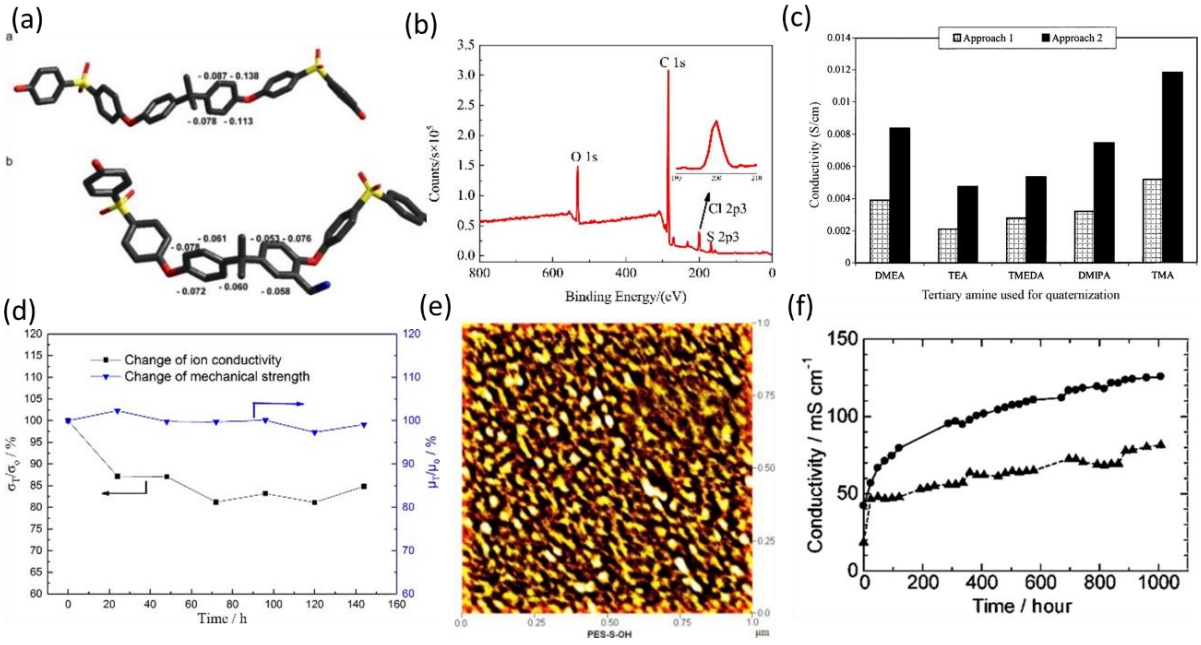

Figure 2.3 (a) Ab-initio calculation of carbon atomic charges. Reproduced with permission from [74]. Copyright (2014), Elsevier. (b) Typical XPS wide scans for chloromethylated PSU. Reproduced with permission from [52]. Copyright (2014), Elsevier. (c) The PSU-based membrane conductivity tethered with different cationic groups. Reproduced with permission from [35]. Copyright (2009), Elsevier. (d) The change of ionic conductivity and mechanical strength of PSU-based membrane in 2 M KOH at 80 °C for a certain time. Reproduced with permission from [50]. Copyright (2018), Elsevier. (e) AFM image of PSU. Reproduced with permission from [68]. Copyright (2016), Elsevier. (f) Time dependence of ionic conductivity. Reproduced with permission from [80]. Copyright (2011), Royal Society of Chemistry.

Different Im-based groups were tethered with PES-based membranes [50, 66]. Lu et al. increased the alkyl line length on the imidazolium (Im) group and obtained two BuIm and EtIm-based membranes [66, 81]. When the alkyl chain length substituted on the imidazole group increases, the membrane's WU, SR, and solubility increase. However, the ionic conductivity decreased. A longer chain allows for more flexibility and expansion, which in turn could increase polymer swelling and water uptake. More water content typically allows for faster ion diffusion from larger water channels. Still, it also dilutes the amount of cationic group per volume, i.e., increasing the distance between them from swelling. Besides, the benzimidazolium (BIm) was also tethered with a PES-based membrane. Perez-Prior et al. used BIm as functional groups via nucleophilic substitution reaction with 1-methyl benzimidazole. The reported ionic conductivity of the PSU-BIm was 0.02 mS cm^{-1} [71]. They put the membranes into a 1 M KOH solution for 100 h. A 35 % loss of BIm groups in the membranes was observed.

PSU-based membranes with other functional groups such as N, N-dimethylhexylammmonium [82], quaternary guanidinium, and sulfonium groups were also investigated. Wang prepared a PSU-based membrane containing pendant quaternary guanidinium groups. The ion conductivity was 51 mS cm^{-1} at 60 ^{o}C [47]. Hossain et al. designed PSU-based AEM with sulfonium as the functional group. The ionic conductivity was above 10^{-2} S cm^{-1} with IEC as 1.37 mmol g^{-1}. The AEM shows no significant weight loss in 1.0 M KOH solution at 60 ^{o}C [68]. The AFM image (Figure 2.3(d)) shows that the surface showed hydrophilic-hydrophobic microphase separation. As is shown in Figure 2.3(e), Li et al. measured the change in ionic conductivity and mechanical strength before and after immersion in 2 M KOH at 80 °C [50]. After 144 h, the ionic conductivity decreased by less than 20 %, and the mechanical strength almost remained the same.

Apart from homogeneous PSU-based polymers, block copolymer-based membranes were also prepared to improve the stability of the membrane. Shin et al. prepared PSUs-based multiblock membranes (PSU-MB) [51]. Introducing a functional group before polymerisation improves performance more than post-polymerisation functionalization. Kim et al. prepared a partially fluorinated (PF) multiblock copolymers-based membrane (PSU-PF) [83], demonstrating well-defined hydrophilic-hydrophobic phase separation behaviour. They used partially fluorinated moiety to improve backbone alkaline stability as the hydrophobic phase excludes hydrophilic nucleophiles. The PF membrane lost 77 % conductivity after immersion in a 1 M KOH solution after 720 h at room temperature. Velu et al. prepared PSU and polyvinylidene fluoride (PVDF) blend membranes. The functionalised PSU segment provides the ionic conductivity while the PVDF segment acts as the hydrophobic polymer enhancing mechanical properties. 50 % and 70 % of PVDF blend membranes showed similar ionic conductivity (54 and 51 mS cm^{-1} at 20 ^{o}C) [84].

Besides, PSU-based composite membranes were also prepared. Moghadasi et al. synthesised quaternised PSU silica as composite AEM. Then three different functionalised silica nanoparticles were mixed with PSU [85]. The content of the nanoparticles had a significant effect on the IEC of the membrane. When containing 3 wt % nanoparticles, the membrane demonstrated high ionic conductivity of 45.46 mS cm^{-1} at 25 ^{o}C.

Table 2.1 The main properties of the PSUs-based membrane.

Code	Functional groups	IEC (mmol g^{-1})	σ^a (mS cm^{-1})	Tensile strength (MPa)	WU (%)	Stability	Ref
PSU	TMA	-	10 (25 °C)	-	100	93.2 % loss of ionic conductivity in 1 M NaOH at 50 °C over 80 h	[86]
PSU	BIm	0.84	0.02 (r.t., 100 % relative humidity and in 0.01 M KOH solution)	-	9.9	35 % decrease of BIm groups in 1 M KOH solution for 100 h	[71]
PSU-PF	TMA	1.7	56 (70 °C)	-	34	65.5 % loss of conductivity in 1M KOH solution at r.t. for 720 h	[83]
PSU	Im	1.54	14.9 (r.t.)	-	67.6	No significant decrease of IEC in 2 M KOH at room temperature. 13 % loss of mass in Fenton's reagent for 200 h.	[66]
PSU	Im	2.19	53 (20 °C)	-	170	-	[81]
PSU	TAM/TMHDA	2.21	46.4 (60 °C)	55.84	20.2	8.2 % loss of IEC in 2 M KOH at 60 °C for 240 h	[57]
PSU	TAM/TMHDA	1.51	22.1 (60 °C)	53.9	29.6	44 % loss of conductivity in 2 M KOH at 60 °C for 50 h	[87]
PES	TMA	1.16	22.3 (r.t.)	53.5	14.3	No physical disintegration in Fenton solution at 80 °C for 8 h	[70]
PSU/PVDF	Im	2.1	73 (60 °C)	-	30	-	[84]
PSU	PMG	z	51 (60 °C)	46.3	39	No significant loss of conductivity in 1 M NaOH at 60 °C for 48 h	[47]
PES	Tertiary sulfonium	1.37	15.6 (60 °C)	-	15.9	No significant mass change 1.0 M KOH solution at 60 °C for 10 days	[68]
PSU	DMH	1.6	48 (60 °C)	22.3	-	81 % loss of IEC in 1 M KOH at 60 °C for 10 days	[82]
PSU-Si	TMA	1.45	45.46 (25 °C)				
PSU	DMIm	0.57	32.4 (80 °C)	40.9	7.5	16.2 loss of conductivity in 2 M KOH at 80 °C for 7 days	[50]
PSU	TMA	-	12	20	106	-	[88]
PSU	DABCO	-	8.8	25	85	-	[88]
PSU/GQD	TMA	1.81	20.56 (30 °C)	11.3	-	-	[89]
PSU	TMA	1.65	25 (20 °C)	15	26.5	-	[52]

PSU	TMA	2.02	11 (30 °C)	-	-	-	[90]
PSU	TEA	1.99	2.8 (30 °C)	-	-	-	[90]

[a] The tested were conducted at 100 % relative humidity, otherwise stated.

2.42 PEKs

Poly(ether ether ketone) (PEEK) is an essential, high-performance engineering polymer with good thermal stability, chemical resistance, and mechanical strength. PEEK and its derivatives, such as poly(ether ketones) (PEK), were investigated as backbones for AEMs. The performance of the PEEKs-based membranes is summarised in table 2.2 using comprehensive sources [73, 91-97].

Different cationic groups were tethered with PEEK-based AEMs. Yan et al. compared the performance of PEEK-based membranes with 1,2-dimethylimidazole (DmIm), 1-Aminoethyl-2,3-dimethylimidazolium (AeIm) and 1-methylimidazole (mIm) with different side chains, namely, PEEK-AeImOH, PEEK-DmImOH, and PEEK-mImOH membranes [98]. As is shown in Figure 2.4(a), the PEEK-DmImOH membrane exhibited a higher WU than the PEEK-mImOH membrane with similar IECs. This was explained by reducing intermolecular force among molecular chains on methyl group addition. PEEK-AeImOH showed the highest WU due to the amine groups introduced in the side chains. The hydroxide conductivity against the IEC for three types of membranes is shown in Figure 2.4(b). The hydroxide conductivity increased expectedly with IEC increase due to the formation of continuous (shorter) path ions hopping. As shown in Figure 2.4(c), after immersion in 1 M KOH at 60 ^{o}C for 168 h. PEEK-AeImOH showed no significant decrease in conductivity since the S_N2 nucleophilic substitution attack of OH^- was reduced due to introducing a long alkyl spacer between the imidazolium group benzene ring on the polymer main.

Wu et al. prepared a PEEK-based membrane with enhanced ionic conductivity using a diquaternisation strategy [99]. As is shown in Figure 2.4(d), they studied ion concentration and the adequate mobility of hydroxide of mono- and di- quaternised membrane. They found that at a certain IEC, multiple quaternised groups on each side chain increase the ionic density and the distance between the neighbouring pendent sites on the polymer backbone, which enhance both hydrophilic-hydrophobic micro-phase separation and adequate hydroxide ion mobility of AEMs.

Yan et al. improved the alkaline stability for AEM through the interactions between strongly polar nitrile groups and available cations. They studied the LUMO energies of benzyl imidazolium, benzyl morpholinium, benzyl imidazolium/benzonitrile, and benzyl morpholinium/benzonitrile (Figure 2.4(e)). They found that the morpholinium functionalized membrane is more stable than the imidazolium one, which might be attributed to the lower swelling ratio of morpholinium functionalized membranes [100].

As is shown in Figure 2.4(f), Chen studied the stability of poly(fluorenyl ether ketone sulfone) (PFEK)-based membranes with both QA and Im as the functional groups. The Im-PFEK-based membrane demonstrated better morphology than QA-PFEK-based membrane [58, 101].

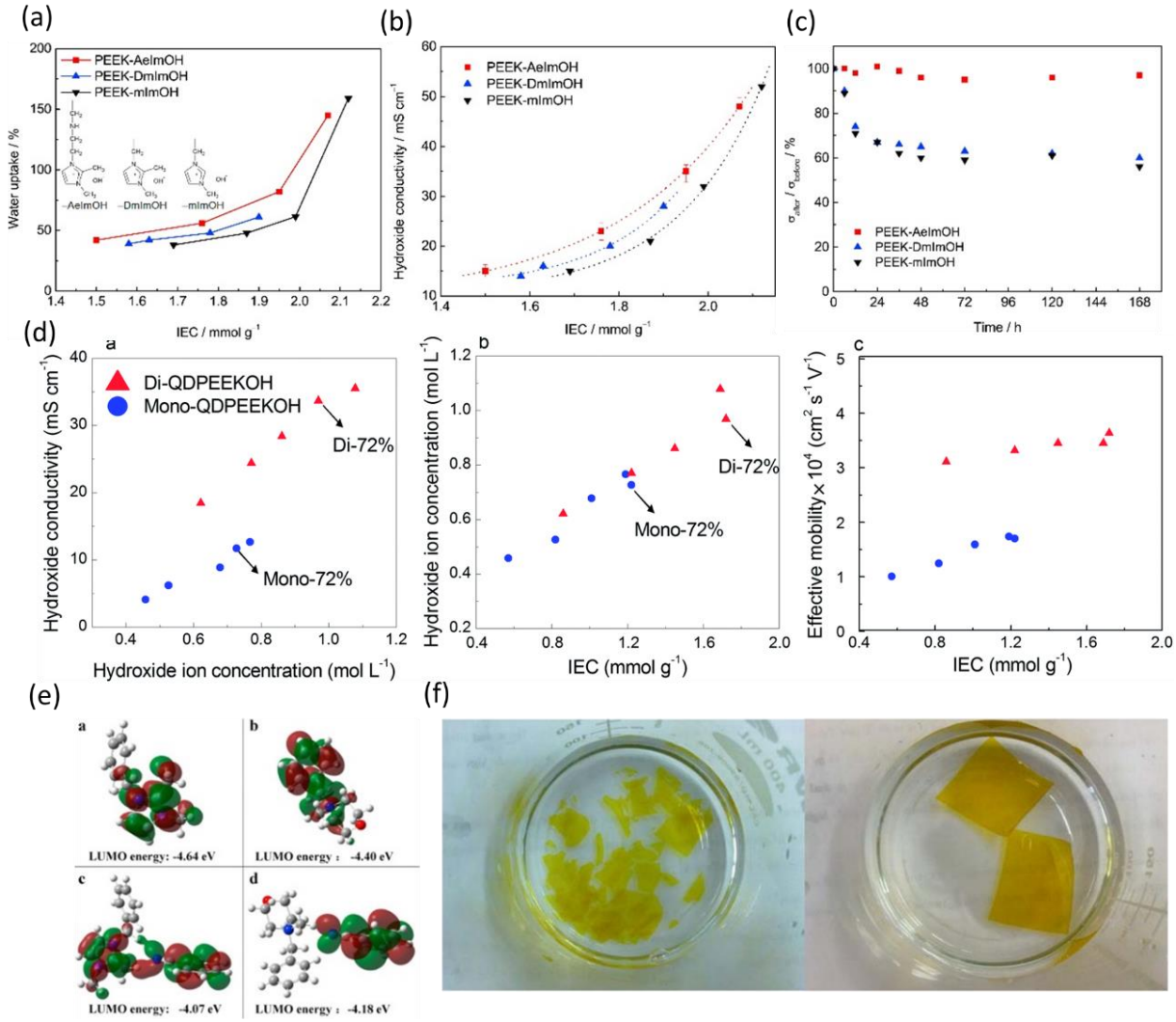

Figure 2.4 (a) Water uptake, (b) hydroxide conductivity and (c) changes of σbefore/ σafter before and after alkaline stability test of PEEK-AeImOH membranes. Reproduced with permission from [98]. Copyright (2016), Elsevier. (d) Concentration and elective mobility of OH- in the mono-and di-QDPEEKOH membrane. Reproduced with permission from [99]. Copyright (2016), Elsevier. (e) The isosurface and LUMO energy (a: benzyl imidazolium; b: benzyl morpholinium; c: benzyl imidazolium and benzonitrile: d: benzyl morpholinium and benzonitrile). Reproduced with permission from [100]. Copyright (2016), Elsevier. (f) Photographs of QA-PFEKS (left) and IM-PFEKS (right) after the degradation test. Reproduced with permission from [101]. Copyright (2012), American Chemical Society

PEEK-based composite membranes were also investigated. Metal-organic frameworks (MOF) are an emergent class of organic-inorganic materials and consist of ordered networks from organic bridging ligands and inorganic metal cations. Owing to the large surface area, low crystal density and tunable pore size, they can be embedded into the polymer matrix to increase the ionic conductivity as multi-functional

fillers. The ion channels can construct either through framework decoration of functional groups or encapsulation of ionic carriers. He et al. incorporated quaternised MIL-101(Cr) into PEEK polymer and prepared ImPEEK/ImMIL-101(Cr) composite membrane. The dimension stability and the mechanical strength of the composite membrane were enhanced. The conductivity of composite membranes of 5.0 wt% ImMIL-101(Cr) is 0.047 S cm^{-1} at 60 °C, 67.9 % higher than that of the pure membrane (0.028 S cm^{-1}) [102]. Besides, bisphenol polycarbonate was also investigated as the backbone. The membrane demonstrated good flexibility and dimensional stability. The ionic conductivity was 31.6 mS cm^{-1} at 80 °C and 100 % relative humidity. After immersion in 1.0 M KOH at 60 °C over 5 days, the ionic conductivity decreased to 23 mS cm^{-1} [60].

2.43 PAEs

Poly(arylene ether)s (PAEs) are a set of polymers containing arylene ether in backbones, including fluorenylidene ether biphenylene groups (FEBG), fluorenylidene biphenylene groups (FBG), fluorinated poly(aryl ether)s (PFAEs), poly(tetraphenyl phthalazine ether sulfone) (PTPES) and poly(tetraphenyl phthalazine sulfone) (PTPS). PAEs were widely investigated as the backbone for AEMs due to their excellent thermal and mechanical properties [80]. Key characteristics of the PAEs-based AEMs are summarised in table 2.2.

PAE-based membranes are typically multiblock membranes. Different blocks were incorporated into the polymer, for instance, the cardo structure, including fluorenylidene ether biphenylene groups (FEBG) and fluorenylidene ether biphenylene groups (FBG) [101, 103, 104]. Cardo polymers are a subgroup of polymers where carbons in the backbone of the polymer chain are also incorporated into ring structures. Cardo groups in the polymer chain can reduce the intermolecular forces and the crystallinity of polymers and thus exhibit specific properties [105]. These backbone carbons are quaternary centres. As such, the cyclic side group lies perpendicular to the plane of the polymer chain, creating a looping structure. These rings are bulky structures that sterically hinder the polymers and prevent them from packing tightly. They also restrict the rotational range of motion of the polymer chain, creating a rigid backbone. Multiblock polymers tend to show phase separation. Li et al. prepared well-defined phase segregation multiblock AEMs with sequential hydrophobic/hydrophilic structures [106-108]. The ionic conductivity was enhanced under strong-field effects. The ionic conductivity of multiblock PAES-X16Y10 membranes (IEC 1.45 mmol g^{-1}) was 27.6 mS cm^{-1} (60 °C). After treatment in 1 M NaOH solution at 60 °C for 132 hours,

89% of the original values remained. Furthermore, instead of bis(3,5-dimethyl-4-hydroxyphenyl)-phenyl methane (BDHPM), they also used 4,4'-sulfonylbis(2,6-dimethylphenol) (SBDMP) to prepare new AEM, QPAE-X8Y8. The ionic conductivity increased to 46.3 mS cm^{-1} 60 °C. QPAE-X8Y8 showed better chemical stability. After the degradation test, the conductivity decreased by 9.7 %.

The chloromethylation reactions occur in the fluorenyl groups at the early stage of the chloromethylation reaction, then on the main chain as the reaction proceeds [104]. FBG can be copolymerized with different groups, for instance, the perfluoroalkane [104]. The solid C-F bond and low polarizability, attributed to fluorine's small size and high electronegativity, result in good hydrophobicity and outstanding chemical and thermal stability [73, 109, 110]. Tetra-quaternary ammonium hydroxide can be obtained in the fluorenyl group [111]. Ozaw et al. prepared perfluoroalky-FBG copolymer (PF-FBG)-based AEMs. The membrane demonstrated showed no practical loss in conductivity after 1100 h [104]. Besides, PSU was also incorporated with FBG as the copolymer. Seo et al. prepared PSU-FBG copolymer-based AEMs with tetra-quaternary ammonium as functional groups. Though many positions were available for chloromethyl substitution, the conductivity was only 30.7 mS cm^{-1} at 80 ^{o}C [111]. Hossain et al. prepared PAEs-based copolymer membranes with imidazolium as a functional group [53]. The membrane with IEC 1.96 mmol g^{-1} demonstrated a conductivity of 28 mS cm^{-1} at 60 °C and 100 % relative humidity. Hydrophilic-hydrophobic microphase separation was observed via atomic force microscopy (AFM). After immersion in 1.0 M KOH solution at 60 °C, the ionic conductivity decreased by 20 %. For PFKS-based backbone. Chen et al. prepared poly(fluorenyl ether ketone sulfone) (PFEKS) and compared the alkaline stability of those two membranes. At 60 °C, QA-functionalised PFEKS lost 18 % of IEC after immersion in 1 M NaOH for 48 h, while Im-functionalised PFEKS lost 22 %. When the temperature increased to 80 °C, QA-functionalised PFEKS suffered 22 % of IEC while Im-functionalised PFEKS lost 57 % of IEC [101]. Figure 2.4(f) shows that QA-PFEKS samples were broken into small pieces after the degradation test, indicating a decrease in mechanical properties and polymer molecular weight [101]. Hossain attached six imidazolium functionalised ionic groups on each PTPES polymer unit. However, the conductivity was much lower than the QA-functionalised one [112]. Compared with quaternary ammonium AEM, the tertiary sulfonium (TS) membrane demonstrated lower water uptake (17.8 %) and lower conductivity (18.3 mS cm^{-1} at 80 ºC) due to the lower IEC 1.51 mmol g^{-1} [113].

Table 2.2 The main properties of the PSUs-based membrane.

Code	Functional groups	IEC (mmol g^{-1})	σ (mS cm^{-1})	Tensile strength (MPa)	WU (%)	Stability	Ref
PAES-X16Y10	TMA	1.45	27.6 (60 °C)	15.2	27.7	25.2 % of conductivity 1 M NaOH solution at 60 °C for 168 h	[106]
QPAE-X8Y8	TMA	1.95	46.3 (60 °C)	20.3	24	9.7 % decrease of conductivity in 1 M NaOH solution at 60 °C for 168 h	[107]
QPE	TMA	1.5	40 (60 °C)	-	133	70 % loss of ionic conductivity in 1 M KOH aqueous solution at 40 °C	[110]
PAEs	Im	1.96	28 (60 °C)	-	35.2	28.6 % loss of conductivity in 1.0 M KOH at 60 °C over 7 days.	[53]
FEBGs	TMA	1.94	35 (60 °C)	30	35	72.3 % loss of ionic conductivity after soaking in 1 $molL^{-1}$ NaOH at 60 °C for 240 h. 8.4 % weight loss after immersion in Fenton's reagent (3% H_2O_2, 2 ppm $FeSO_4$) at 80 °C for 1 h.	[103]
PFES	TSH	1.51	18.3 (80 °C)	-	17.8	-	[113]
FBGs	TMA	1	70 (80 °C)	-	1.23	5 % loss of the IEC (in Cl^- form) in M KOH over 1000 h at 60 °C	[104]
FEBGs	TMA	1.73	30.5 (80 °C)	-	68.7	-	[111]
FEBGs	TMA	1.7	40 (20 °C)	-	30	-	[114]
PEEK	TMA	1.15	14.6 (30 °C)	-	28.7	12.15 % weight loss, 16.39 % conductivity loss after socked in 10.0 M KOH for 24 h at 100 °C	[94]
PEEK	TMA	1.4	17 (20 °C)	-	70	-	[91]
PEK	Imidazolium	2.15	31.6 (80 °C)	-	42.8	22.5 % decrease of ionic conductivity after immersion in 1.0 M KOH solution at 60 °C over 5 days	[60]
PAEs	TMA	1.45	10.8 (60 °C)	17.5	15.7	16.7 % decrease of conductivity and 11.4 % decrease of tensile strength in 1 M NaOH at 60 °C for 120 h	[97]
PEK	TEA	-	2 (60 °C)	-	-	No significant decrease in conductivity in 1 M KOH at 100 °C.	[73]
PEK-C	TMA	0.11	5.06 (60 °C)	-	3.33	2.1 % loss of weight after immersion in Fenton's reagent at 60 °C for 168 h	[92]
PEEK	AeImOH	2.07	71 (60 °C)	-	150	The conductivity of the PEEK-AeImOH membrane has almost no change at room temperature for 168 h	[98]
PEEKK	DImOH	1.65	19 (20 °C)	22	250	25 % loss of conductivity and IEC at 60 °C for 192 h	[96]

PEEK	TMA	1.39	12 (30 °C)	-	-	-	[93]
PEEK	Im	2.03	52 (20 °C)	18	150	-	[95]
PEEK	DABCO	1.22	24.4 (50 °C)	14.6	125	41.5 % loss of conductivity in 2 mol L^{-1} KOH at 60 °C	[99]
ImPEEK/ImMIL-101(Cr)	Im/ImMIL-101(Cr)	2.2	30 (30 °C)	32	22	25 % loss of ion conductivity in 2 mol L^{-1} NaOH at 80 °C for 48 h	[102]
PEN	Im	1.8	32 (30 °C)	-	80	28 % decrease of ionic conductivity in 1 M KOH 60 °C for 120 h	[100]
PEN	Mm	2.11	25 (30 °C)	-	15	12 % decrease of ionic conductivity in 1 M KOH 60 °C for 120 h	[100]
FEBGs	TMA	1.59	37.2 (30 °C)	67.4	52	27.2 % loss in conductivity at 70 °C in a 2 M NaOH for 120 h	[45]
FEBGs	TMA	1.23	5.3 (30 °C)	48	38	50 % loss of the ammonio groups in water 80 °C for 1000 hours	[80]
FEBG	TMA	1.93	95 (40 °C)	14	110	40 % loss of IEC In hot water at 80 °C for 500 h	[44]
PFEKS	TMA	1.80	22.3 (25 °C)	-	59	18 % loss of IEC in 1 M NaOH at 60 °C and 22 % loss of IEC in 1 M NaOH at 80 °C	[101]
PFEKS	Im	1.64	17.1 (25 °C)	-	48	17 % loss of IEC in 1 M NaOH at 60 °C and 57 % loss of IEC in 1 M NaOH at 80 °C	[101]
FPAE	TMA	2.05	43.9 (30 °C)	-	350	-	[109]
PDBBES	TMA	1.69	27 (80 °C)	-	84	-	[115]
PTPES	TMA	1.8	40 (30 °C)	-	75.6	73 % loss of ionic conductivity in 1 M KOH over 10 days	[116]
PTPES	Im	2.41	38.4 (80 °C)	-	46.8	27.7 % of conductivity in 1 M KOH solution at 60 °C for 7 days	[112]

2.44 PPO

Poly(phenylene oxide) (PPO) was used as AEM backbone due to its excellent physicochemical properties [52, 82, 117, 118]. The characteristics of PPO-based AEMs are summarised in table 2.3 and compared to other items. Expectedly, the degree of chloromethylation (DC) significantly affects the performance [67, 117, 118].

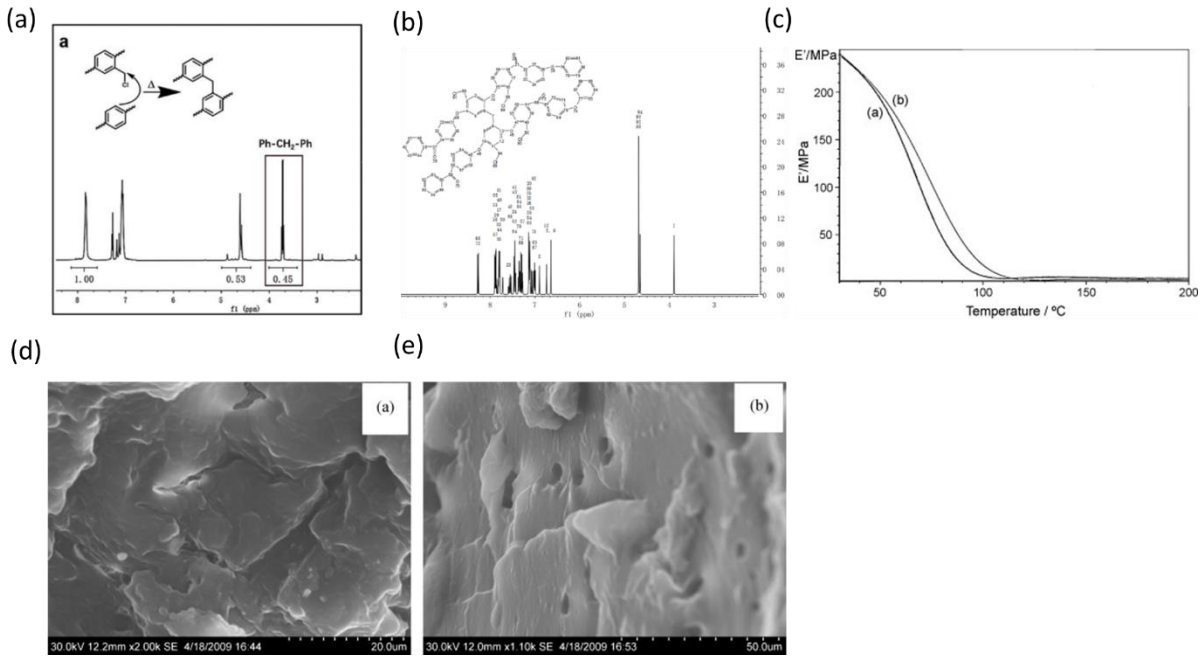

Figure 2.5 (a)1H NMR spectrum of self-crosslinked HCM-PEEK preserved for two months. (b) Simulation of self-crosslinked CMPEEK by the software MestReNova 11 (Mestrelab company). Reproduced with permission from [69] and Appendix A. Supplementary data. Copyright (2016), Elsevier. (c) Storage modulus vs temperature at 1 Hz for PSEBS and QAPSEBS. The SEM images of (d) surface and (e) cross-section of SEBS-based membrane. Reproduced with permission from [15]. Copyright (2016), Elsevier.

PPO-based composite membranes were also investigated. Manjula et al. modified PPO-AEMs with inorganic reduced quaternised graphene oxide (rQGO) by using 1-benzylimidazole (BZM) as a quaternising reagent after chloromethylatioin. The mechanical property was primarily strengthened after modification. The QPPO/rQGO composites showed a high Young's modulus of 340.5 compared with 116 MPa for unmodified AEMs. As shown in Figure 2.5(a), a new sharp signal at 3.8 ppm, attributing to the methylene-H between two benzene rings, appeared after preserving the sample at room temperature for two months. And this agrees with the simulation results, as is shown in Figure 2.5(b) [69]. The Van der Waals interaction was developed due to the high electron density of benzene rings in the polymer chains. The benzene rings of PPO possess high electron density owing to two strong electron-donating oxygen atoms and two moderate electron-donating methyl groups tethered in every single benzene ring in the PPO polymer.

Table 2.3 The main properties of the PPOs and other backbone-based membrane.

Structure	Functional group	IEC (mmol g^{-1})	σ (mS cm^{-1})	Mechanical strength (MPa)	WU (%)	Stability	Ref
PPO	TMA	0.70	4.36 (30 °C)	-	25	-	[67, 119]
QPPO/QGO	BZM	1.26	0.16	-	22	showed stable cell voltage of 0.65-0.68 V at constant current density of 0.1 A cm^{-2} at 60 °C for 10 h	[117]
PPO	TMA	2.2	3.7 (25 °C)	40.7	29	86.5 % loss of conductivity in 2 M NaOH at 80 °C for 3 days	[32]
PPO	TMA	1	12 (30 °C)	28.8	26.4	30 % loss of IEC in 1 M KOH at 60 °C for 10 days	[82]
PPO	DMH	0.9	20 (30 °C)	32.9	22.4	33 % loss of IEC in 1 M KOH at 60 °C for 10 days	[82]
PPO-PSF	TMA	3.73	2.23 (20 °C)	-	137	15 % loss of ionic conductivity in at r.t. for 250 h	[120]
PPO	TMA	1.62	7.5 (30 °C)	-	64	34 % loss of ionic conductivity and 32 % loss of IEC in 4 mol dm^{-3} KOH at 30 °C for 300 h	[121]
C12-PPO	TMA	2.11	49.2 (20 °C)	38	58.4	17.9 % of ionic conductivity in 1 M KOH at 60 °C for 500 h	[122]
PPO	QPOH	1.25	55 (20 °C)	-	-	-	[123]
PPO	TMA	1.61	76.7 (30 °C)[a]	-	26.2	-	[118]
PPO	TMA	2.2	59 (20 °C)	14	430	67 % loss of IEC in 1 M KOH at 60 °C for 500 h	[124]
PEI	TMA	1.23	44.2 (90 °C)	-		71.7 % loss of ionic conductivity in Fenton's reagent at 60 °C for 200 h	[125]
PEI	TMA	0.983	3.5 (60 °C)	-		No differences in conductivity were found after immersion in 0.5 and 1.0 M KOH at 60 or 80 °C. The membrane deteriorated at 100 °C	[126]
QPEI-HN		1.58	26.8	-	-	-	[55]
QPEI-EN		1.92	30.7	-	-	-	[55]
QPEI-MN		2.07	32.2	-	-	-	[55]
PFS-b-PS	TMA	0.58	3.67 (23 °C)	-	3.9	-	[33]
SEBS	TEA	0.578	0.69	-	-	-	[15]
PTPEDBP	Im	2.08	30.5 (80 °C)	-	-	16.9 % loss of ionic conductivity in 1.0 M KOH at 60 °C for 5 days	[127]
Parmax	Im	2.14	26.3 (80 °C)	-	20.3	11.5 % loss of conductivity in 1.0 M KOH solution at 60 °C	[128]
Parmax	QA	2.36	28.1 (80 °C)	-	28.5	28.5 % loss of conductivity in 1.0 M KOH at 60 °C	[128]
PA	TMA	2.0	138 (80 °C)	-	70	No significant decrease in 1 M KOH at 40 °C for 300 h	[41]
Terpolymers	TMA	1.46	62 (30 °C)	10	80	99 % loss of conductivity in 1 M KOH at 40 °C for 1000 h	[129]

[a]Measured in equilibrium with 0.01 M NaCl solution at 30 °C by Nyquist plot.

2.45 Other backbones

Other backbones containing aromatic structures were reported to prepare the AEM via F-Cs reaction, including polyetherimide (PEI), poly(phenylene) [89, 127, 128], and polystyrene (PS) [56], due to their high glass transition temperature, chemical resistance and thermomechanical properties over a wide range of temperatures [55, 125, 126, 130]. The characteristics of these AEM are summarised in table 2.3. As a thermoplastic polymer, PEI-based AEM possessed good thermal stability and tolerance to KOH. No significant difference in conductivity was observed after being immersed in 80 °C for 24 h. However, the conductivity was 3.5 mS cm^{-1} (60 °C) due to low IEC (0.98 mmol g^{-1}) [126]. Oh et al. prepared PEI-based AEMs and investigated the morphologies of membranes by using AFM and SAXS. They found that the nanophase-separated morphology was associated with ionic conductivity [125]. Vinodh et al. prepared a polystyrene-b-poly(ethylene-co-butylene)-b-polystyrene (SEBS)-based membrane. As is shown in Figure 2.5(c), the membrane demonstrated the typical behaviour of an amorphous polymer [15]. They also studied the microstructure via SEM, shown in Figure 2.5(d)&(e), and rough fractured surfaces were observed, which means the uniformity of the membrane. Those membranes showed poor conductivity 0.69×10^{-3} S cm^{-1}. Ono et al. prepared fluorinated ammonium terpolymer-based AEMs, composed of perfluoroalkylene, alkylene, and quaternised phenylene groups. They investigated the effect of the main chain aliphatic groups on the properties of the membrane. After immersion in 1 M KOH at 80 °C for 1000 h, the conductivity decreased from 43.0 mS cm^{-1} to 2.3 mS cm^{-1} [129].

Hu et al. prepared poly(2,3,4,5,6-pentafluorostyrene)-b-poly(styrene) (PFS-b-PS) by atom transfer radical polymerisation (ATRP) and functionalised the polymer via chloromethylation. The PFSb-QAPS(OH) membrane demonstrated low conductivity (3.69 mS cm^{-1}) due to low IEC (0.21 mmol g^{-1}) [33]. Poly(phenylene)s were also employed to prepare AEMs [89, 127, 128]. The commercial membrane, Parmax 1200, is a poly(phenylene) polymer without ether linkages. The poly(phenylene) structure provides a stiff and chemically stable backbone. The benzoyl groups can be chemically modified to improve solubility.

Polystyrene (PS) are also widely used to prepare the AEM [131]. However, without modification, the stand-alone PS cannot fabricate the AEM with good mechanical properties due to high rigidity, forming very brittle AEMs. As a result, PS-based copolymers were investigated. By employing the one-step bromoalkylation, Jeon et al. prepared polystyrene-b-poly(ethylene-co-butylene)-b-polystyrene (SEBS)-based

AEMs [36]. The tether length between the cation headgroup and the backbone is adjustable by changing the alkyl chain length. In addition, other aromatic hydrocarbons, for instance, triptycene groups [132], were employed as the AEMs.

2.5 Cell performance

2.51 The effect of the MEA

Most studies focused on the conductivity and stability of the AEMs. Despite a significant number of literature regarding AEM preparation, only less than 10 % of them conducted the cell test [133]. For validating the performance of the AEMs, the membrane is assembled in a membrane electrode assembly (MEA). Different AEMs prepared via F-C reaction were utilised to prepare the MEA, including PSU, PES, PPO, PEEK, etc. The cell performance of the AEMs is presented in table 2.4. Nearly all the AEMs are applied in fuel cells, and very little is used in water electrolysers.

Different types of AEMs with high conductivity were achieved. Nevertheless, more efforts are required for cell performance. The same as ion conductivity, TMA functionalised AEMs showed the best performance [134]. As is shown in Figure 2.6(a), the peak power density and limiting current density of AEMFC has improved significantly over the last two decades [133], with power densities of AEMFCs reaching 2.58 W cm^2 peak power density (>7.6 A cm^{-2} current density, 0.39 mg cm^{-2} Pt-Ru/C) at 80 ^oC, as is shown in Figure 2.6(b) [135, 136]. The power density of the cell is affected mainly by the AEM conductivity and electrode polarization. The advancement in power density was made by improved ionomer and the use of fragile membranes below 20 µm resulting in fast water transport mitigating anode flooding and low area-specific resistance or ohmic losses. Apart from power density, durability is also a significant challenge for AEMFC commercialisation. Most AEMFCs suffer a substantial reduction in life over the first 200 hours of the operation. It is reported that the cells can work at 67 °C 0.4 A cm^{-2} over 1000 h, as is shown in Figure 2.6(c) [137]. Several aspects need to be improved for the cell performance to outperform the incumbent technologies, including decreasing the cost and increasing durability and performance. In addition, to prepare the MEA, an ionomer is added to the catalyst ink to increase the conductivity and reduce the resistance. Typically, the AEM and ionomer can be the same materials because of the better compatibility. However, the adsorption of ionomer may also deteriorate the activity of the catalyst or even poison the catalyst due to the adsorption [66, 138]. Two specific adsorptions are occurring on the catalyst's surface, limiting the cell's performance: cation-hydroxide-water co-adsorption and phenyl group adsorption.

2.52 The effect of the CO_2

CO_2 plays multiple roles in AEMFC and AEMWE. Hydroxide ions in AEMs efficiently react with the CO_2 in the ambient air and form the more essential and less mobile bicarbonate (HCO_3^-) and carbonate (CO_3^{2-}). The conductivity suffers a significant decrease once the carbonation process is completed. Therefore, precautions should exclude CO_2 [139, 140]. Three methods are used in the literature to avoid AEM carbonation effects. The first is to use the N_2-purged water and conduct the test as soon as possible. This method needs to be completed in water. The second is to test the cell in a CO_2-free environment, such as an inert gas glovebox. The third is to apply an external electric current through the membrane to convert all the HCO_3^-/CO_3^{2-} to OH^- effectively self-purging. It is reported that the CO_2 of ambient air has a detrimental effect on the performance of AEM fuel cells. As shown in Figure 2.6(e) and (f), Ziv et al. studied the impact of the temperature and humidity on the properties of AEM in three relevant anion forms (OH^-, HCO_3^- and CO_3^{2-}). Using an ex-situ conductivity technique, they measured the transient effective conductivities of AEMs during the carbonation and de-carbonation process. An increase of 2-10 fold in conductivity is obtained using this method.

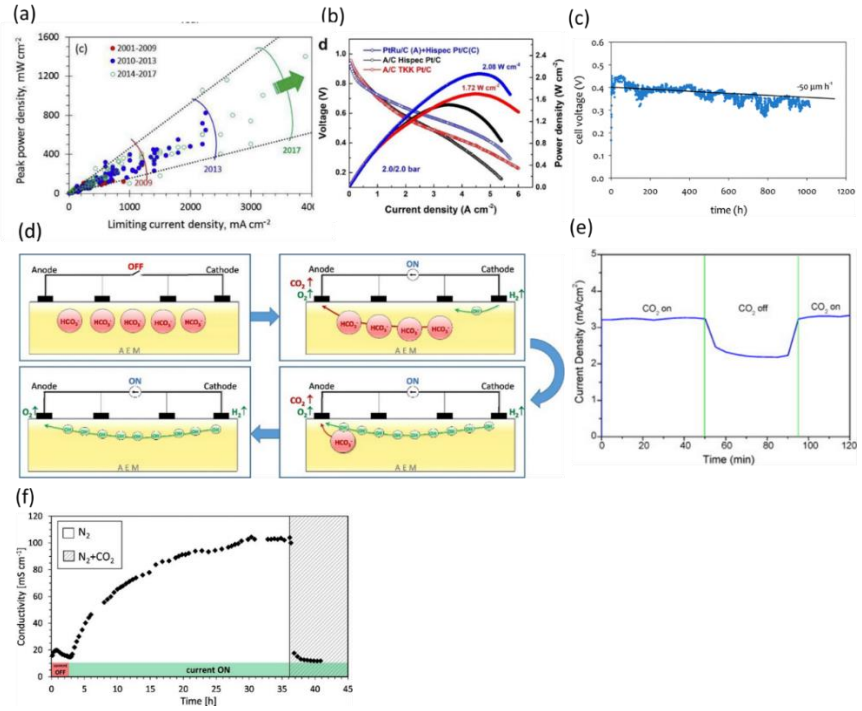

Figure 2.6 (a) Peak power density reported in the AEMFC fuel cell. Reproduced with permission from [133]. Copyright (2017), Elsevier. (b) Power density is reported in the literature. (c) Durability test at 0.4 A cm^{-2} at 67 ◦C over 1000 h. Reproduced with permission from [137]. Copyright (2020), Royal Society of Chemistry. (d) The processes in the AEM while conducting the electrochemical test. Reproduced with permission from [140]. Copyright (2018), Elsevier. (e) The effect of CO_2 on the performance of current density. Reproduced with permission from [86]. Copyright (2009), Elsevier. (f) Conductivity changes before, during and after applying 100 μA direct current. Reproduced with permission from [140]. Copyright (2018), Elsevier.

Table 2.4 the cell performance

Backbone	Functional group	Application	Catalyst	Current density (mA cm^{-2})	Power Density (mW cm^{-2}) or Cell voltage (V)	Conditions	Ref
PSU	TMA	Fuel cell	Pt/C (20 wt %), 1 $mgcm^{-2}$	12.5	4.1 mW cm^{-2}	100 % humidified at 25 °C, flow rate of 3 and 6 mL min^{-1} for O_2 and CO_2, respectively	[86]
F-PSU	TMA	Fuel cell	Anode and cathode: Pt/C, 0.45 mg cm^{-2}	310	186 mW cm^{-2}	100 % humidified at 70 °C	[83]
PES	Im	Fuel cell	Anode and cathode: Pt catalyst, 0.4 mg cm^{-2}	55	30 mW cm^{-2}	100 % humidified at 45 °C, flow rate of 50 and 100 mL min^{-1} for O_2 and CO_2, respectively	[66]
PSU	TMA/TMHDA	Fuel cell	Anode: Pt/C (40 wt %), 0.5 mg cm^{-2}. Cathode: Ag/C 2.0 mg cm^{-2}	75	30 mW cm^{-2}	100 % humidified at 60 °C	[141]
PSU	TAM/TMHDA	Fuel cell	Anode and cathode: Pt/C (40 wt%), 0.5 mg cm^{-2}	195	110 mW cm^{-2}	100 % humidified at 60 °C, flow rate of 100 and 200 mL min^{-1} for H_2 and O_2, respectively	[87]
PES	TMA	Fuel cell	Anode and cathode: Pt/C (20 wt%), 0.5 mg cm^{-2}	445	162 mW cm^{-2}	100 % humidified at 30 °C, flow rate of 50 and 100 mL min^{-1} for H_2 and O_2, respectively	[70]
PSU	DMIm	Fuel cell	Anode and cathode: Pt/C (70 wt%), 0.5 mg cm^{-2}	100	37.76 mW cm^{-2}	100 % humidified at 60 °C, flow rate of 100 mL min^{-1} for H_2 and O_2, respectively	[50]
PSU	1)TMA 2) TEA	Fuel cell	Anode and cathode: Pt/C (20 wt%), 0.5 mg cm^{-2}	-	1) 142 mW cm^{-2} 2) 300 mW cm^{-2}	100 % humidified at 60 °C, a stoichiometry of 1.5 and 2 at 1 A cm^{-2} for H_2 and O_2, respectively.	[90]
PAES	TMA	Fuel cell	-	300	148 mW cm^{-2}	60 °C, H_2 and O_2 as the fuel and oxidant	[142]
PPO	TMA	Fuel cell	Anode and cathode: Pt/C (40 wt%), 0.5 mg cm^{-2}	250	58 mW cm^{-2}	humidified at 30 °C, flow rate of 200 mL min^{-1} for H_2 and O_2, respectively	[67, 119]
PPO/QGO	BZM	Fuel cell	Anode: Pd/NG, 3 mg cm^{-2}. Cathode: Pt/C, 0.5 $mgcm^{-2}$	250-315	125 mW cm^{-2}	60 °C, methanol as the fuel	[117]
PPO	TMA	Fuel cell	Anode and cathode: Pt/C (40 wt%) catalyst 0.5 mg cm^{-2}	250	111 mW cm^{-2}	100 % humidified at 30 °C, flow rate of 200 mL min^{-1} for H_2 and O_2, respectively	[67]
PAEs	TMA	Fuel cell	Anode: NiZn, 2.6 mg cm^{-2}, Cathode: iron phenanthroline, 1.0 mg cm^{-2}	451	176 mW cm^{-2}	26 % humidified, 80 °C, a flow rate of 2 mL min^{-1} for air and 500 mL min^{-1} for hydrogen	[110]

PEEK	TMA	Fuel cell	Anode and cathode: Pt, 4 mg cm^{-2}	109.3	48.09 mW cm^{-2}	100 % humidified at 30 °C, flow rate of 50 and 100 mL min^{-1} for H_2 and O_2, respectively	[94]
PEEK	AeIm	Fuel cell	Anode and cathode: Pt, 0.5 mg cm^{-2}	260	120 mW cm^{-2}	100 % humidified at r.t., flow rate of 20 and 10 mL min^{-1} for H_2 and O_2, respectively	[98]
PEEKK	Im	Fuel cell	Anode and cathode: Pt/C (70 wt%), Pt, 0.5 mg cm^{-2}	100	46.16 mW cm^{-2}	100% humidified at 60 °C, flow rate of 500 cm^3 min^{-1} for H_2 and O_2, respectively	[96]
FBOG	TMA	Fuel cell	-	270	130 mW cm^{-2}	100 % humidified at 60 °C, flow rate of 500 cm^3 min^{-1} for H_2 and O_2, respectively	[45]
FBOG	TMA	Fuel cell	Anode and cathode: Ni powder and Co	826	297 mW cm^{-2}	100 % humidified at 80 °C.	[44]
PEPES	TMA	Fuel cell	-	250	100 mW cm^{-2}	100% humidified at 80 °C.	[116]
FPAE	TMA	Fuel cell	Anode: NiZn, 2.6 mg cm^{-2}. Anode: iron phenanthroline 1 mg cm^{-2}	1200	510 mW cm^{-2}	Anode: a mixture of 1.0 M potassium hydroxide and 5.0 wt% hydrazine aqueous solution to the anode at a flow rate of 2 mL $min^{-1,}$ Cathode: 500 mL min^{-1} for 26 % humidified oxygen or air at 80 °C	[41]
PSU	1)TMA 2)DABCD	Electrolyser	Anode: $NiCo_2O_4$, 5 mg cm^{-2}. Cathode: Ni foam	1)130 2)170	1) 2V 2) 2V	10 wt% KOH at 50 °C	[134]
PPO-PSF/ZnO	TMA	Fuel cell	Anode and cathode: Pt, 2 mg cm^{-2}	220	69 mW cm^{-2}	50 °C, methanol (2 M) and KOH (2 M) at a 1:1 ratio.	[120]
PPO	TMA	Fuel cell	Anode and cathode: Pt, 2 mg cm^{-2}	25	8.5 mW cm^{-2}	Anode: flow rate of 2 mL min^{-1} for 2 mol dm^{-3} aq. methanol cathode: flow rate of 200 mL min^{-1} oxygen at 30 °C	[121]
C12-PPO	TMA	Fuel cell	Anode and cathode: Pt/C 46.2 wt%	98	60 mW cm^{-2}	95% RH at 60 °C, flow rate of 200 mL min^{-1} and 400 cc min^{-1} for H_2 and O_2, respectively	[122]
SEBS	TMA	Fuel cell	Anode: PtRu/C, 0.5 $mgcm^{-2}$. Cathode: Pt/C, 0.6 mg cm^{-2}	900	520 mW cm^{-2}	Fully humidified at 60 °C, flow rates of 2000 and 1000 sccm for H_2 and O_2, respectively.	[36]
PPO	QPOH	Fuel cell	Anode and cathode: Pt 0.2 mg cm^{-2}	500	242 mW cm^{-2}	Fully humidified at 60 °C, flow rates of 0.2 mL min^{-1} for H_2 and O_2, respectively.	[123, 143, 144]

2.6 Discussion

2.61 Chloromethylation and crosslinking

As for chloromethylation, the exact substituted positions on aromatic rings are still controversial in the literature [74]. For instance, some literature reported the substitution for FBG to take place in fluorenyl groups. In contrast, others reported that both fluorenyl and backbone were involved, i.e., di-substitution and tetra-substitution [103, 104]. The order of substitution positions for chloromethylation on fluorenylidene needs to be studied [111]. The proper substitution range is determined by the solubility. If the degree of chloromethylation (DC) is too low, the chloromethylated polymer cannot dissolve in the solvent (NMP), preventing the following membrane preparation process. If the degree of substitution is too high, the membrane obtained is easily dissolved in water due to the high ratio of functional groups. On the premise of membrane preparation, the optimum degree of chloromethylation can be achieved by maximizing the ionic conductivity [145, 146]. A trade-off in the degree of chloromethylation is required to prepare AEM with good conductivity while retaining swelling and mechanical property AEMs with high DC become soluble in water. The proper substitution range is between degrees 33.2 to 70.6 %.

For chloromethylation reaction conditions, most studies revealed that a longer reaction time is beneficial for chloromethylation. DC is increased almost linearly with the chloromethylation time [91]. However, it is reported that time dependence is a pseudo-first-order reaction kinetics [74]. Besides, methods to calculate the degree of chloromethylation for the same polymer are inconsistent in different literature. Take PPO polymer as an example. NMR spectroscopy is used to determine the number of chloromethyl groups. The most utilised way is to compare the number of tethered chloromethyl groups over all the aryl units in the backbone, as shown in equation 2.1 [80].

$$DC = \frac{\text{-}CH_2Cl \text{ tethered}}{\text{aryl units}} \qquad (2.1)$$

Another calculation method replaces the aryl units with the unsubstituted ones. For instance, Manohar et al. calculated DC using unsubstituted ones, and the results were much higher than aryl units [118].

Crosslinking easily occurs due to the side reaction during chloromethylation and leads to solution gelation. The most widely employed method is using a solvent extraction method, named the gel fraction (GF), to measure the degree of crosslinking [35, 89]. The sample was dried in an oven overnight and then immersed in a solvent such as

NMP or chloroform. The undissolved solid was dried in the oven until no change in weight was observed [65]. Some researchers might also use boiling and reflux solvents to dissolve the sample as much as possible. The GF was calculated using the mass difference before and after immersing in the solvent, as shown in equation (2.2).

$$\text{Gel fraction (\%)} = \frac{\text{final sample weight}}{\text{initial sample weight}} \times 100 \quad (2.2)$$

Where m_1 and m_2 are the mass of dried samples before and after dissolving in the solvent.

The wide recognition is that crosslinking occurs mainly at high temperatures, as heating is necessary to trigger the crosslinking reaction [147]. However, the crosslinking phenomenon was observed at room temperature [69].

Gel formation could be avoided under appropriate control of the reaction conditions [54]. Gu et al. prepared crosslinking-free AEMs with tris(2,4,6-trimethoxyphenyl) quaternary phosphonium hydroxide (QPOH) as cationic groups by strictly controlling the reaction condition [123]. Sufficient chloromethylating reagents are required to prevent the gelation, reducing the possibility of the phenyl rings participating in the alkylation reaction. Besides, the catalyst needs to be added dropwise or injected slowly to control the reaction rate [52]. However, an appropriate crosslinking degree (CLD) improves mechanical strength, chemical resistance, and dimensional stabilities [35]. Crosslinking needs to be balanced against the decrease in IEC, affecting ionic conductivity. It is reported that CLD can be controlled by the adjusted chloromethylation time [56]. To prepare the crosslinked membrane, apart from the side reaction caused by halomethylation process, the commonly used method is to add diamine as the crosslinker in the amination process, such as TMEDA, which can improve the ionic conductivity and thermal stability simultaneously [35]. Due to the considerable steric hindrance, the crosslinked AEMs showed better dimensional stability, mechanical strength, and alkaline due to the significant steric hindrance.

Wang et al. obtained a PSU-based membrane of high DC without gelation by controlling the amount of catalyst [47]. Typically, the higher the DC, the higher the ionic conductivity. For instance, Yan et al. prepared PSU-based AEM with imidazolium as functional groups. DF of the chloromethylated PS ranges from 42 % to 132 %, and their corresponding IEC increases from 0.78 mmol g^{-1} to 2.19 mmol g^{-1}. AEMs with the highest DF shows the highest conductivity (53 mS cm^{-1} at 20 °C) [81].

Apart from crosslinking, crosslinkers can also increase the number of functional groups after the amination process by using the bi-quaternisation of the diamine, such as the

N,N,N',N'-tetramethyl-1,6-hexanediamine (TMHDA) and N,N,N',N'-tetramethylethylenediamine (TMEDA) [57, 58, 87]. Park et al. used two amination agents, TMA and TMHDA, to quaternise the chloromethylated PSU using a mixture of monoamine (TMA) and diamine (TMHDA) [148]. Wang et al. prepared the TMA-functionalised AEMs, and TMEDA was utilised as the crosslinker. The crosslinked membranes demonstrated good dimensional stability and higher ion conductivity [57]. Crosslinking is a significant side reaction in F-C reactions. The strong covalent bonds can markedly reduce the solubility and flexibility of the polymer, resulting in poor membrane processability and severe embrittlement.

2.62 Ionic conductivity and water uptake

The ionic conductivity is directly associated with IEC, hydration level and micro-morphology of the membrane [149]. Typically, higher IEC generally results in higher ionic conductivity and water uptake. The trade-off between ionic conductivity and water uptake needs to be made to ensure the excellent performance of the membrane.

A high degree of chloromethylation results in higher ion exchange capacity (IEC) and higher ionic conductivity. However, AEMs with high DC did not consistently demonstrate expected conductivity [32]. For instance, Gopi et al. prepared PPO-based AEMs with TMA as functional groups. They found the optimum DC for chloromethylated PPO ClPPO is 40 %, with a conductivity of only 4.3 mS cm^{-1} at 30 °C [67]. It is reported that the alkyl spacers between the backbone and functional group can mitigate the degradation and enhance alkaline stability. However, it is not valid for PPO. As is shown in Figure 2.5(a), the IEC of TMA-C6-PPO-based membrane with hexyl pendant chains decreased by 39 % in 1 M NaOH at 60 °C after 30 days [150].

Hydroxide ion concentration is also utilised to characterise the performance of the AEM. It is expressed by the moles of the ionic group per unit volume of water-hydrated membrane, which takes both IEC and water uptake into account. Adequate ion mobility gives information regarding the ion dissociation degree, ionic channel tortuosity and spatial proximity of neighbouring ion groups.

2.63 Chemical stability

One of the most critical challenges restricting cell durability is AEM's chemical stability, which contains alkaline and oxidative stability [151]. The chemical stability is dependent mainly on the headgroup. Different methods have been employed to evaluate the chemical stability of AEMs. The most widely utilised measure is the loss

of weight, ionic exchange capacity (IEC) or ionic conductivity after immersion in a specific solution, such as NaOH, KOH or Fenton solution [71, 152].

Alkaline stability

In OH ion electrophilic attack degradation, the degradation rate is accelerated with increasing alkali metal hydroxide concentration, immersion/reaction time and temperature. It is reported that model cationic compounds and AEMs degrade faster at lower hydration conditions as the activation energy of the nucleophilic attack of the OH^- with the cationic model molecules is decreased with fewer water molecules. In other words, OH^- is a stronger nucleophile when it is less hydrated [153]. A thermogravimetric method was also proposed to quantify the IEC decrease, in which weight changes are measured under controlled temperature and relative humidity that are close to these in a fuel cell environment [154]. Tanaka utilised the ammonio-substituted fluorenization as functional groups to increase the ion conductivity of QAEs-based membrane [80]. The ionic conductivity was up to 50 mS cm^{-1} at 30 °C. They tested the membrane's durability in water at 80 °C for 1000 h and found that the ammonia groups were partially lost, and the polymer main chains were intact. Besides, Gao combined fluorinated poly(aryl ether) (PFAE) and fluorene units [103]. The conductivity was 35 mS cm^{-1} at 60 °C. After soaking in 1 $molL^{-1}$ NaOH at 60 °C for 240 h, the ionic conductivity decreased 72.3 %.

Most of the research focuses on the alkaline stability of AEMs. The AEMs degrade quickly under the attack of nucleophilic OH^- in an alkaline environment due to the vulnerability of the functional groups. However, the pristine polymer backbone shows good stability in the same conditions.

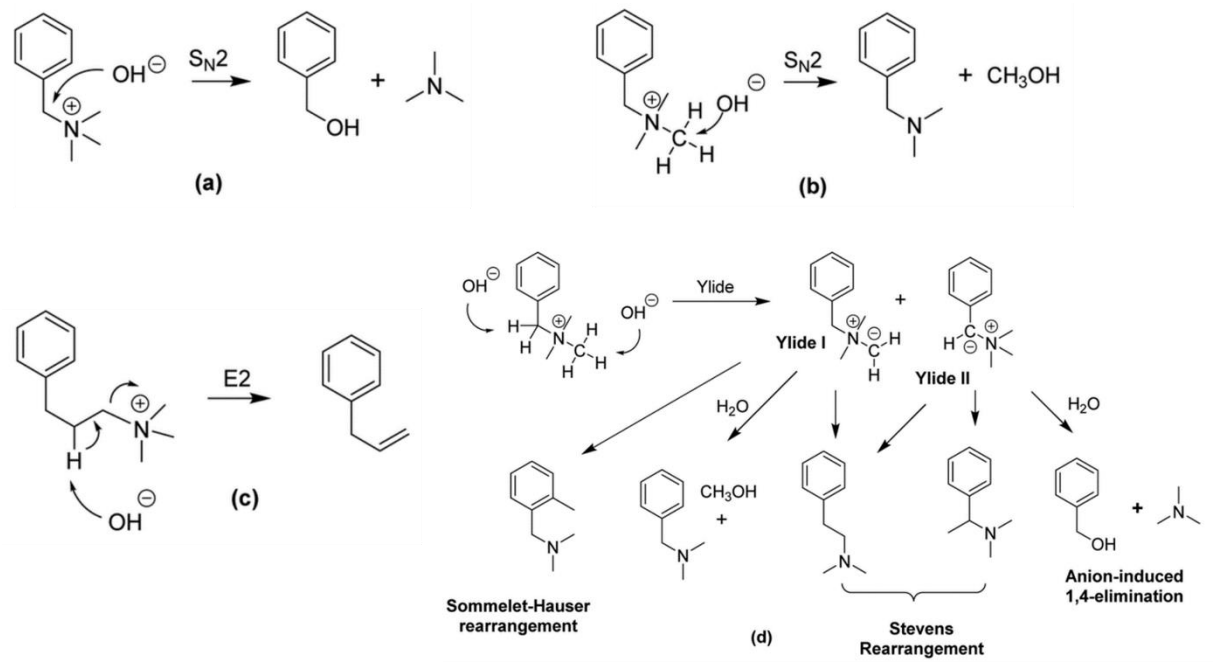

Figure 2.7 Possible degradation pathways for quaternary ammonium groups (a) S_N2 benzyl substitution (main, nucleophilic substitution), (b) S_N2 methyl substitution (minor, nucleophilic substitution), (c) β-elimination substitution (Hofmann elimination), (d) ylide-intermediated rearrangements. Reproduced with permission from [137]. Copyright (2020), Royal Society of Chemistry.

QA cations degrade under alkaline conditions due to the OH^- attack. And the decomposition rate will increase with temperature increase. For decades, different QA groups have been investigated as potential cationic groups for AEMs, and some of them demonstrated excellent alkaline stability towards hydroxide in lab-scale experiments. Several factors affect the stability, including the nucleophilic activity, basicity, and adjustability of amine groups. As is shown in figure 2.7, there are four main degradation mechanisms via hydroxide ion attack: S_N2 benzyl substitution (main, nucleophilic substitution), S_N2 methyl substitution (minor, nucleophilic substitution), β-elimination substitution (Hofmann elimination) and nucleophilic substitution, and ylide-intermediated rearrangements [40, 79, 137, 152]. Hofmann elimination is an E2 reaction in which the elimination of a tertiary amine from the neighbouring carbon quickly happens when OH^- ions attack the neighbouring β-hydrogen. Otherwise, if β-hydrogen is not present, the nucleophilic attack, specifically the S_N2 reaction, could occur on both the backbone and the functional group as OH^- is a strong nucleophile [155]. However, the proximity of available groups to OH^- usually makes them more vulnerable. For example, as is shown in Figure 2.7, in the case of benzyl trimethyl ammonium hydroxide, the nucleophilic substitution occurs not only on the α-carbon, converting the quaternary ammonium group into a tertiary amine and producing alcohol

which is the minor pathway but could also attack the benzylic carbon atom leading to the loss of a tertiary amine which is the main pathway [82, 156].

As for the ylide formation pathway, OH^- ions abstract an α-proton from the methyl group, which produces a nitrogen ylide intermediate. This intermediate is then converted to tertiary amine and water via the Stevens or Sommelet-Hauser rearrangements, determined by complicated factors such as temperature, nucleophile strength and concentration. However, it was suggested in some work that this reaction is reversible and doesn't lead to significant net degradation [20].

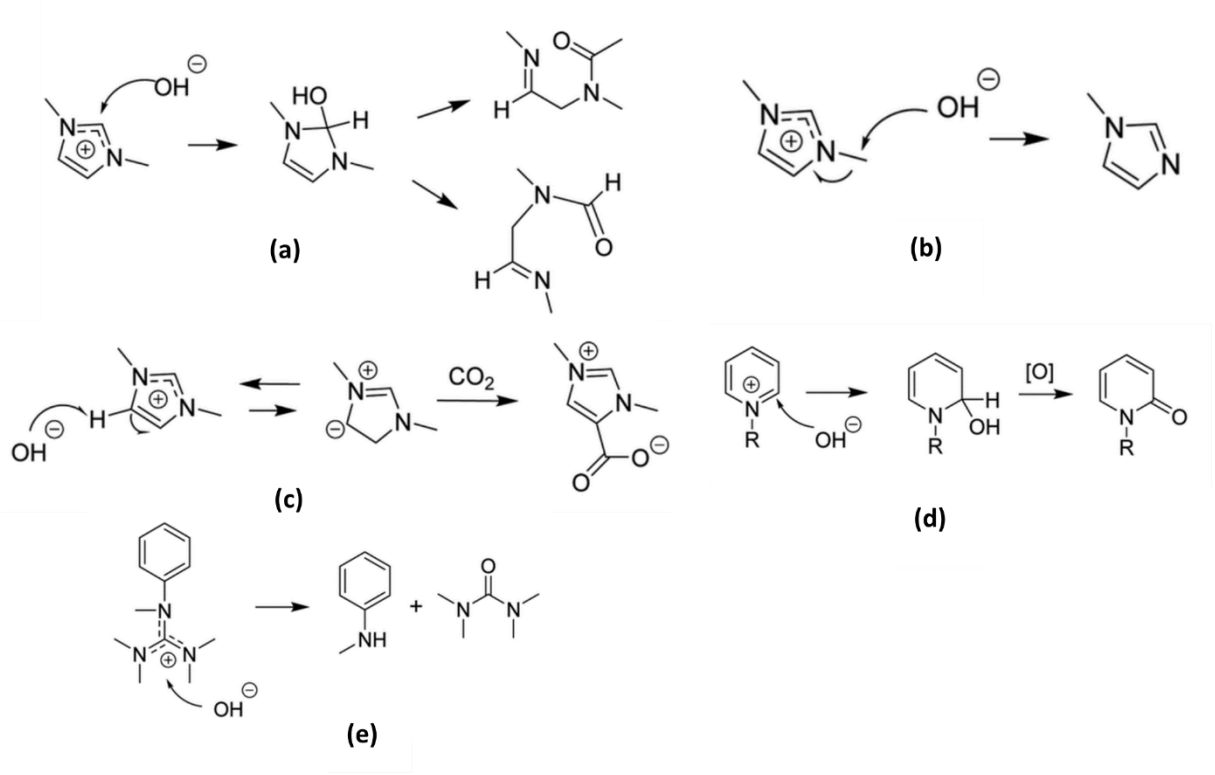

Figure 2.8 (a) ring opening (imidazolium), (b) S_N2 methyl substitution (imidazolium), (c) heterocycle deprotonation (imidazolium), (d) S_N2 and ring opening (piperidinium, pyrrolidinium and morpholinium), (e) nucleophilic degradation (guanidinium). Reproduced with permission from [137]. Copyright (2020), Royal Society of Chemistry.

Imidazolium (Im) groups are also widely investigated since the ring's structure provides Im functionalised AEM with improved chemical stability in high pH solutions compared to QA-functionalised AEMs [66, 68]. However, as is shown in Figure 2.8 (a), (b) and (c), imidazolium (Im) groups suffer ring-opening, S_N2 methyl substitution, and heterocycle deprotonation. The ring-opening reaction of Im is when an OH^- attacks the C2 position of Im, which results in the opening of the Im ring [98]. The electro-donating groups and steric hindrance are two effective methods to avoid the degradation of functional groups in anion exchange membranes [157]. In the electron donation method, the electron distribution in the functional group is stabilized by introducing

electro-donating groups, for example, C2-methyl-substitution of the imidazolium group, which protects against nucleophilic attack. In the steric hindrance method, the functional group is protected duo to the bulk structure. The alkaline stability improves when the C2 position is occupied by electron-donating groups, such as 1,2-dimethylimidazole (DmIm) [98]. Long-spacer was tethered to the imidazolium, such as 1,2-dimethylimidazole (DmIm), 1-butylimidazole (BuIm) 1-ethylimidazole (EtIm), and 1-aminoethyl-2,3-dimethylimidazolium (AeIm) [81, 98]. The long spacer was suggested to mitigate the degradation of the functional groups. However, others did not see this conclusion and is still debated [141]. Wang et al. reported that the increased length of a long alkyl affixed to the N-3 position in Im decreases the functionalised membranes' alkaline stability [158]. Besides the aliphatic substitution, benzyl substitution provides better alkaline stability due to steric hindrance, such as 1-benzyilimidazole (BZM) [117]. Apart from the QA and Im, the other cationic groups also suffered from OH^-. As is shown in Figure 2.8 (d) and (e), pyridinium suffered from nucleophilic addition and displacement, and guanidinium suffered from nucleophilic degradation [137].

The OH^- degradation reaction is reported to be mitigated in the presence of electron-donating groups or when the electron-withdrawing substituents are leaving reducing. For example, for PPO-based AEM, DMH cation, compared to the TMA cation, mitigated PPO backbone hydrolysis when exposed to alkaline media. However, this mitigation of DMH cation was not seen when using the PSU backbone due to the inherent presence of the electron-withdrawing sulfone group [82]. Besides, MOF can also improve AEMs' alkaline stability due to the interaction between the strongly polar nitrile groups, such as benzonitrile, with the side-chain functional cations, e.g., quaternary ammonium reducing their interaction with OH^-. The energy level of the unoccupied molecular orbital (LUMO) energies of benzyl imidazolium, benzyl morpholinium, benzyl imidazolium/benzonitrile, and benzyl morpholinium/benzonitrile were calculated to be −4.64, −4.40, −4.07 and −4.18 eV, respectively (Figure 2.4(e)) [100]. The benzyl morpholinium shows higher LUMO energy than benzyl imidazolium. After introducing the benzonitrile groups, the LUMO energies for both imidazolium and morpholinium increased due to the interaction between the benzonitrile and functional groups. The high energy of the LUMO means lower stabilization of transferred electrons and lower acidity. In other words, the cationic head groups become weaker Lewis acids with lower interaction with OH^- ion.

Apart from the cationic group. The backbone can also be attacked by the OH^-. The backbone suffers from possible scission triggered by cation groups via quaternary

carbon and ether hydrolysis in alkaline media [159]. The degradation mechanism of the backbone under high pH conditions is shown in Figure 2.9 [160].

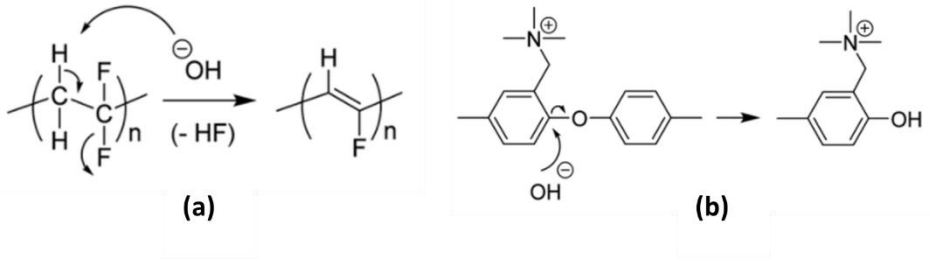

Figure 2.9 the degradation mechanism of polymer backbones (a) dehydrofluorination, (b) S_NAr aryl ether cleavage. Reproduced with permission from [160]. Copyright (2021), Royal Society of Chemistry.

The stability of the backbone is also altered and affected by the functional groups after functionalisation and depends on charge distribution in the functionalised polymer. The ether group in the backbone, such as PPO and PSF, is reported to be attacked by the OH^- after their functionalisation [137, 161].

Oxidative stability

Apart from OH^- attack, radicals like hydroxyl ($OH^{\cdot}$) and peroxyl radicals ($OOH^{\cdot}$) are formed either from electrode electrochemical reactions, e.g., at fuel cell cathode or electrolyser anode or from a chemical reaction involving oxygen or OH^- counterion and cationic head group. Their transport and the hydroxide ion causes severe and irreversible membrane degradation [22].

For the practical operation of the cell, alkaline stability is insufficient to ensure membrane durability [22]. Alkaline stability in well-hydrated AEMFC and AEMWE fed with deionised water is not directly relevant. Under such conditions, oxidative stability becomes an essential factor. Though nucleophilic degradation has a critical effect on IEC and ionic conductivity, the significant decrease in mechanical strength cannot be explained [162]. It is found that apart from the ions, free radicals, especially the reactive oxygen species (ROS), such as hydroxyl free radicals ($^{\bullet}OH$) and superoxide anion radicals ($O_2^{\bullet-}$), might be the reason for chain scission of the polymer electrolyte. They could accelerate the degradation of membrane electrolytes due to the visible changes in membrane colour and loss of mechanical properties after the stability test [163]. According to the degradation tests under different atmospheres, the degradation rate under oxygen was more than four times faster than under nitrogen, implying that oxygen might be essential in accelerating the degradation process. By analysing chemicals and identifying the degradation products, Espiritu and co-workers [5] reported that the membrane degraded because of the loss of the functional groups and

the removal of the benzene ring that connected functional groups and backbones. They also found that the degradation of the membrane has a close relationship with the oxidant concentration. Besides, Parrondo and co-workers found that the degradation rate was much faster when molecular oxygen was present by using 5-diisopropoxyphosphoryl-5-methyl-1-pyrroline-N-oxide (DIPPMPO) as a spin-trap and ^{31}P NMR spectroscope to detect the free radicals [7]. These findings illustrate the importance of the oxidative stability of AEMs. It is much more meaningful for AEMs to improve oxidation resistance. The formation of hydroxyl ($^{\cdot}OH$) and superoxide anion radicals ($^{\cdot}O^{2-}$) is shown in Figure 2.10 [156]. There are three main steps. Step 1, in alkaline conditions, carbanions are generated by deprotonation. Step 2, the carbanion reduces dioxygen to produce the superoxide anion radical and an organic free radical. Step 3, the hydroxide ion transfers an electron to the organic free radical, regenerating the carbanion and producing the highly reactive hydroxyl free radical. At high pHs, the hydroperoxyl radical ($^{\cdot}HO_2$, pK_a of 4.8.) will be deprotonated to $^{\cdot}O^{2-}$.

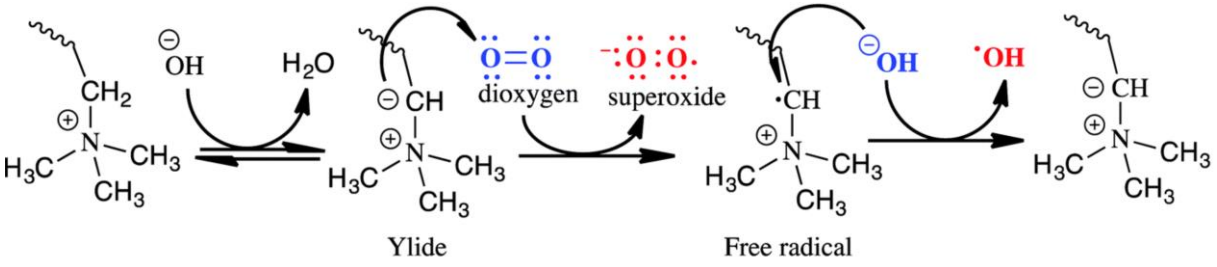

Figure 2.10 The mechanism for generating reactive oxygen species by one-electron reduction of dioxygen under alkaline conditions. Reproduced with permission from [156]. Copyright (2016), Royal Society of Chemistry.

To evaluate oxidative stability, the most widely utilised method is to measure the weight loss, ionic exchange capacity (IEC) loss, or ionic conductivity decreased after immersion in oxygenated DI water for long periods or in Fenton's solution (3 wt% H_2O_2 added 2 ppm $FeSO_4$) in short periods [75, 79].reduction of OH^- lead to the formation of oxidising solid, $^{\cdot}OH$ and $^{\cdot}OOH$ radicals/H_2O_2 [94, 164]. Moreover, oxygen can be reduced to produce superoxide ions. The reduction of OH^- and oxygen can be the catalyst by the head group ylide and the catalyst in the presence of an electrocatalyst. In oxygen, OH and $O_2^{\bullet-}$ were detected during AEMs oxidative stability tests [156, 165]. Quaternary ammonium radicals are generated when the oxygen molecules capture the electron of the ylides. The quaternary ammonium radicals degrade into ethylene and tertiary amines [152, 165]. Wierzbicki et al. detected and identified the radical during and after long-term AEMFC operation using electron paramagnetic resonance (EPR)

spectroscopy [162, 166]. Four types of AEMs were investigated, including hydrocarbon backbone membrane with quaternary ammonium groups, Tokuyama A201; radiation grafted membrane containing covalently bonded benzyltrimethylammonium head-groups fabricated low-density polyethylene (LDPE), membrane composed of 2,2″,4,4″,6,6″-hexamethylpterphenylene, and N-methylated poly(benzimidazolium)s, denoted PMBI, and commercial FAA-3-PK-130 membrane, marked FAA3. The primary detected adducts during the operation of the micro-AEMFC are DMPO-OOH and DMPO-OH on the cathode side and DMPO-H on the anode side.

Free radical scavengers, such as ceria and sulfide groups, can be introduced into the membrane structure to increase oxidative stability. They were effective in PEM sister technology, e.g., in PEMFC. For instance, Bu et al. prepared 1,2,4-Triazole functionalized poly(arylene ether ketone) (PAEK)-based PEM with enhanced oxidative stability. The membranes with the sulfide group exhibited excellent oxidative resistance and retained their shapes for more than 50 h in Fenton's solution [167]. In AEM, these strategies are yet to be tested. The addition of the phenolic group in solution improves AEM oxidative stability; however, these groups are not regenerated and will provide limited protection as sacrificial attack sites [165]. Arylimidazolium was stable for 10,000 h in 3 M KOH but had poor conductivity and electrolyser performance even when using high concentration KOH [168].

2.64 Mechanical property

AEMs may suffer the forces under vibrating and pressure conditions in the operation process [169]. Thus, the mechanical properties of AEMs also have a critical effect on cell durability. The mechanical failure of AEM results in catastrophic performance loss. For AEM, mechanical failure originates from three aspects. The first one is related to the degradation of the backbone. As discussed in section 2.63, some polymer backbone degradation can be attacked by the OH^- under high alkaline conditions. The mechanical strength was decreased because of the cleavage of the backbone. Besides, the water uptake also affects the mechanical strength. High water uptake (or high IEC, ionic conductivity) may cause a high swelling ratio and poor dimension stability, resulting in poor mechanical strength. For instance, the higher degree of grafting (DOG) of LDPE-based AEM, the lower the membrane's ultimate tensile strength [170]. The trade-off between ionic conductivity (or IEC) and water uptake must be made. Furthermore, long-term operation and elevated working temperature may cause the membrane to creep as continuous compaction works on the hydrated AEM [15].

2.7 Overview

There are several approaches to improving the stability of AEMs. This can be divided into OH^- ion, oxidative, and mechanical stability. It is reported that the alkyl spacers can be used to improve water uptake and alkaline stability. However, the effects of the alkyl spacers on AEMs conductivity and stability are still debated. There is a correlation between the various properties of the membrane. For example, ionic conductivity and water uptake are positive correlations. High ionic conductivity shows a high attraction to water molecules resulting in increased water uptake. In turn, the increased water uptake is beneficial for ionic conductivity. However, two high water uptake AEM may cause poor dimensional stability and delamination in the catalyst layer. Thus, a trade-off between the swelling ratio and ionic conductivity needs to be made. Multiblock copolymer membranes offer an excellent option to tune AEM properties producing well-defined aggregate structures and hydrophobic/hydrophilic phase segregation [104, 106].

Another promising approach is reinforcing AEMs using a porous substrate such as porous membranes or fibres. The porous substrate can either be inert, e.g., PTFE, or contains charged groups providing ionic crosslinking with pore filed AEM. The composite membrane approach significantly increased mechanical strength with moderate sacrifice in ionic conductivity [89, 171-173].

Functional groups play a significant role in membrane chemical stability. Several strategies are used to improve the alkaline stability of the head group, including a spacer between the head group and backbone, bulkier head group, and adjacent electron-donating groups to reduce the acidity of quaternised head group and its vulnerability to nucleophilic attack. While these strategies were shown to be effective in some instances depending on the backbone and head group used, they moistly come at the cost of reduced ionic conductivity. For example, inserting a long space chain between functional groups and the polymer main chain may improve the stability of the membranes [66, 98]. For instance, alkyl imidazolium was more stable than benzyl imidazolium. Introducing the long space chain could effectively reduce the S_N2 nucleophilic substitution attack of OH^- to the functional group by stabilizing the transition state of the attack reaction, which enhanced the alkaline stability of the anion exchange membrane [98, 174]. However, this wasn't observed when used in other AEM backbones, such as PPO [98].

In addition, dense functional groups may have better conductivity than loose ones. The di-quaternised membrane shows a bigger scattering for ionic clusters than the mono-

quaternised membrane [99]. Increasing the steric hindrance can also protect the functional groups. For instance, incorporating adjacent bulky groups near the reactive C2 position of the benzimidazolium group can hinder nucleophilic attack by OH^- because of steric crowding [71, 175]. Furthermore, the membrane contains the quaternary ammonium groups on the side chain rather than the main chain, decreasing the aromatic backbone's steric hindrance and promoting phase separation [70]. However, this may reduce the ionic conductivity accordingly.

In terms of chemical stability, it is essential to avoid vulnerable bonds in the backbone structure, e.g., towards nucleophilic or radical attacks. Perfluorinated polymers are known for their excellent chemical stability. However, there is a drive to reduce their use due to environmental and cost concerns. Backbones rich in aromatic structures, such as poly(phenylene) (PPP) and PPO, has been attracting attention due to their good oxidative stability and lower cost [176]. However, it should be stressed that upon functionalisation, the chemical stability of the backbone can be altered, e.g., as seen in PPO vulnerability towards OH^- ion attacks after functionalisation. In our area of interest of water electrolysers using AEM, oxidative stability is a critical factor in stability when deionised water feed or low-concentration KOH is used. This is because nucleophilic attacks become negligible when AEM is fully hydrated due to a low concentration of accessible OH^-. When selecting the AEM backbone for AEMWE, benzylic hydrogen and C=O containing AEMs should be avoided due to their high vulnerability towards reactive oxygen radical attacks. PPO is a good candidate to investigate AEMWE due to its good solubility in solvents for functionalisation and good oxidative stability. PPP is also a promising candidate. However, limited solubility in common solvents makes its functionalisation more difficult.

The more intensive the ion aggregation, the more distinct the phase separation [142]. The synergism of the dense function groups per segment with the size effect of the phase blocks largely determines the properties of the resulting polymers [106]. The hydrophilic features enhanced hydroxide ion mobility and provided wide ion transport channels due to the strong-field effects of the sense functional clusters. In contrast, the hydrophobic segments, such as fluorinated hydrophobic moiety [83], decreased the possibility of hydroxide attack and improved the stability of the backbone [50, 53].

Chapter 3. Research Aim and Objectives

3.1 Aim

This project aims to investigate the stability and viability of polyphenylene oxide (PPO)-based polymer as AEM for AEMWE applications with target ionic conductivity >6×10^{-2} S cm^{-1} at 50 °C.

3.2 Objectives

- AEMs-based on PPO, PPO/PTFE will be synthesised, fabricated, and characterised.
- Evaluate the thermal and oxidative stability.
- Identify degradation by-products and mechanisms
- Electrolyser tests with the most promising materials. The membranes with the best comprehensive performances will be prepared for membrane electrode assembly (MEA), and their single water electrolyser properties will be tested.

Chapter 4. General methodology and techniques

4.1 Materials

Poly(2,6-dimethyl-1,4-phenylene oxide) (PPO, product number 181781, white powder), *N*-methyl-2-pyrrolidinone (NMP), 1, 3, 5-trioxane, chlorotrimethylsilane (TMCS), $SnCl_4$ (product number 208930), chloroform, trimethylamine (TMA, in 45 % solution in H_2O), potassium hydroxide, methanol, sulphuric acid and sodium chloride were purchased from Sigma-Aldrich and used without further purification. PTFE (LOT No. 00624440, pore size 0.5 μm) was purchased from Toyo Roshi Kaisha, Ltd, Japan.

4.2 The preparation of the PPO-based membrane

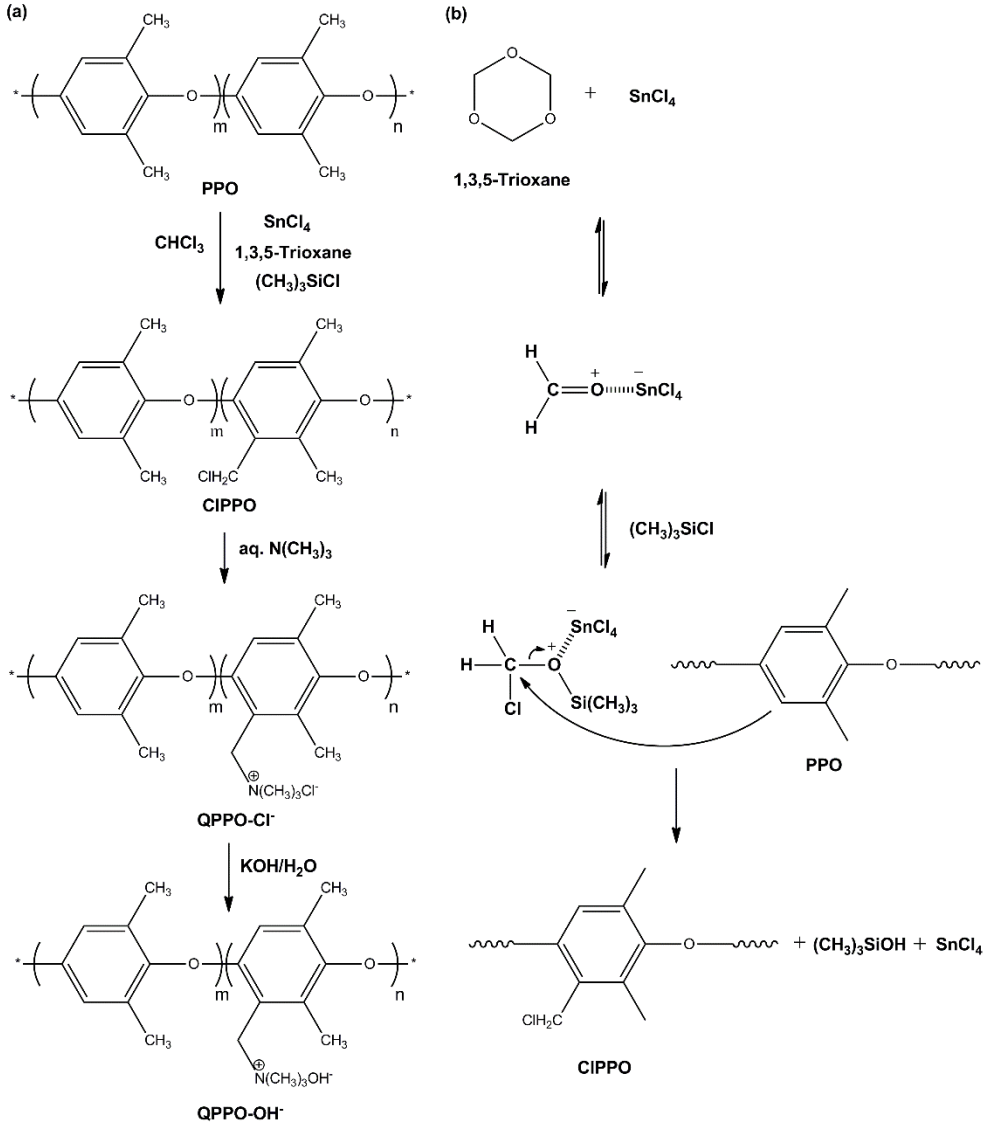

Figure 4.1 (a) Synthetic route for PPO-based AEM. (b) Mechanism of chloromethylation of PPO.

As is shown in Figure 4.1(a), the AEM was obtained through sequential chloromethylation, quaternisation and ion exchange steps. The mechanism of

chloromethylation is shown in Figure 4.1(b) [177, 178]. 1,3,5-trioxane undergoes a tautomeric process to form formaldehyde, with protonation occurring in the presence of $SnCl_4$. Then, the intermediate with chlorotrimethylsilane and phenyl rings react. For example, unless otherwise specified, PPO (4.0 g) and chloroform (250 ml) were added into a three-neck round bottom flask fitted with a reflux condenser under continuous nitrogen purging. After complete dissolution, 1,3,5-trioxane (1.7 g) and chlorotrimethylsilane (7.2 ml) were added. The $SnCl_4$ catalyst (0.8 ml) was injected slowly into the flask with a syringe. The mixture was then stirred for 10 h at 35 °C. After precipitation, the chloromethylated PPO (ClPPO) was obtained precipitation in a methanol/water mixture (150 ml/ 150 ml). ClPPO was purified by re-dissolution in chloroform, precipitated by methanol, and dried overnight under a vacuum (60 °C).

The process of quaternisation was done both in homogenous and heterogeneous methods. The polymer solution was prepared for the homogenous method by dissolving ClPPO (120 mg) in NMP (4 ml). Quaternisation was performed by adding an appropriate amount of trimethylamine solution (45 wt% in water) into the mixture. The solution was agitated and left still for 24 h at room temperature. The membranes were formed by casting the yellow transparent polymer solution onto a flat glass plate at 70 °C for 3 days. After the solvent evaporated, the films were obtained and could be easily removed from the glass surface by immersing the glass in deionised water. The quaternised PPO membranes were obtained in chloride form (Q-PPO-Cl^-). To convert the (Cl^-) counter ion to hydroxide (OH^-), membranes were immersed into 1 M KOH solution for 1 h whilst changing the KOH solution every 20 min. The membrane films were washed with deionised water several times to remove the excess KOH. Finally, the Q-PPO-OH^- was obtained (150~170 μm). For the heterogeneous quaternisation, the ClPPO was dissolved in $CHCl_3$ and cast into the membrane first. After being dried in an oven at 70 °C overnight, the membrane obtained was immersed in TMA solution for 24 h and washed thoroughly with deionised water [145, 179]. Several factors affect the kinetics of the heterogeneous amination process. The quaternisation time varies according to reaction conditions, including the polymer type, TMA concentration and temperature [180, 181].

4.3 The preparation of the PPO/PTFE composite membrane

0.5 g chloromethylated PPO (ClPPO) was dissolved in 4 ml THF to prepare the ClPPO solution. And then, the porous white PTFE membrane was immersed into a beaker

containing ClPPO /THE solution. The mixture was sonicated for two minutes until the solution thoroughly impregnated the PTFE pores and the PTFE membrane became transparent/wet. Then the impregnated PTFE membrane was moved out from the beaker and kept in the air to dry. After the solvent evaporation, the ClPPO/PTFE composite membrane was obtained. The difference in mass between pristine PTFE and dried ClPPO/PTFE membranes is the mass of the ClPPO in the newly prepared composite membrane.

4.4 Fourier-transform infrared spectroscopy (FTIR) and nuclear magnetic resonance (NMR)

FTIR and NMR were used to characterise the structure of the polymer. A Varian 800 FT-IR in Attenuated Total Reflectance (ATR) mode was used to verify the successful introduction of functional groups. FTIR analysed samples of PPO, ClPPO and QPPO. ^{1}H NMR spectra of PPO and ClPPO were recorded on a Bruker Av-400-WB instrument using $CDCl_3$ as solvent [67].

4.5 Scanning electron microscope (SEM) analysis

The scanning electron microscope (SEM) was employed to analyse the surface morphology of the substance. A focused beam of electrons was shot from the SEM and interacted with specimen atoms. Secondary electrons were collected, producing SEM images that contain lots of information about the sample, such as the surface topography and composition. SEM analysis of the pure PTFE and PPO/PTFE composite was performed using a JEOL JSM-5300LV machine.

4.6 Ion exchange capacity (IEC), water uptake (WU), swelling ratio (SR) and hydration number

Ion exchange capacity (IEC) was calculated by measuring the OH^- ions concentration in NaCl solution exchanged from the membrane with acid-base titration using Methyl red as the indicator. Before titration, the membrane in hydroxide form was immersed in a known volume of 1 M NaCl solution for 24 h to liberate the hydroxide ions. Then, 10 ml of the solution was titrated with a known concentration of H_2SO_4 solution until colour change was observed. The measurement was repeated 3 times to get an average. The membrane was then washed thoroughly with deionised water (DI) to remove the excess salt on the surface of the membrane. Finally, the membrane was dried in the oven overnight at 60 °C and weighed. The IEC was calculated using the

amount of OH^- in millimoles divided by dry membrane weight in grams, shown in equation 4.1.

$$IEC = \frac{2 \times V_{H_2SO_4} \times C_{H_2SO_4}}{W_{dry}} \quad (4.1)$$

Where the $V_{H_2SO_4}$ is the volume of H_2SO_4 solution consumed in the titration, $C_{H_2SO_4}$ is the concentration of H_2SO_4 solution and W_{dry} is the weight of the dry membrane.

Water uptake (WU), swelling ratio (SR) and hydration number (λ) were measured by calculating the change of membrane weight and dimension before and after hydration, respectively. The OH^- form membrane was soaked in deionised water for 48 h at room temperature. Then, the surface of the wet membrane was wiped with tissue paper to remove the water on the surface and weighed immediately. The hydrated membrane was dried in the oven at 60 °C overnight. For the calculation of WU, equation 4.2 was used.

$$WU = \frac{W_{wet} - W_{dry}}{W_{dry}} \times 100\% \quad (4.2)$$

Where W_{wet} and W_{dry} were the weight of wet and dry membranes, respectively.

SR was measured as the average swelling in width, length, and thickness of the membrane before and after drying. This was measured by using equation 4.3.

$$SR = \frac{D_{wet} - D_{dry}}{D_{dry}} \times 100\% \quad (4.3)$$

Where D_{wet} is the studied dimension of the wet membrane, such as width, length, or thickness, and D_{dry} is the corresponding dimension after the membrane was dried.

The hydration number is the number of water molecules per counterion in the membrane [182], and it was calculated using equation 4.4.

$$\lambda = \frac{m_{H_2O}}{M_{H_2O} \times IEC} \times 1000 \quad (4.4)$$

Where λ is the hydration number, m_{H_2O} is water uptake (m_{H_2O} = weight of wet film – the weight of dry film). M_{H_2O} is the molecular weight of water (g mol^{-1}) [183].

4.7 Thermal stability

The thermal stability of the PPO-based samples was measured by thermogravimetric analysis (TGA) and differential scanning calorimetric (DSC). TGA was performed on a Perkin Elmer, TGA 4000 instrument. The sample was heated from 50 °C to 650 °C with a heating rate of 10 °C min^{-1} under a nitrogen atmosphere. DSC was investigated under a nitrogen atmosphere using TA Instruments, Q20. The sample was heated

from 50 °C to 350 °C in an open alumina pan with a heating speed of 10 °C min^{-1} under a nitrogen atmosphere.

4.8 Mechanical properties

Tensile testing of QPPO was performed using a Model-Tinius Olsen H25KS to obtain the stress-strain plot with a constant crosshead velocity of 2 mm min^{-1} for all the tests.

4.9 Dynamic gravimetric vapour sorption (DVS)

Dynamic gravimetric vapour sorption (DVS) can determine materials' vapour sorption isotherms. Hidden Isochena (Advancing sorption analysis) was used for those studies to measure the weight change as the function of time at target relative humidity. An ultromicrobalance is used to measure the uptake and loss of vapour gravimetrically. The instrument with high mass resolution and baseline stability can identify the adsorption and desorption of tiny amounts of probe molecules. PPO and PPO/PTFE-based membranes were tested. The dry membranes' weight was 17.12 mg and 14.12 mg, respectively.

4.10 Ionic conductivity and activation energy

The membrane through-plane conductivity was measured using an in-house test cell with an electrode area of 1.77 cm^2. To avoid direct reaction with the CO_2 in the air, the membrane was submerged in deionised water while loaded in conductivity cell and tested under an N_2 atmosphere. The membrane was sandwiched between two gas diffusion layer carbon electrodes in the cell with 100 % relative humidity and elevated temperature, verified by temperature and humidity sensors, respectively. The ionic conductivity was calculated by using equation 4.5.

$$\sigma = \frac{4L}{R(\pi d^2)} \quad (4.5)$$

Where σ is the hydroxide ionic conductivity, L is the membrane thickness, R is the resistance derived from the impedance value at a zero-phase angle, and d is the diameter of the actual testing area. The impedance was measured using the same procedure previously reported [152].

The activation energy (Ea) of ion transport is consistent with the energy barrier of anion diffusion [184]. Ea can be determined with the Arrhenium relationship between conductivity and temperature. Equation 4.6 is as follows.

$$Ea = -b \times R_g \quad (4.6)$$

Where b is the slope of linear regression of $\ln\sigma$ versus 1000/T, and R_g is the gas constant.

4.11 Alkaline stability

The alkaline stability of the membrane was measured by immersing the membrane in 1 M KOH solution at room temperature and 60 °C for 500 h. Then, the IEC and weight loss were calculated-based on the data before and after alkaline treatment.

4.12 Oxidative stability

Oxidative stability of the membrane was measured by immersing the membrane in N_2-saturated DI water at room temperature and 60 °C for 10 months. Then, the weight and IEC of the membrane were analysed after treatment. Also, the membrane was immersed in Fenton's solution (3 wt% H_2O_2 added 2 ppm $FeSO_4$) at 60 °C for 24 h. The IEC and weight loss change were calculated on the data before and after treatment.

4.13 Electrochemical measurements

The electrochemical performance of the membrane and the ionomer were tested in electrolyser cells by preparing a membrane electrolyte assembly (MEA) using Pt/C catalyst at the cathode (0.4 mg cm^{-2}) and $NiCo_2O_4$ at the anode (2 mg cm^{-2}) [177]. At the anode side, titanium fibre felt GDL with a thickness of 0.3 mm and 78 % porosity (Bekaert Toko metal fibre Co., Ltd.) was used for the oxygen evolution reaction. The anode catalyst ink, consisting of $NiCo_2O_4$, 28 wt% ionomer and N-Methylpiperidine solvent, was sprayed on the Titanium GDL directly. As for the hydrogen evolution reaction, the electrode was used for non-wet proofed carbon GDL with MPL (product code H2315 C9, Freudenberg Germany). The catalyst at the cathode was 20 % Pt/ C, 28 wt% ionomers and isopropanol. PPO membrane and ionomers synthesised in the current study were compared against bench-mark LDPE-based AEM and SEBS ionomers reported previously [170, 177]. Besides, the PPO/PTFE composite membrane was also tested for electrochemical performance with PPO as the ionomer. The electrochemical measurement, including cyclic voltammetry (CV), electrochemical impedance spectroscopy (EIS) and potentiostatic durability test, were made using the Autolab potentiostats instrument (PGSTAT302 N). The experiments were operated by circulating 0.1 M NaOH to both the anode and cathode. CV was studied by cycling between 1.3 to 2 V at a scan rate of 1 mV s^{-1}. EIS was measured at 1.7 V at 40 °C. For the durability test of the electrolyser, the voltage was set to 1.7 V at 40 °C.

Chapter 5. Preparation and characterisation of PPO-based membrane

Poly(2,6-dimethyl-1,4-Phenylene Oxide) (PPO) is considered a good membrane candidate due to its excellent physicochemical properties, such as high glass transition temperature (Tg), excellent mechanical strength and good chemical stability [185-188]. PPO-based AEMs are usually prepared in three steps: chloromethylation (or bromination), quaternisation and hydroxide ion exchange [189]. Among those steps, chloromethylation is crucial as it enables further PPO functionalization, which determines the functional groups of the polymer and influences the anion conductivity. To chloromethylate PPO, the Friedel-Crafts reaction plays a significant role. The conventional methods usually use $ZnCl_2$ or $AlCl_3$ as the Lewis acids catalyst and carcinogenic chemicals as chloromethylating reagents [120], such as chloromethyl methyl ether (CMME) or bis-chloromethylether (BCME). Greener and more efficient chloromethylation methods have been researched, for example, by using $SnCl_4$ as catalyst and paraformaldehyde ($(HCHO)_n$) and chlorotrimethylsilane (TMCS) as chloromethylating reagents to replace the carcinogenic ones. Those new methods present an eco-friendly and simplified synthetic route for chloromethylation. Several studies employed this new method to chloromethylate the PPO. However, the ionic conductivity was too low for the cell operation [13] even under the high degree of chloromethylation [32, 67, 118, 121], which raised the need to investigate the process of chloromethylation further. Arges and co-workers [82] prepared PPO-based AEMs using SnCl4 as the catalyst. The ionic conductivity of the membrane in hydroxide form they obtained was 13 mS cm^{-1} at 30 °C with 13 % for the degree of chloromethylation (DC). Becerra-Arciniegas and co-workers prepared a PPO-based membrane with grafted trimethylammonium groups, and the ionic conductivity in hydroxide form was 5.9 mS cm^{-1} at 60 °C with 54 % for DC. In addition to the low ionic conductivity, gelation was observed during the membrane preparation process, and the solvent extraction method was used to calculate the degree of gelation [67]. However, this method lacks high accuracy and has limited application, only suitable when the gel content is high enough to detect. We and others prepared cholоromethylated polystyrene-b-poly (ethylene/ butylene)-b-polystyrene (SEBS) by using 1,3,5-trioxane to replace paraformaldehyde in the presence of $SnCl_4$ as catalyst [177, 190].

Given the research gap and previous studies, PPO-based AEMs and ionomer were prepared via Friedel-Crafts reactions using $SnCl_4$ as catalyst and 1,3,5-trioxane and chlorotrimethylsilane as chloromethylating reagents. Compared with other head groups, for instance, the imidazolium cation, benzyl ammonium provides relatively high ionic conductivity, acceptable stability and a good environment (low adsorption on the catalyst) [138]. For the performance of anion exchange membrane fuel cell, trimethylammonium (TMA) cation showed the highest power density than 1,2-dimethylimidazolium (DMIm) and N-methylpiperidinium (Pip) cations [191]. Thus, benzyl ammonium is supposed to meet the requirement. The membrane is expected to be applied in a water electrolyser when the working condition is close to a pH-neutral environment [152]. In addition, the steric hindrance of the crosslinking structure is expected to protect the benzyl ammonium group to some extent [138]. As a result, TMA was chosen as the cation. A variety of characterisation techniques were used to measure ionic conductivity and thermal, mechanical, and alkaline stabilities. The overlooked cross-linking side reaction was studied and explained. New and more accurate calculation methods for DC and cross-linking degree (CLD) were proposed. Finally, in comparison with our previously studied membrane (low-density polyethylene, LDPE) [152] and ionomer (SEBS) [177], electrochemical testing with QPPO as both membrane and ionomer was done in electrolysis.

5.1 FTIR spectroscopy

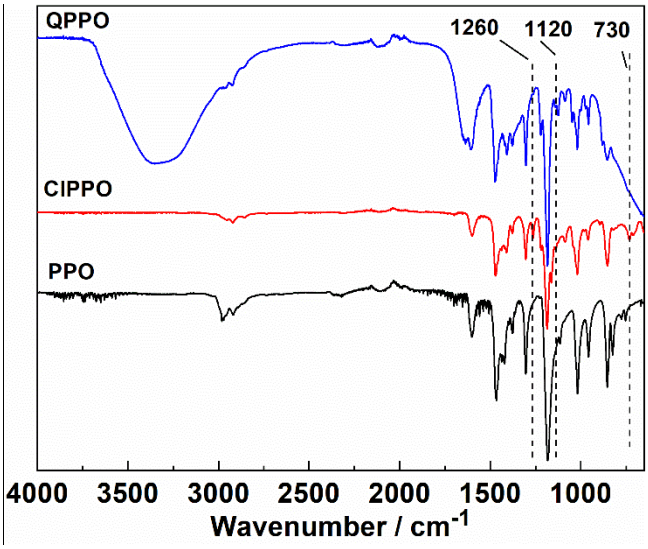

Figure 5.1 FTIR spectroscopic comparison of Q-PPO, ClPPO and PPO.

Figure 5.1 shows the FTIR spectra of pristine PPO, ClPPO, and Q-PPO collected in the ATR mode. The signals at 1600 cm^{-1} and 1189 cm^{-1} were assigned to C=C bonds

stretching in aromatic rings and C-O-C stretching, respectively, and the polymer backbone [192]. After chloromethylation, new peaks at 1260 cm^{-1} and 730 cm^{-1} were observed, which are assigned to the C-Cl bonds [145], confirming the successful chloromethylation of the polymer. The broad bands at 3380 cm^{-1} were assigned to the stretching vibration of O-H bands in water. Furthermore, a new peak at 1120 cm^{-1} observed after quaternisation were assigned to the C-N vibration [120], indicating the successful introduction of the quaternary ammonium group [145].

5.2 Degree of substitution and crosslinking

5.21 ^{1}H and ^{13}C NMR spectroscopy

^{1}H and ^{13}C NMR spectroscopy were used to confirm the structure of ClPPO and calculate the degree of chloromethylation. Figure 5.2(a) shows the ^{1}H NMR spectra of pristine PPO (bottom), partially chloromethylated PPO (middle) and fully chloromethylated PPO (top). Taking partially chloromethylated PPO as an example, additional signals in the spectra compared to pristine PPO can be seen. The signal at δ = 6.5 ppm corresponds to the aryl proton of PPO (labelled as a). Due to the electrophilic substitution, some aryl protons are shifted to δ = 6.1 ppm (labelled as d). The signal at δ = 5 ppm was assigned to the chloromethyl group (labelled as c), confirming the chloromethylation. Owing to the deactivating effect of the chloromethyl group, mono-chloromethyl substituted aromatic compounds are obtained [32, 122, 193]. The signal at δ = 2.0 ppm was assigned to the methyl groups. Due to changes in its chemical environment and the effect of surrounding protons, the chemical shift, and multiplicities of ClPPO were different from those of pristine PPO. To make it clearer in the following explanation, protons in the methyl groups were labelled as b, b'& b'' (Figure 5.2(a)).

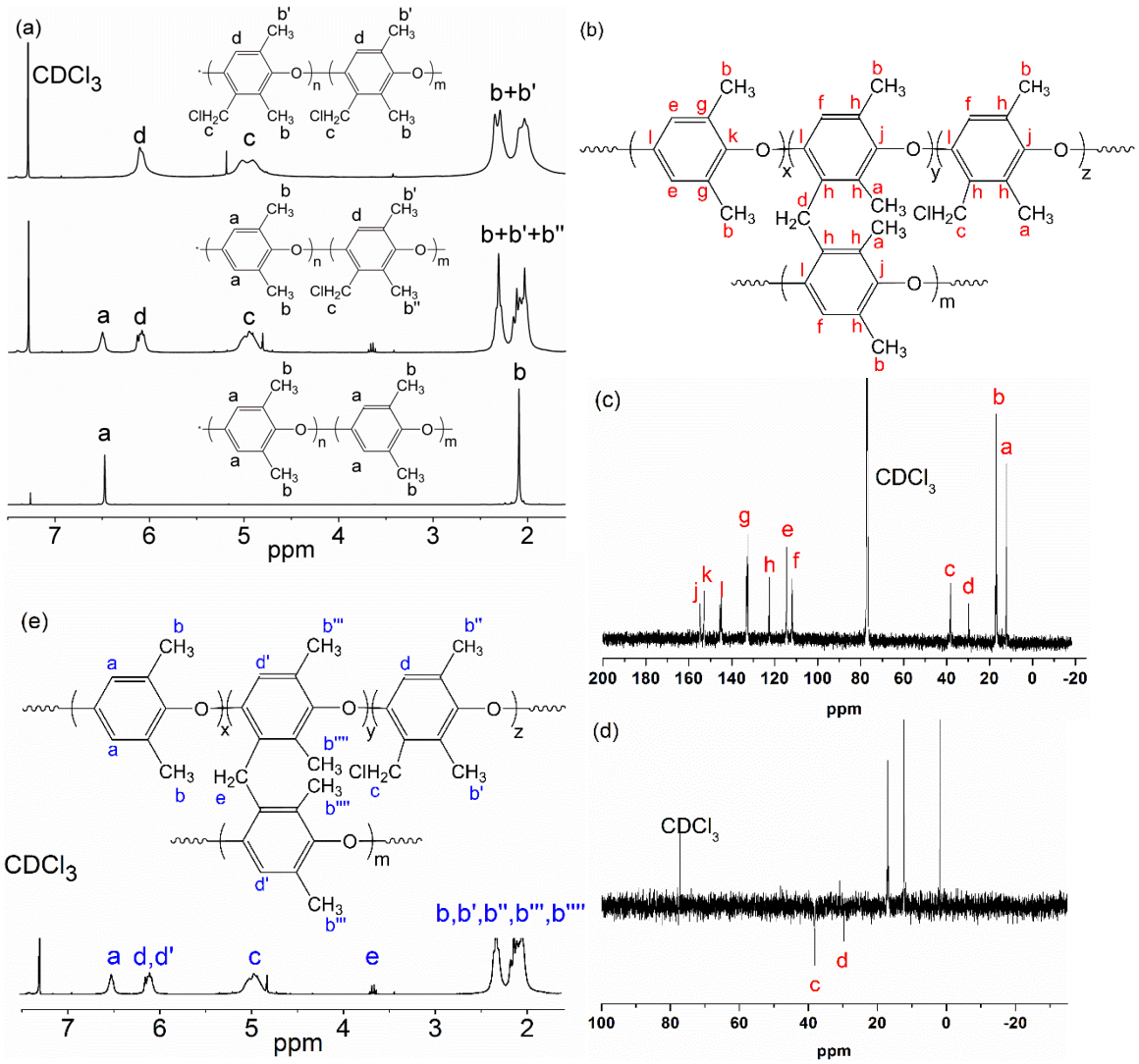

Figure 5.2 ^{1}H NMR spectra of pure PPO (bottom), partially chloromethylated PPO (middle) and fully chloromethylated PPO (top) ($CDCl_3$, 400 MHz). (b) The proposed cross-linked structure of ClPPO. (c) ^{13}C NMR ($CDCl_3$, 100MHz) of (b). (d) ^{13}C NMR DEPT 135 spectra of (b). (e) the ^{1}H NMR spectra of cross-linked ClPPO.

The degree of chloromethylation (DC) was one of the significant parameters to characterize the degree of functionalization. The most used equation for DC in the literature is equation 5.1 [67, 123, 145, 194].

$$DC_1\,(\%) = \frac{A(H_d)}{0.5A(H_a)+A(H_d)} \times 100 \quad (5.1)$$

A: The integrated area of the aryl proton signal in the ^{1}H NMR spectra.

As is shown in Figure 5.2(a), once chloromethylation occurs, the chemical shift at position d changes from δ = 6.5 ppm to δ = 6.1 ppm. Thus, the area of protons (AP) at position d can be used to characterize the degree of chloromethylation.

Manohar and co-workers used a different equation, 5.2, which uses a similar method and will be discussed in the following [118].

$$DC'(\%) = \frac{2A(H_c)}{A(H_d)} \times 100 \quad (5.2)$$

A: The integrated area of the proton signal in the ^1H NMR spectra.

Table 5.1 shows the degree of chloromethylation (error ± 5%) of ClPPO obtained under different experimental conditions, such as temperature, the ratio between reactants and catalyst, reaction time, and reactants' concentration. Theoretically, once the chloromethylation reaction occurs, the signals for H_d and H_c should appear simultaneously. The integration of the H_d peak, i.e. $A(H_d)$, should be half of that of H_c since the amount of hydrogen at position c is twice as much as that at position d, i.e. $A(H_d)/A(H_c) = 0.5$. However, as shown in table 5.1, the A(Hd) and A(Hc) ratios are not 0.5 for all prepared ClPPO samples, suggesting a side reaction.

In the case of PPO, the alkylation could link two aromatic rings with a methylene bridge under a Lewis acid environment ($SnCl_4$) and produce a crosslinked PPO structure. This is also reported for other polymers, such as polystyrene [195, 196]. As is shown in Figure 5.3, there appears to be a competition between the chloromethylation reaction (Route A) and the crosslinking reaction (Route B). The side reaction between the chloromethyl groups and the aromatic rings should be considered. Therefore, we proposed a crosslinked polymer structure after chloromethylation in Figure 5.2(b) and the crosslinking process route B, as shown in Figure 5.3.

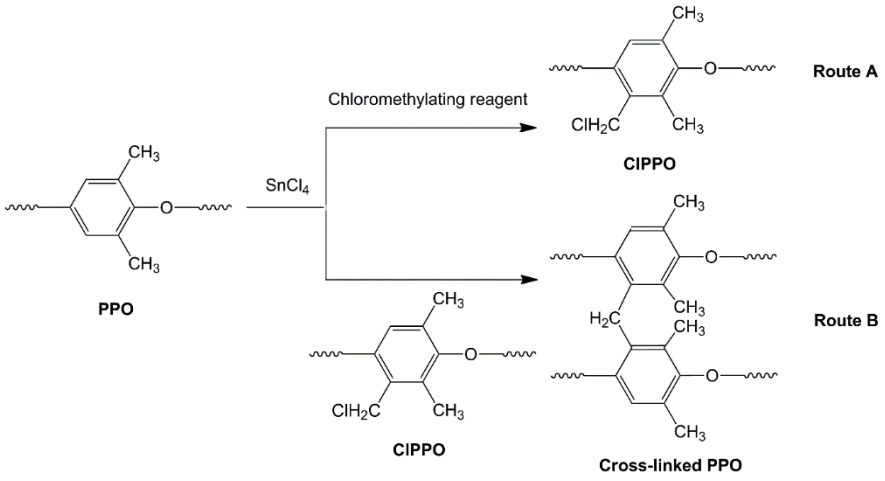

Figure 5.3 The competition between chloromethylating reagent and substituted benzyl chloride for unsubstituted PPO.

Table 5.1 Degree of chloromethylation and crosslinking calculated under different reaction conditions.

Code number	$n_{PPO}: n_{Tri}: n_{Sn}$ [a]	t (h)	T (°C)	n (wt%[b])	A(a)	A(d)	A(c)	A(d)/A(c)	A(e)	A(d)-0.5 A(c)	DC_1 (%)[c]	DC_2 (%)[d]	CLD (%)[e]
ClPPO-1[f]	1:2:0.75	1	20	1.7	0	1	1.69	0.59	0	0.59	1	84.5	-
ClPPO-2[f]	1:2:0.75	18	20	1.7	0	1	1.56	0.64	0.06	0.64	1	75.5	-
ClPPO-3	1:1:0.5	4	20	1.7	1	5.9	10.8	0.54	0.5	0.47	92.1	84.9	4.1
ClPPO-4	1:0.5:0.25	4	20	1.7	1	0.03	0.05	0.6	0.01	0	56.6	4.7	0.9
ClPPO-5	1:0.5:0.25	7	20	1.7	1	1.01	1.72	0.59	0.14	0.14	67.1	57.0	4.8
ClPPO-6	1:0.5:0.25	7	15	1.7	1	0.26	0.40	0.61	0.07	0.06	35.9	29.5	4.7
ClPPO-7	1:0.5:0.25	15	10	1.7	1	0.29	0.54	0.52	0.03	0.02	36.7	34.2	1.9
ClPPO-8	1:0.5:0.5	20	10	1.7	1	1.58	3	0.53	0.09	0.08	75.9	72.1	2.2
ClPPO-9[f]	1:0.5:0.5	5	35	1.7	0	1	1.24	0.81	0.12	0.27	1	62	-
ClPPO-10[f]	1:1.5:0.5	5	35	1.7	0	1	1.46	0.68	0.07	0.28	1	71.5	-
ClPPO-11[g]	1:0.5:0.5	0.5	35	2.0	-	-	-	-	-	-	-	-	-
ClPPO-12[g]	1:0.5:0.5	5	35	1.7	-	-	-	-	-	-	-	-	-
ClPPO-13	1:0.5:0.2	5	35	1.7	2.84	1	1.9	0.53	0.09	0.1	41.3	39.3	1.8
ClPPO-14	1:0.5:0.2	10	35	1.7	1	0.54	1.02	0.53	0.04	0.05	51.9	49	1.9
ClPPO-15[g]	1:0.5:0.2	20	35	1.7	-	-	-	-	-	-	-	-	-
ClPPO-16	1:0.5:0.2	4	35	1.7	2.46	1	1.86	0.54	0.07	0.07	44.8	41.7	1.6

[a]The mole ratio among PPO (repeating unit), 1,3,5- trioxane and $SnCl_4$ fed in reaction. [b]The wt% of PPO. [c]The degree of chloromethylation calculated by equation 4.1. [d]The degree of chloromethylation is calculated by equation 4.3. [e]The degree of crosslinking is calculated by equation 4.4. [f]The solubility is very low due to the crosslinking. [g]The gelation occurs during the chloromethylation process data obtained because of the gelation.

The proposed crosslinking structure was verified by ^{13}C NMR spectra, as shown in Figure 5.2(c). The signal at δ = 29.71 ppm corresponds to the methylene carbon (position d) in Figure 4.2(b), confirming the presence of crosslinking, and the signal at δ = 38.27 ppm corresponds to the chloromethyl carbon (position c) confirming the polymer chloromethylation [150, 197]. To verify the proposed crosslinked polymer structure further, ^{13}C NMR DEPT 135 spectroscopy of ClPPO was conducted. With this technique, CH and CH_3 carbon atoms appear as positive signals, CH_2 as negative signals, and quaternary carbon atoms do not show any signal. Figure 5.2(d) shows that two signals (δ = 29.71 ppm and δ = 38.37 ppm) appear under the X-axis, corresponding to methylene and chloromethyl carbon, respectively, confirming the proposed crosslinking structure.

As is shown in Figure 5.3, chloromethylation and crosslinking are competitive reactions, even though crosslinking only occurs after the chloromethylation reaction. These two reactions occur at the same benzene ring (position a). At a short reaction time, the chloromethylation reaction is swift. It will be the dominant reaction as the number of available aromatic rings is high, with an increase in reaction time, an increase in substituted aromatic rings, and a decrease in aromatic rings available for substitution crosslinking reaction.

Therefore, we re-analyse the ^{1}H NMR in Figure 5.2(e). Taking partially chloromethylated PPO as an example, after chloromethylation, the area of protons (AP) at position c should be twice that at position d. Once crosslinking occurs, one methylene group will be generated and connected to two benzene rings. Thus, the AP at position e should be equal to that at position d''. Furthermore, the AP at position c or d can therefore be used to estimate the unreacted chloromethyl groups, which corresponds to the reasonable degree of chloromethylation after crosslinking. The AP at position d' or e can be used to estimate the number of methylene groups and the crosslinking degree. However, the protons at positions d and d' have similar chemical shifts (ca. 6.1 ppm), making it difficult to distinguish between them and determine the degree of crosslinking. Therefore, when calculating the degree of chloromethylation, the protons at position c should be considered. Thus, a new equation has been proposed by here using the ratio among $A(H_c)$, $A(H_a)$ and $A(H_d, H_{d'})$as equation (5.3), (designated as DC_2).

$$DC_2\ (\%) = \frac{0.5A(H_c)}{0.5A(H_a)+A\left(H_d,H_{d'}\right)} \times 100 \quad (5.3)$$

As discussed above, the generation of the methylene bridge (position e) indicates the crosslinking of ClPPO, and there are two protons in the methylene bridge. Therefore, CLD should be half of AP at position e. CLD can therefore be calculated by equation (5.4)

$$\text{CLD}\ (\%) = \frac{0.5A(H_e)}{0.5A(H_a)+A\left(H_d,H_{d'}\right)} \times 100 \quad (5.4)$$

and AP at position e should be the same as at position d'. In other words, CLD can also be expressed as the difference between DC_1 and DC_2. Thus, CLD can also be calculated by equations (5.5) and (5.6).

$$\text{CLD}\ (\%) = \frac{0.5(A\left(H_d,H_{d'}\right)-0.5A(H_c))}{0.5A(H_a)+A\left(H_d,H_{d'}\right)} \times 100 \quad (5.5)$$

or

$$\text{CLD}\ (\%) = 0.5\ (DC_1-DC_2) \quad (5.6)$$

Therefore, if equation 5.1 calculates the degree of chloromethylation, the result should include both degree of chloromethylation and crosslinking degree. Given this, estimating the degree of chloromethylation will be inaccurate using equation 5.1, i.e., DC_1. This might be the main reason for the differences of $A(H_d)/A(H_c)$ between the theoretical and calculated values in table 5.1. As a result, the alkylation reaction would produce the crosslinked structure with a methylene bridge and give a higher crosslinking degree (CLD) value if equation 5.1 was used. This might explain the phenomenon of a high degree of chloromethylation but low ionic conductivity. As for equation 5.2, the protons at position a are not considered, and this will cause an overestimate of DC.

5.22 Effect of reaction conditions

The effects of reaction conditions, namely the molar ratio of PPO, 1,3,5- trioxane and $SnCl_4$ feed, reaction time, concentration, and temperature on chloromethylation and crosslinking reactions, were studied. $SnCl_4$ was chosen due to its higher catalytic efficiency than other catalysts, such as $AlCl_3$ or $ZnCl_2$ [27]. Chloromethylation and crosslinking are competitive reactions. Crosslinking reaction occurs only after the corresponding chloromethylation reaction since the tethered chloromethyl group is involved in the crosslinking reaction. It is worth mentioning that the crosslinking reaction was observed at room temperature [69]. The higher the degree of crosslinking, the higher the viscosity. Some prepared samples had poor solubility due to the high cross-linking degree, such as ClPPO-1, ClPPO-2, ClPPO-9 and ClPPO-10. Similarly, gelation was observed during the chloromethylation process for some samples,

namely ClPPO-11 and ClPPO-12 and ClPPO-15. The ratio between reactants and catalyst are significant.

As is shown in table 5.1, the reaction conditions have a significant effect on DC_2 and CLD. When other reaction conditions are fixed, a high ratio/concentration of catalyst is more beneficial for chloromethylation at low temperatures, while long reaction time and high temperature facilitate cross-linking. Finding a suitable range for DC_2 and CLD has a significant influence on the membrane preparation process and largely determines the properties of anion exchange membranes. When the degree of cross-linking is high (>4.8 %), the polymer becomes insoluble in chloroform and after filtration. No NMR signal of the polymer could be detected.

When a large amount of catalyst is used concerning PPO mass, the chloromethylation and crosslinking reaction reactions proceed rapidly, resulting in a high crosslinking degree. The polymer obtained is hard to dissolve (ClPPO-1 and ClPPO-2). Higher reaction temperature increases the reaction rate constant of both chloromethylation and crosslinking reactions. If catalyst content is high and the reaction temperature is >20 ºC, a further increase in temperature is expected to be more beneficial for crosslinking over the chloromethylation reaction. In comparison, for low catalyst loading and at low temperatures <20 ºC, the opposite effect is expected at low to medium time scales. Similar to a higher catalyst ratio, at high $n_{PPO}: n_{SnCl_4}$ ratio of 1:0.5 at 20 ºC, ClPPO-3 shows DC_2 of 84.9 % in comparison to ClPPO-9 at 35 ºC showing DC_2 of 62 %.

When a low catalyst ratio of 1:0.25 and relatively medium reaction time (7 h) are used, the temperature increase has a more significant impact on the chloromethylation reaction rate than the crosslinking rate. When the temperature increased from 15 to 20 ºC, DC_2 risen from 29.5 % (ClPPO-6) to 57 % (ClPPO-5), while CLD decreased from 4.7 to 4.8 %.

As discussed above, as the chloromethylation reaction proceeds, the cross-linking side reaction becomes more significant with a longer reaction time and a higher degree of chloromethylation. For example, as the reaction time extends from 5 h (ClPPO-13) to 10 h (ClPPO-14), the DC_2 increases from 39.3 % to 49 % and CLD increases from 1.8 % to 1.9 %. After 20 h, ClPPO-15 become highly crosslinked and turns into the gel as a longer reaction time decreases the DC_2 and increases the CLD due to the involvement of chloromethyl groups in the crosslinking reaction. This can also be seen in ClPPO-1 and ClPPO-2 cases. When reaction time increased from 1 h to 18 h, the DC_2 decreased from 84.5 % to 75.5 %. A higher concentration of PPO and reagents

for a given molar ratio (lower solvent content) should increase the chloromethylation and crosslinking reaction rates but seems to favour the latter under the studied conditions. For example, at a high temperature of 35 ºC and catalyst molar ratio n_{PPO}:n_{SnCl_4} of 1:0.5, i.e., when the chloromethylation reaction rate is fast, increasing the concentration of reagents and PPO from 1.7 to 2 % (ClPPO-12 to ClPPO-11), the resulting polymer became gel very rapidly after 0.5 h. In addition to the rapid increase in chloromethylation, this can also be caused by increased solution viscosity and slow diffusion of chloromethylated products resulting in higher crosslinking rates.

If high DC and low CLD are required to produce membranes with good conductivities but with acceptable solubility/processability, higher catalyst concentration >1:0.2 and short reaction time <15 h and low temperature of 20 ºC should be used.

5.23 Optimal degree of chloromethylation

Polymers with different DC_2 and CLD will produce AEMs with different chemical stability, IEC, WU and SR and conductivity after quaternisation. Significantly, DC_2 and CLD will also affect polymer processability. On the one hand, when chloromethylation is too low, ClPPO will have limited solubility in NMP (required for homogenous quaternisation). On the other hand, when the degree of chloromethylation is too high, the membrane prepared will possess a very high swelling ratio and water uptake after quaternisation, resulting in unacceptable mechanical properties, e.g., ClPPO-3 with DC_2 of 85.9 %. A trade-off between these two effects should also be achieved in agreement with the reported chloroacetylation process of PPO [145].

Similarly, crosslinking limits water uptake and membrane swelling and potentially improves the polymer chemical stability, however, at the cost of lowering DC and conductivity and membrane solubility in solvent for processing and casting. During Friedel-Crafts reactions, when crosslinking degree is too high (>5 %), the solution will become gel quickly, and the polymer cannot be dissolved in NMP thoroughly. Membrane fabrication becomes impossible, e.g., ClPPO-11 and ClPPO-15.

To ensure the solubility in NMP during quaternisation process, ClPPO polymers with DC_2 higher than 29.5 % and CLD lower than 4.8 % were found to be suitable for quaternisation and membrane processing.

5.3 Quaternization

Quaternisation is a crucial procedure in the preparation of AEMs. We have explored two different methods to quaternise PPO, namely the homogenous method, where both the polymer and the quaternising agent are dissolved in solvent/solution, e.g.,

NMP and heterogeneous method, where the polymer is immersed in solid form the aqueous solution of the quaternising agent. As discussed above, not all the synthesized ClPPO were suitable for AEMs preparation. When the mass of PPO was fixed, for example, 120 mg, and a sufficiently long quaternation reaction time of 24 h is used, the degree of quaternisation was controlled in the heterogeneous method by altering the molar ratio between chloromethyl groups in the 120 mg PPO and added amount of TMA to water. In a homogenous way, the PPO concentration in NMP was kept constant, and the TMA amount/concentration in NMP was altered to achieve the desired quaternisation degree. Table 5.2 compares these two different methods using ClPPO-7 at room temperature.

Table 5.2 Comparison of two different quaternization methods of ClPPO-7.

Heterogeneous quaternization		Homogenous quaternization	
n_{chloro}/n_{TMA}[a]	IEC (mmol g^{-1})	Concentration of TMA (M)	IEC (mmol g^{-1})
1:120	0.9	1.12	1.4
1:200	1.3	2.52	1.7
1:700	1.4	3.65	1.7

[a]The molar ratio between chloromethyl groups and TMA.

Ion exchange capacity (IEC) is the ability of the membranes to exchange the ions, calculated using equation 4.1. Water uptake (WU), Swelling Ratio (SR) and hydration number (λ) were calculated using equations 4.2, 4.3 and 4.4, respectively. Table 5.2 shows the IEC obtained from different quaternisation methods. It can be observed that IEC increases exponentially with increasing TMA concentration using the homogenous quaternisation procedure. The IEC increases by increasing the concentration of the quaternising agent, TMA in the solution. For a fixed polymer amount, the theoretical IEC ($IEC_{theoretical}$) of ClPPO-7 is 2.21 mmol $g^{-1,}$ and the experimental IEC obtained through homogenous and heterogeneous quaternisation was 1.72 mmol g^{-1} and 0.92 mmol g^{-1}, respectively. Homogenous quaternisation results in higher IEC than heterogenous method despite using around half the TMA concentration (3.65 vs 6.5 M). This can be explained by enhancement in mass transport, i.e., faster TMA diffusion in NMP-ClPPO solution than slower diffusion of TMA through solid Cl-PPO. As a result, homogenous quaternisation was chosen as the preferred quaternisation method. The experimental IEC is significantly lower than the theoretical IEC (ca. 78 %). The incomplete exchange between Cl can partially explain this^{-} and OH^{-} during the exchange process and incomplete quaternisation in 24 h period, which was observed in other AEMs we believe that the significantly lower IEC obtained is caused by the

nature of the PPO backbone aromatic rigid polymer chains resisting the conformational changes necessary to form charged domains limiting and slowing the quaternisation process. This can be particularly at high IEC. This seems consistent with rapid change in water uptake at higher IEC, as discussed below.

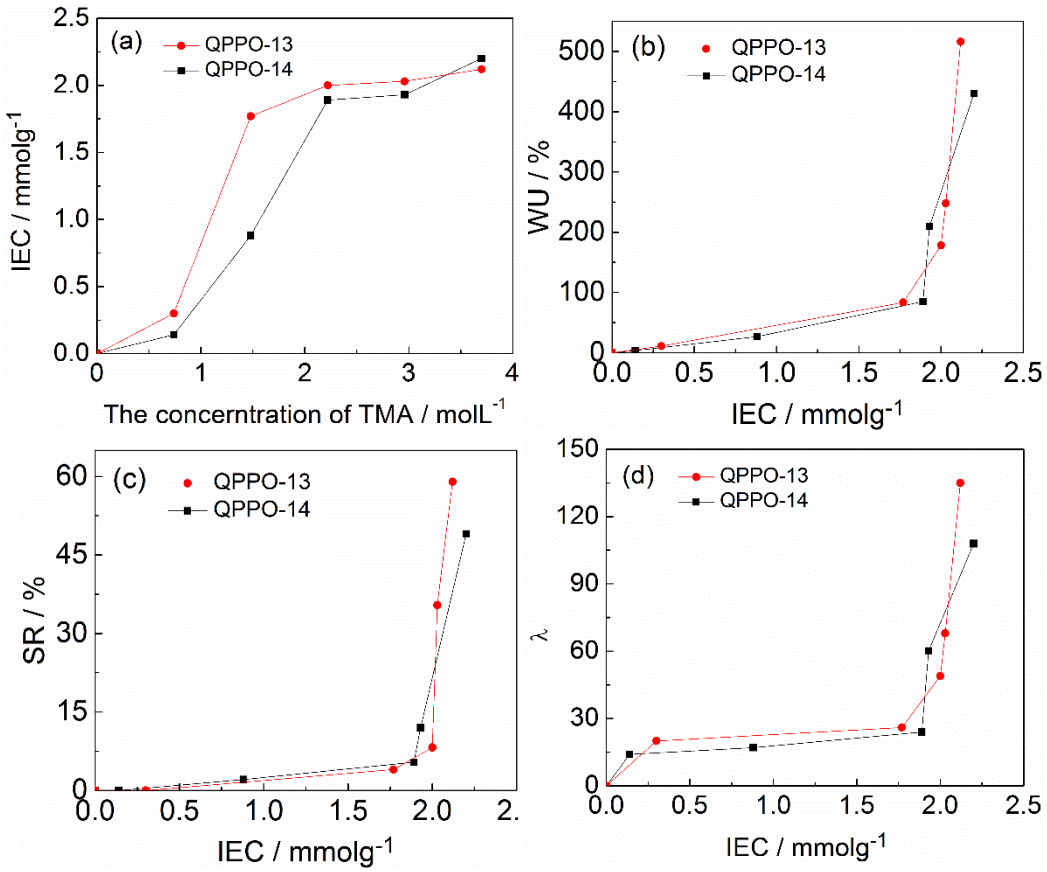

Figure 5.4 (a)IEC of QPPO-13 and QPPO-14 under different concentrations of TMA using homogenous quaternisation procedure, (b)water uptake, (c)swelling ratio and (d)hydration number of QPPO-13 and QPPO-14 with different IEC.

The quaternisation process of ClPPO-13 and ClPPO-14 was studied at different concentrations of TMA. The corresponding IEC, water uptake, swelling ratio and hydration number were analysed. The $IEC_{theoretical}$ of ClPPO-13 and 14 are 2.59 mmol g^{-1} and 2.89 mmol g^{-1}, respectively. As shown in Figure 5.4, when TMA concentration was 2.96 mmol L^{-1}, IEC rapidly approached a steady value (around 2.0 mmol g-1) and then increased much more slowly beyond that value, indicating that $IEC_{theoretical}$ is not easy to reach. Water uptake (WU) and swelling ratio (SR) both rose slowly initially with the increase of IEC (and TMA concentration) but then exhibited a sharp increase when IEC reached around 1.9 mmol g^{-1} (WU 150-300 %, SR 5 %-30 %, Figure 5.4(b) and Figure 5.4(c)). Similar observations were reported in proton exchange membranes for sulfonated poly(arylene ether sulfone) membranes [198], which results from the phase

separation. The prepared membranes are composed of hydrophobic backbones and hydrophilic functional groups. The water uptake is caused principally by the hydrophilic ion clusters. The results indicate that, for low IEC membranes, the hydrophilic parts are isolated and surrounded by the continuous hydrophobic phase, which reflects by low water uptake and low conductivity. After the IEC reaches a particular value (1.9 mmol g^{-1}), the hydrophilic ionic domains continue, and large channels for water transportation are formed, which is reflected by a sudden increase in water uptake and conductivity. Such sudden change in polymer properties with IEC is common in aromatic polymers, e.g. functionalised poly ether ether ketone becomes water-soluble after a narrow increase in IEC [199].

Interestingly, ClPPO-13 could reach higher IEC than ClPPO-14 for a given TMA concentration (Figure 5.4a). Additionally, at higher IECs, ca. 2 mmol g^{-1}, QPPO-13 showed higher WU and SR than ClPPO-14 despite having a lower degree of chloromethylation. This can be caused by a lower crosslinking of ClPPO-13 and a higher degree of amination of the available chloromethylated groups. More amination of chloromethylated groups in ClPPO-13 against ClPPO-14 means that there is more homogeneity in water and headgroup distribution in ClPPO-13 in comparison to ClPPO-14. ClPPO-14 will contain larger fractions of un-quaternised chloromethyl group resulting in a lower volume fraction of homogenous/continuous conduction path as discussed further below in the conductivity section and as seen in the NMR study in the degradation study chapter. As will be seen in the degradation chapter below, the distribution of quaternary ammonium is in the polymer, not necessarily homogenous, resulting in regions of AEM with high swelling and other regions of lower swelling. This could explain the rapid increase in swelling ratio for little change of IEC seen above.

Similarly, PPO is a rigid semi-crystalline polymer with a glass transition temperature of 160 °C (Figure 5.4(a)), high tensile strength and very low elongation at the break below 5 %. The rigidity of aromatic chains towards the conformational changes required to allow the formation of continuous ion ionic domains could be the reason for the seen sudden change. From Figure 5.4(d), taking QPPO-13 as an example, it could be seen that the hydration number almost doubled when IEC increased from 2.0 mmol g^{-1} to 2.1 mmol g^{-1}, which means more water molecules were gathered near the functional groups. Moreover, the higher water content will result in membrane swelling and increased spaces between the polymer chains and flexibility, promoting increased hydration of the functional groups.

5.4 Solubility

Table 5.3 Solubility of PPO, ClPPO and QPPO in common organic solvents.

	Samples	NMP	THF	Chloroform	Methanol	DMF
PPO	n.a [a]	–[b]	+[c]	+	–	–
ClPPO (DC_2 >30 % & CLD< 5%)	ClPPO-14	+	+	+	–	–
ClPPO (DC_2 >30 % & CLD>5%)	ClPPO-11	–	–	–	–	–
ClPPO (DC_2 <30 %)	ClPPO-4	–	–	+	–	–
QPPO-OH^{-d}	QPPO-14	–	–	–	–	–

[a]n.a represents not applicable. [b]+ represents soluble in this solvent. [c]– represents insoluble in this solvent.

Table 5.3 shows the solubility of PPO, ClPPO and QPPO in common organic solvents. The solubility of ClPPO is influenced by both DC_2 and CLD, as discussed above. At DC_2 <30 %, e.g., ClPPO-4 5.6 %, ClPPO polymer has very few chloromethylated chains or charged groups and behaves like pristine PPO, i.e., insoluble in polar NMP while soluble in chloroform. On the other hand, when CLD is too high, >15 %, ClPPO will not dissolve in NMP because of a high degree of crosslinking, such as ClPPO-11. Thus, ClPPO with appropriate DC_2 (>30 %) and CLD (<5 %) was soluble in chloroform, THF and NMP. It should be noted that when TMA was added into polymer-THF solution or polymer-chloroform solution, the polymer started to phase out of the solution and eventually became insoluble. When TMA was added to the polymer-NMP solution, the mixture became opaque and transparent. And there was no precipitation in the solution. Therefore, NMP was the suitable solvent for quaternisation, as described above. This can be explained by NMP's high polarity and compatibility with polar charged quaternary ammonium head group.

5.5 Morphology

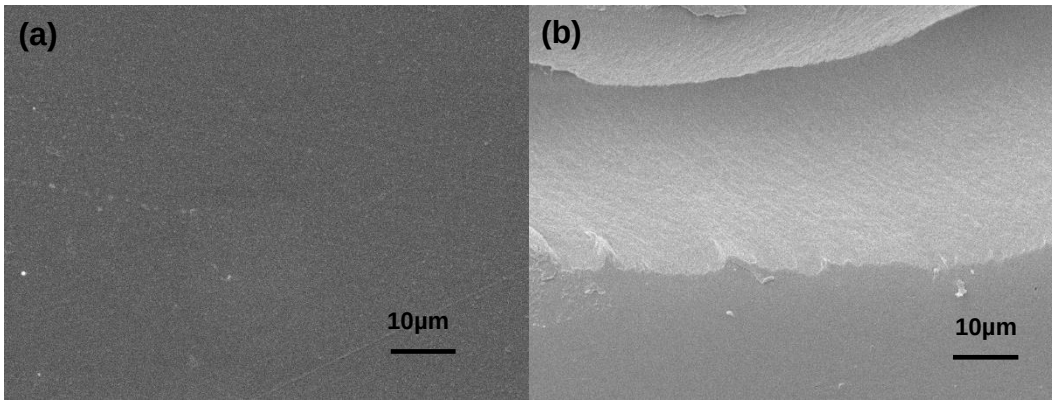

Figure 5.5 The SEM images of (a) surface and (b) cross-section of QPPO-14 (dry, thickness 110 μm).

The surface and cross-section SEM images are shown in Figures 5.5 (a) and (b). A uniform and smooth structure indicates a homogeneous and dense membrane [118, 200].

5.6 Thermal stability

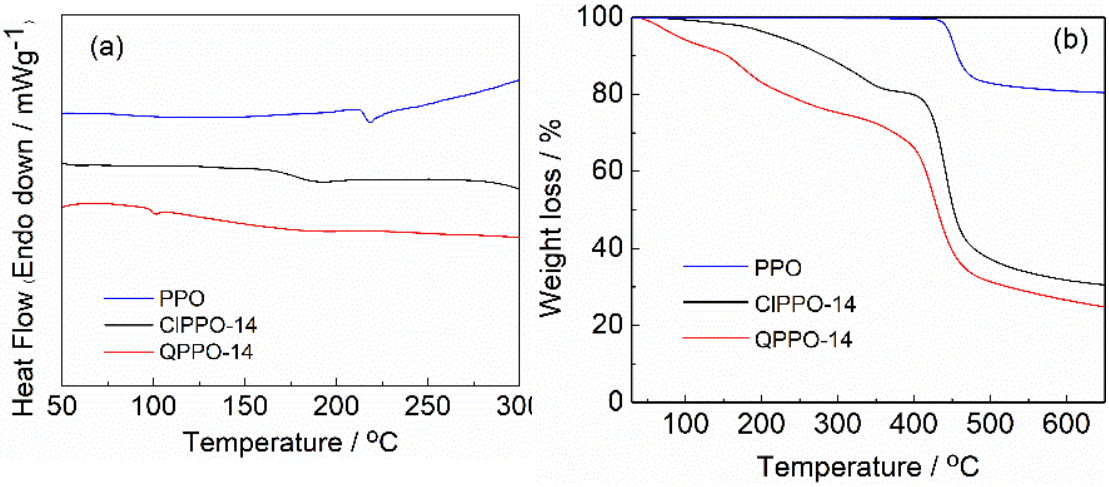

Figure 5.6 (a) The DSC and (b) TGA curves of pure PPO, ClPPO-14 and QPPO-14.

The thermal stability of the functionalized polymer is also an essential property of AEMs; thus, DSC and TGA were used to study QPPO thermal properties under a nitrogen atmosphere. Figure 5.6 (a) and (b) show the DSC and TGA curves of ClPPO and Q-PPO. ClPPO exhibits an apparent glass transition temperature of around 160 °C. For QPPO, there is a small endothermic peak at 100 °C caused by the vaporisation of residual water from the membranes. For TGA curves, the Q-PPO AEM exhibits a slight mass loss (<5 %) below the temperature of 150 °C, which is attributed to water loss from the polymer [201]. As discussed earlier, QPPO shows good water uptake. Before the thermal stability tests, the membranes were thoroughly dried in a vacuum oven at 60 °C. The QPPO rapidly absorbed water from the air during sample transfer to the TGA instrument. The onset decomposition seen at 170 °C in Q-PPO is due to the degradation of the head group [202]. Finally, the second weight loss stage occurs at around 400 °C can be assigned to backbone chain decomposition.

Table 5.4 Degradation temperature of the polymer.

Sample	$T_{d5\%}$ / °C [a]	$T_{d10\%}$ °C [a]
ClPPO	223	301
QPPO[b]	188	289

[a] $T_{d5\%}$ means the temperature when the weight loss is 5 %. $T_{d10\%}$ means the temperature when the weight loss is 10 %.
[b] $T_{d5\%}$ and $T_{d10\%}$ of QPPO was calculated by subtracting the water loss.

As shown in table 5.4, $T_{5\%}$ of the polymer is above 189 °C, suggesting that PPO-based membranes have good thermal stability under non-oxidizing conditions and the potential use in water electrolyser at temperatures <100 ºC.

5.7 Mechanical Properties

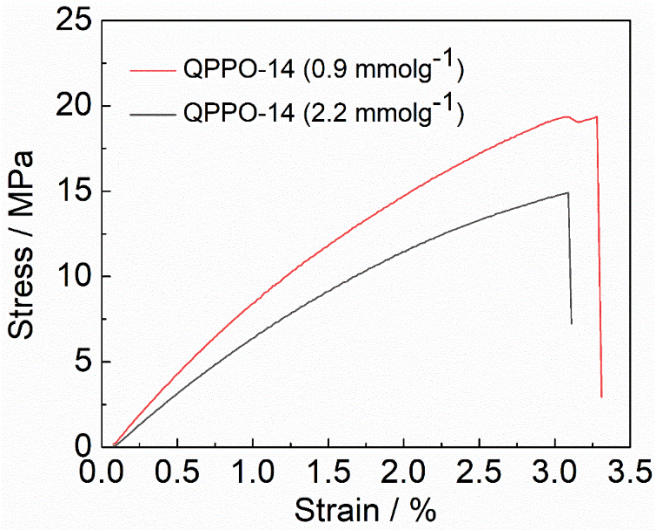

Figure 5.7 Stress-strain curves of QPPO-14 (0.9 mmol g^{-1}) and QPPO-14 (2.2 mmol g^{-1}) at room temperature.

Mechanical properties of QPPO-14 with different IEC were tested at room temperature. The membranes in hydroxide form were submerged in water for 1 h before testing. As shown in Figure 5.7(c), QPPO-14 was chosen due to the suitable degree of chloromethylation and its potential application in water electrolysers. The stress of break and elongation of QPPO-14 (2.2 mmol g^{-1}) is >12 MPa and 3 %, respectively, which is in agreement with the values reported by Wu and co-workers (17 MPa and 3.5 %, shown in table 5.5) for similar IEC membrane (2.10 mmol g^{-1}) [192]. However, our QPPO-14 exhibited over 7 folds increase in ionic conductivity and water uptake in comparison to that of Wu et al. As expected in comparison to lower IEC reported Q-PPO membrane (table 5.5, 1.0 mmol g^{-1}) [82], QPPO-14 (2.2 mmol g^{-1}) shows an order of magnitude lower elongation at break and half the ultimate tensile strength, due to high IEC and high swelling degree but over 8 folds higher ionic conductivity and water uptake.

A comparison of membrane properties among ion exchange membranes-based on varieties of backbones is shown in table 5.5. In contrast to CMPPO-TMA, which was also prepared via Friedel-Crafts reaction using different chloromethylation reagents, QPPO-14 shows a higher ionic conductivity and IEC. Besides, compared with radiation grafted low-density polyethylene with vinylbenzyl chloride functionalised with TMA (LDPE-g-VBC-TMA) [170], QPPO-14 shows the same level of ionic conductivity but a

much higher ultimate tensile strength. PPO-1 and CMPPO-TMA were also prepared by using Friedel-Crafts reaction but with different chloromethylation reagents, exhibiting a much lower IEC and ionic conductivity. Compared with commercial perfluorosulfonic acid membranes Nafion 212 (9 MPa at 100% RH) [170, 203], QPPO-14 demonstrated higher ultimate tensile strength despite having more than double the IEC, which is the result of the rigid aromatic structure of the PPO backbone. Unlike the linear structure of Nafion 212, Q-PPO in this work shows high water uptake (WU), which inevitably increases the swell ratio (SR). The crosslinking design prevents further expansion of the molecular chain when more water molecules gather near the functional groups. Compared with the commercial AEMs FAA3, QPPO-14 shows higher ionic conductivity [13]. The PPO-based membrane needs to be modified to reinforce the strength, reduce the water uptake, and improve the dimension stability.

Table 5.5 The properties of different membranes at room temperature.

Sample	IEC[a] (mmol g^{-1})	Thickness (wet, μm)	σ (mS cm^{-1})	WU (wt%)	SR[d] (wt%)	Ultimate tensile strength (MPa)	Elongation at break (%)
Q-PPO (this work)	2.2	160	58.3	430	49	14	3.1
Q-PPO [192]	2.1	151	7.9	24	–[e]	17	4.3
LDPE-g-VBC-TMA [170, 177]	2.3	96 & 120	54	254	38.8	2.4	41
Nafion 212 [170, 203]	0.91	51	77.4[bc]	14.93	39.6	9	85
Q-PPO [82]	1	–	7	26.4	–	28.8	43.4
Fumasep® FAA3 [13]	1.7-2.1	25-35	40	-	2(Br)	40	20-40

[a]IEC is mmol Cl^- per gram. [b]The conductivity was tested at 30 °C. [c]The ionic conductivity of Nafion 212 was proton conductivity. [d]The length changes were measured. [e]- means no data was obtained.

5.8 Ionic conductivity

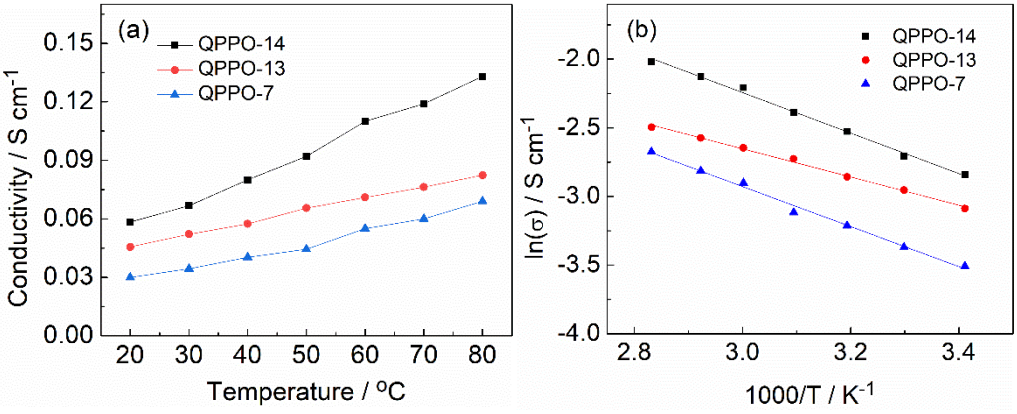

Figure 5.8 (a) Ionic conductivity of membranes with different IEC as a function of temperature. (b) The Arrhenius-type temperature plots.

Ionic conductivity is another important AEMs characteristic affecting the area-specific resistance (ASR) and IR loss in water electrolysers. Higher ionic conductivity allows for thicker membranes with improved mechanical properties while maintaining ASR. The ionic conductivity and activation energy of OH^- hopping in hydrated AEM were calculated by using eq. 5 and eq. 6, respectively. Figure 5.8(a) shows the through-plane conductivity of different membranes. QPPO-14 (2.2 mmol g^{-1}), QPPO-13 (2.0 mmol g^{-1}) and QPPO-7 (1.8 mmol g^{-1}) were tested from room temperature to 80 °C at 100 % RH. All these three membranes showed an increase in conductivity with the temperature rise to 80 °C. As expected, membranes with higher IEC and more significant water volume fraction (swelling) displayed higher conductivity at a given temperature. Higher IEC will result in higher ion concentration in AEM and shorter hopping distance, while higher water content will result in more facile ion diffusion. For example, at 20 °C, the ion conductivity of QPPO-14 is around 0.058 S cm^{-1}, which is higher than that of QPPO-13 (0.045 S cm^{-1}) and QPPO-7 (0.027 S cm^{-1}). QPPO-14 exhibited one of the highest ionic conductivities (0.133 S cm^{-1} at 80 ^oC) in comparison to other reported PPO-based membranes in the literature (with a higher degree of chloromethylation also prepared via Friedel-Crafts reaction) [32, 67, 82, 118, 120]. The ionic conductivity at elevated temperatures was also presented as the Arrhenius plot. Ion conduction is facilitated when the activation energy is low. As is shown in Figure 5.8(b), the OH^- conductivity shows an approximate exponential temperature dependence [204]. The relationship between ionic conductivity and temperature fits the thermally activated process presented by the Arrhenius equation. Active energy (Ea) is the minimum energy required for OH^- diffusion. The lower the Ea, the lower the energy barrier for hydroxide transport [205, 206]. The fitted Ea values of QPPO-14, QPPO-13 and QPPO-7 were 12.26, 8.53 and 12.13 KJ mol^{-1}, respectively, lower than that reported for other AEMs (18 KJ mol^{-1}) [207, 208] and similar to that to high conductivity radiation grafted LDPE -based AEM [152, 170]. This suggests rapid hydroxide transport in prepared QPPO AEMs [208-210]. QPPO-13 exhibited the lowest Ea value, which indicates the facile transport of OH^- ions through ion channels which can be attributed to higher water uptake and more homogenous distribution of quaternised groups (higher degree of quaternisation of available chloromethylated groups as discussed above). The crosslinking degree of QPPO-13 is also slightly lower than that of QPPO-14 and QPPO-7, contributing to higher WU. More unquaternised chloromethylated groups and, consequently, non-continuous conduction path and the

tighter crosslinking structure with lower WU of QPPO-14 and QPPO-7 will result in an adverse effect on the ionic conductivity [211, 212].

The water uptake and the swelling ratio of QPPO, LDPE and Nafion 117-based membranes are shown in table 1. The swelling occurs in all directions, including length, width, and thickness. It is not difficult to observe that the water uptake is relatively high for QPPO while Nafion is low (430 % VS 14.93 %). This might be due to Nafion's higher molecular weight than H_2O since Nafion is perfluorosulfonic acid membrane and the IEC of Nafion is relatively low. When absorbing the same amount of water, Nafion will show lower water uptake. But for PPO, the formula weight (92.1 g mol^{-1}) is relatively low. Thus, the water uptake is quite high. The high water uptake was also observed for the LDPE membrane [170].

5.9 Alkaline stability

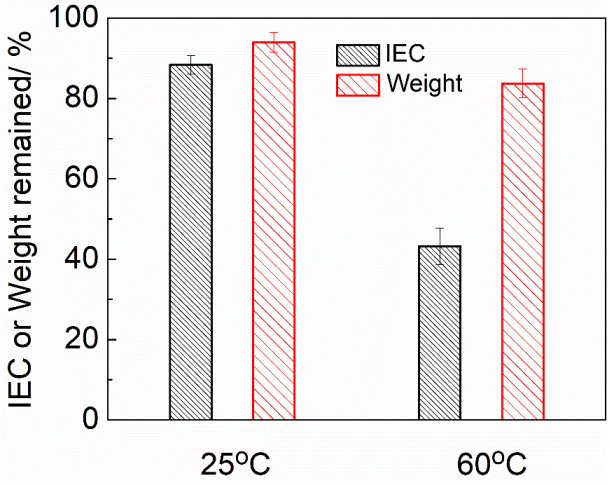

Figure 5.9 IEC and weight remained of QPPO-14 after immersing in 1 M KOH at 25 °C and 60 °C for 500 h.

AEMs need to have good chemical stability for long-term application in water electrolysers. While ideally, AEM can be fed with deionised water, there is a need in some instances to use support electrolytes, e.g., 0.1-1 M KOH, for example, to enhance OER activity and stability when using transition metal oxide catalyst. The IEC and weight change of QPPO-14 (2.2 mmol g^{-1}) were measured after immersion in 1M KOH at 25 °C and 60 °C for 500 h. As is shown in Figure 5.9, the temperature has a vital influence on the degradation rate. The aged QPPO-14 retained >88 % of its IEC and > 94 % of its original mass at 25 °C after 500 h. On the other hand, at 60 °C, QPPO-14 retained only 43 % of its IEC but 84% of its original mass, suggesting that most of the degradation affects the head group instead of the backbone. However, the decrease in the IEC is expected from alkaline degradation involving the TMA head

group and not the PPO backbone. As reported in the literature [40, 170], TMA is a good leaving group, and the degradation is mainly due to the OH^- attack on the TMA cation group via nucleophilic substitution in a high alkaline environment (pH>13). Benzylic alcohol is produced consequently. Stevens rearrangement for the benzyl-TMA group is also a minor decomposition route [159]. In this process, a ylide intermediate is formed first, and then a tertiary amine and water are produced finally. Our tests aim to use low-concentration alkaline supporting electrolytes of 0.1 M and ideally deionised as of PEMWE systems. We will be dedicating separate chapter 6 below to a detailed understanding and study of PPO-based AEM degradation in an environment relevant to water electrolyser [213].

As is shown in table 5.7, crosslinked QPPO with IEC of 2.2 mmol g^{-1} showed a 67 % loss of IEC after 21 days in 1M KOH at 60 °C, higher than that of the uncrosslinked QPPO with IEC of 1.78 mmol g^{-1} -based membrane showing 40 % loss of IEC after 21 days in 1 M KOH at 60°C [156]. This agrees with the lack of crosslinking protection effect on the head group/TMA and is consistent with a faster degradation rate from higher IEC (head group concentration) for a given OH^- ions concentration [214]. Another critical factor is that higher IEC results in a significantly higher swelling degree, e.g., 7 % vs 60 %, resulting in faster OH^- diffusion in AEM and a faster degradation rate. As discussed, the poor alkaline stability at 60 °C in 1M KOH is mainly due to the poor stability of benzyltrimethylamonium headgroup in comparison with the other [215-218] head groups, e.g. the imidazole group (Im) [219]. While IEC and swelling degrees affect the degradation rate, they also impact the ionic conductivity. On the other hand, compared with different functional groups, benzyl ammonium has relatively low alkaline stability. Therefore, the membrane needs to be reinforced to protect the functional group in future work.

Table 5.6 Alkaline stability comparison of reported membranes.

Sample	IEC (mmol g^{-1})	σ (mS cm^{-1})	Testing condition	Stability result	Ref
QPPO	2.2	59 (20 °C)	1 M KOH at 60 °C for 500 h	67 % loss of IEC	This work
Uncrosslinked QPPO	1.78	-	1 M KOH at 60 °C for 30 days	40 % loss of IEC	[156]
QMter-co-Mpi-100%	2.42	35 (30 °C)	1 M KOH at 60 °C for 500 h	3.3 % loss of IEC	[217]
PES-Im-38	1.86	57.6 (80 °C)	1 M KOH at 60 °C for 168 h	7.5 % loss of IEC	[219]
MBPES	2.03	105 (80 °C)	1 M KOH at 60 °C for 200 h	10.8 % loss of IEC	[215]
QAPS-OH	1.34	18 (30 °C)	1 M NaOH at 60 °C 342 h	5.2 % loss of IEC	[216]

5.10 Electrolysis test

The electrochemical performance of the QPPO-14 membrane and ionomer were tested in electrolyser cells by preparing a membrane electrolyte assembly (MEA) using Pt/C catalyst at the cathode (0.4 mg cm^{-2}) and $NiCo_2O_4$ at the anode (2 mg cm^{-2}) [177]. The active area is 1 cm^2. The performance was recorded through steady-state linear sweep voltammetry at a scan rate of 1 mVs^{-1} between 1.3 and 2 V in 0.1 M NaOH at 40 °C [12]. In this section, QPPO-14 (2.2 mmol g^{-1}) was used as both membrane (M, 160 μm) and ionomer (I) due to the consideration of ionic conductivity and compatibility between the membrane and ionomer. Using the same QPPO, the membranes and the ionomer will have similar properties, offering better contact in the interface and reducing contact resistance. The test was benchmarked against radiation grafted low-density polyethylene (LDPE) AEM membrane (2.3 mmol g^{-1}, 120 μm) reported elsewhere [40]. The PPO-based ionomer was also benchmarked against uncross-linked quaternised polystyrene-b-poly(ethylene-*co*-butylene)-b-polystyrene (SEBS) (1.9 mmol g^{-1}) ionomer with bulky ionic clusters (60 % wt styrene) reported elsewhere [177]. Despite QPPO-14 having higher IEC than SEBS-based ionomer, its rigid structure, CLD of 3.8% and lower SR results in significantly lower ionic conductivity at 40 °C of 0.08 vs 0.13 S cm^{-1} for SEBS [177]. While desired for membrane mechanical stability, the lower swelling ratio is expected to show slower water permeation through the membrane/ionomer, a critical factor for superior AEM performance [220]. Figure 5.10(a) compares the electrolyser performances using the different membrane and ionomer combinations, M_{LDPE}-I_{SEBS}, M_{LDPE}-I_{SEBS}, M_{PPO}-I_{PPO} and M_{PPO}-I_{SEBS}. Their corresponding impedance data are shown in Figure 5.10(b). The electrolyser with the PPO membrane and SEBS ionomer performed lower than the other three electrolyser samples over the full testing voltage range. To obtain the current density of 100 mA cm^{-2} with a supporting electrolyte of 0.1 M NaOH at 40 °C, cell voltage for M_{LDPE}-I_{PPO}, M_{LDPE}-I_{SEBS}, M_{PPO}-I_{PPO}, and M_{PPO}-I_{SEBS} electrolysers were 1.74 V, 1.73 V, 1.74 V and 1.77 V, respectively. At 1.75 V, the current density of the four different combinations of membranes and ionomers were 102 mA cm^{-2} (M_{LDPE}-I_{PPO}), 127 mA cm^{-2} (M_{LDPE}-I_{SEBS}), 120 mA cm^{-2} (M_{PPO}-I_{PPO}) and 73 mA cm^{-2} (M_{PPO}-I_{SEBS}), respectively. There was a slight difference in MLDPE-IPPO, MLDPE-ISEBS and MPPO-IPPO samples compared to that $M_{PPO}I_{SEBS}$. At the studied conditions of low supporting electrolyte concentration (pH 13), ionomer conductivity plays an essential role in catalyst layer utilisation and electrolyser performance. Equally, the interaction of ionomer-membrane and

membrane mechanical properties is equally important. The chemical and mechanical compatibility between ionomer and membrane will significantly affect contact and area-specific resistance (ASR). Membrane mechanical properties will also affect the catalyst layer performance indirectly. Softer membranes with lower tensile strength will result in better contact of the catalyst layer with the membrane resulting in lower contact resistance and improved catalyst layer utilisation. However, soft membranes with low tensile strength will suffer from faster failure. More soothing membranes will be compressed and thin under compression while initially resulting in lower area-specific resistance. This will eventually result in a short circuit with time. For example, the LDPE membrane failed after 50 h of operation [177, 221]. Compared with LDPE-based membrane [222], PPO-based membrane is more rigid due to the high content of aromatic rings in the backbones, which will cause lower-dimensional including thickness changes. The changes in the area-specific resistance calculated from the impedance at the cell voltage of 1.7 V are shown in table 5.7. ASR for four the studied samples were 116 mΩ cm^{-2} (M_{LDPE}-I_{PPO}), 104 mΩ cm^{-2} (M_{PPO}-I_{PPO}), 150 mΩ cm^{-2} (M_{LDPE}-I_{SEBS}) and 184 mΩ cm^{-2} (M_{PPO}-I_{SEBS}) PPO-based membranes (in combination with PPO ionomer) showed slightly lower ASR to that of LDPE-based AEM which is desired for use in electrolysers despite the higher thickness of PPO membrane in comparison to LDPE-based membrane [177]. The lower ASR values for M_{LDPE}-I_{PPO} and M_{PPO}-I_{PPO} in comparison to that of M_{LDPE}-I_{SEBS} and M_{PPO}-I_{SEBS} can be explained by better compatibility between membrane and ionomer resulting in lower contact resistance. On the other hand, the similar chemical and mechanical compatibility between LDPE and SEBS explains the lower ASR of LDPE-SEBS compared to that of PPO-SEBS.

As is shown in Figure 5.10(b), the total charge transfer resistance (CTR) of both HER and OER (two electrodes measurement) was measured at 1.7 V for the M_{LDPE}-I_{PPO}, M_{PPO}-I_{PPO}, M_{PPO}-I_{SEBS}, and M_{LDPE}-I_{SEBS} electrolysers were 1.24 Ω cm^{-2}, 1.23 Ω cm^{-2}, 1.71 Ω cm^{-2} and 0.92 Ω cm^{-2}, respectively. This supports the earlier discussion on the effect of ionomer conductivity and water permeability on performance and catalyst utilisation. Most ion transport in the catalyst layer occurs via the ionomer using low supporting electrolyte concentration. Hence, the most active fraction of the catalyst layer is that adjacent to the membrane, which is primarily influenced by the good intimate contact and a continuous ionic path between the catalyst layer and the membrane. Significantly, higher conductivity and SR of SEBS compared to QPPO ionomer resulted in 26 % lower charge transfer resistance when used with the same LDPE membrane.

In contrast, poor compatibility between QPPO membrane and SEBS ionomer resulted in seen highest charge transfer resistance of M_{PPO}-I_{SEBS} of 1.71 Ω cm^{-2}. This highlights the importance of ionomer properties and compatibility with membrane on AEM water electrolysis performance at lower voltages and current densities (< 0.2 A cm^{-2} and 1.78 V). As current density increases and membrane IR loss or ASR become more dominant energy loss over kinetic losses, QPPO-based membrane AEMWE showed similar performance to that of LDPE-based AEMWE despite having a 25 % higher thickness. This shows the promising potential of using QPPO as an AEMWE membrane, offering lower ASR and SR and consequently lowering energy loss and stability towards mechanical failure. Ionomer's study reveals ionomer properties' importance and membrane compatibility on AEM water electrolysis performance. It displays the critical trade-off between ionic conductivity and catalyst utilisation of the ionomer on the one hand and SR, rigidity, and mechanical properties on the other hand, with SEBS-based ionomer having superior properties of the former and QPPO on the latter.

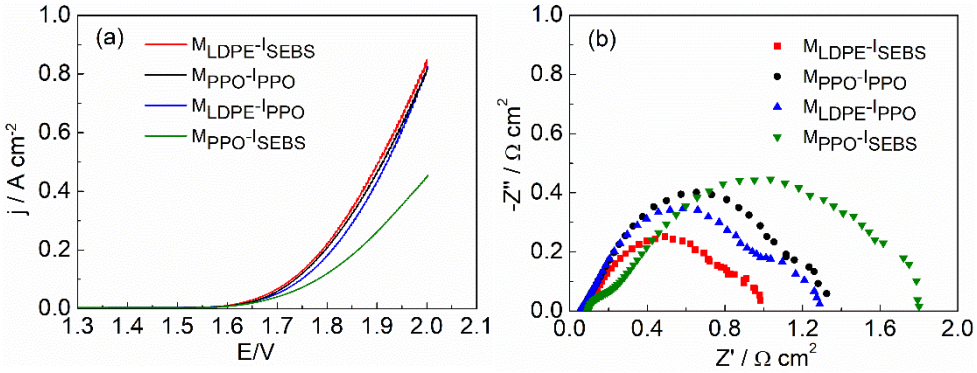

Figure 5.10 Polarization curves (a) and corresponding impedance data (b) of different combinations of membrane and ionomer. M_{LDPE}-I_{SEBS} means LDPE as membrane and SEBS as ionomer, M_{LDPE}-I_{PPO} means LDPE as membrane and PPO as ionomer, M_{LDPE}-I_{SEBS} means LDPE as membrane and SEBS as an ionomer. M_{PPO}-I_{PPO} means PPO as membrane and ionomer, and M_{PPO}-I_{SEBS} means PPO as membrane and SEBS as an ionomer. The tests were conducted in 0.1 M NaOH at 40 °C.

Table 5.7 The area-specific resistance of different membranes electrolysers.

Sample	M_{LDPE}-I_{PPO}	M_{PPO}-I_{PPO}	M_{PPO}-I_{SEBS}	M_{LDPE}-I_{SEBS}
ASR[a] / mΩ cm^2	116	104	184	150 [177]
CTR[b] / Ω cm^2	1.24	1.23	1.71	0.92

[a]The ASR means the area-specific resistance. The resistance was calculated at 1.7 V. Thickness of the hydrated LDPE-based membrane is 120 µm, and the thickness of the hydrated PPO-based membrane is 160 µm. [b]CTR means charge transfer resistance.

Apart from the comparison with the electrolyser performance with LDPE membrane. More PPO-based membrane and ionomer tests were conducted at different temperatures and alkaline conditions. Figure 5.11 shows the polarization curves and

the impedance with PPO as both membrane and ionomer. The test was conducted at 20 °C, 40 °C, and 60 °C and at 1 M NaOH.

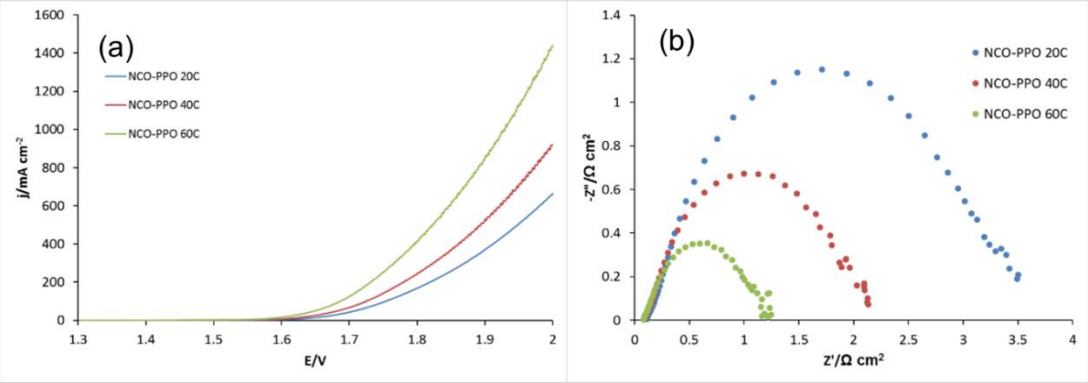

Figure 5.11 Polarization curves (a) and corresponding impedance (b) at 20 °C 40 °C and 60 °C in1 M NaOH. PPO was used as both membrane and ionomer.

Figure 5.11(a) shows that the temperature significantly affects electrolyser performance. When the current density reaches 100 mA cm^{-2}, the corresponding voltage for 20 °C, 40 °C and 60 °C is 1.754 V, 1.725 V and 1.686 V, respectively. When the voltage is at 1.75 V, the corresponding current density at elevated temperature is 95 mA cm^{-2}, 143 mA cm^{-2}, and 252 mA cm^{-2}. The area-specific resistances at 20 °C, 40 °C and 60 °C are 108 mΩ cm^2, 90 mΩ cm^2 and 80 mΩ cm^2, respectively. Their corresponding CTR is 3.49 Ω cm^2, 2.13 Ω cm^2 and 1.22 Ω cm^2. The increase in conductivity and activity with temperature is expected for thermally activated OH- ion conduction/diffusion and oxygen evolution reaction.

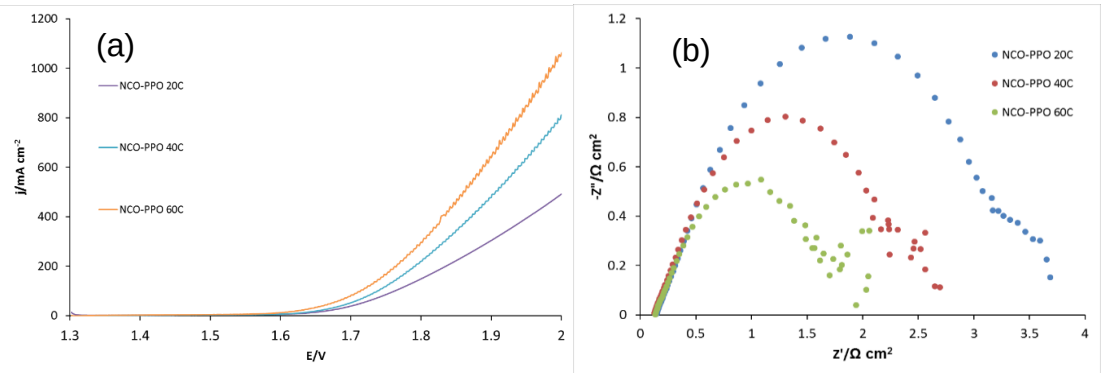

Figure 5.12 Polarization curves (a) and corresponding impedance (b) at 20 °C, 40 °C and 60 °C in 0.1 M NaOH. PPO was used as both membrane and ionomer.

The electrolyser performance at 0.1 M NaOH was also evaluated. As shown in Figure 5.12, the performance at different temperatures is similar to that when using 1 M NaOH. At 100 mA cm^{-2}, the corresponding voltage at 20 °C, 40 °C and 60 °C was 1.762 V, 1.737 V and 1.714 V, respectively. At 1.75 V, the current density at 20 °C, 40 °C and

60 °C was 84.74 mAcm^{-2},117.64 mA cm^{-2}, 166.56 mA cm^{-2}, respectively. The area-specific resistances at 20 °C, 40 °C and 60 °C were 144 mΩ cm^2, 126 mΩ cm^2 and 135 mΩ cm^2, respectively. Their corresponding CTR are 3.68 Ω cm^2, 2.69 Ω cm^2 and 2,04 Ω cm^2.

The electrolyser performance was also tested at 0.01 M NaOH. When the concentration of NaOH decreases to 0.01 M, the amount of mobile ions in the supporting electrolyte drops significantly, and OH^- conductivity is mainly facilitated by AEM and ionomer, resulting in worse performance than that at higher NaOH concentration. As shown in Figure 5.13, at 100 mA cm^{-2}, the corresponding voltage at 20 °C, 40 °C and 60 °C was 1.885 V, 1.826 V and 1.794 V, respectively. At 1.75 V, the current density at 20 °C, 40 °C and 60 °C are 40.59 mA cm^{-2}, 55.48 mA cm^{-2}, 73.68 mA cm^{-2}, respectively. The area-specific resistances at 20 °C, 40 °C and 60 °C are 285 mΩ cm^2, 250 mΩ cm^2 and 273 mΩ cm^2, respectively. Their corresponding CTR is 5.89 Ω cm^2, 4.69 Ω cm^2 and 4.46 Ω cm^2.

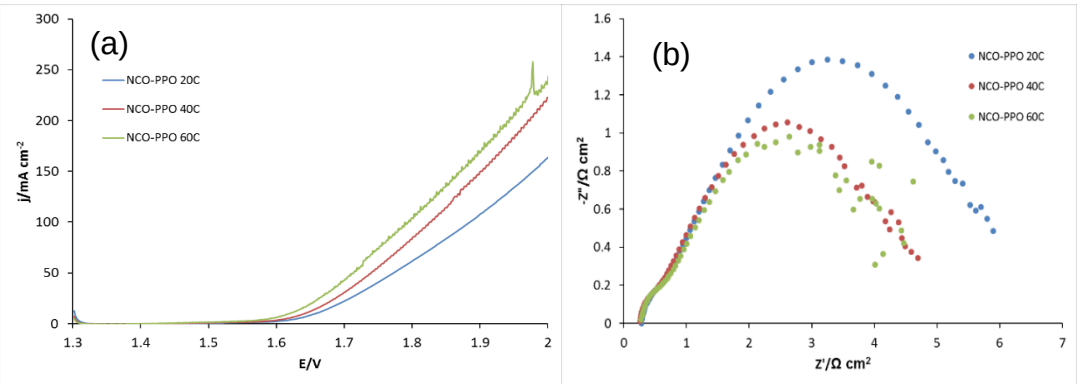

Figure 5.13 Polarization curves (a) and corresponding impedance (b) at 20 °C, 40 °C and 60 °C in 0.01 M NaOH. PPO was used as both membrane and ionomer.

5.11 Long-term tests

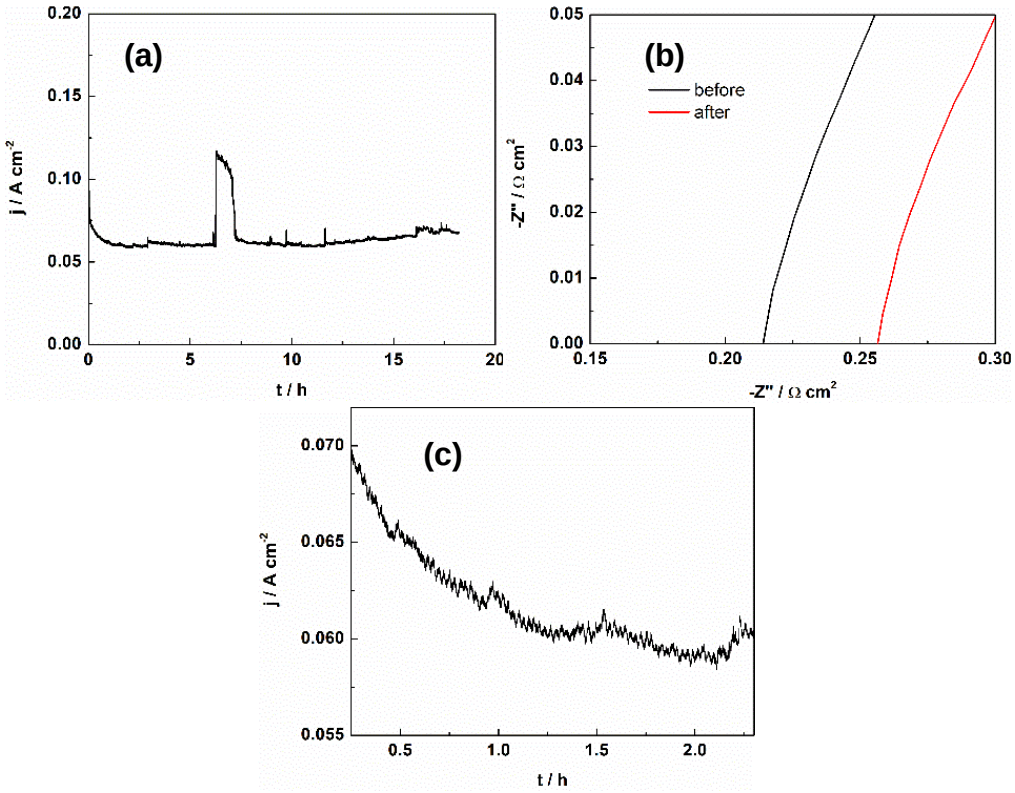

Figure 5.14 (a) Long-term test of PPO at 1.7 V in 0.1 NaOH at 40 ºC, (b) EIS of PPO before and after 18 h electrolysis tests. (c) The decrease of current density with time within the first two hours.

The long-term test was conducted in 0.1 NaOH at 40 ºC. As is shown in Figure 5.14(a), the current density decreases at the beginning within 2 hours and then becomes stable gradually. The gradual decay over 2 h can either be attributed to catalyst deactivation or dehydration of a small section of MEA due to poor liquid flow. Catalyst OER activity is the function of OH^- concentration (as seen above) and potential, which dictates surface coverage with OOH active groups. The current density at studied 1.7 V of 60-70 mA cm^{-2} is minimal compared to 800 mA cm^{-2} at 40 °C (Figure 5.12). This means that mass transport limitation, e.g., due to bubble or OH^- transport, is insignificant under understudied conditions. However, there was a sudden increase in current density from 60 to 120 mA cm^{-2} after 6 hours, followed by a sudden decrease at 7 hours. These sudden changes in performance are consistent with poor flow, e.g., similar to flooding characteristics seen in fuel cells on liquid build-up in part of electrodes/channels. The performance at 1.7 V during linear sweep (Figure 5.12) is consistent with the base current density of 60-70 mA cm^{-2}. This could suggest the cell design using a serpentine flow field designed for the fuel cell is not ideal for an electrolyser. Optimising flow field flow and electrolyte flow is beyond the scope of this work. However, it shows the significant role of MEA hydration on electrolyser performance and durability.

Bubble generation and flowing away affect electrolysis performance [223].

After the 18 h durability test, the area resistance increased by 18 %, from 0.22 mΩ cm^2 to 0.26 mΩ cm^2, as shown in Figure 5.14(b). The decrease of current density with time within the first two hours was fast (Figure 5.14(c)). Two main reasons might cause this. The first is the loss of the functional groups of AEMs due to OH^- nucleophilic attack. However, the rate of IEC loss seen above is significantly slower and can't explain the rate observed. The rate of IEC loss was 12 % and 57 % after 500 h at 25 and 60 °C, respectively. This average to an estimated loss of 35 % at 40 °C after 500 h or 1.26 % after 18 h. The other explanation is the combined effect of ionomer degradation, including oxidation (which was shown to promote degradation rates by over 5 times compared to N_2) and possible surface restructuring of spinel anode to less electrically conductive oxides.

Chapter summary

Quaternised Poly(2,6-dimethyl-1,4-phenylene oxide) (QPPO)-based anion exchange membranes were prepared successfully via Friedel-Crafts reaction using $SnCl_4$ as catalyst and 1,3,5-trioxane and chlorotrimethylsilane as 'environmentally friendly' chloromethylating reagents. The overlooked cross-linking side reaction during the chloromethylation process was analysed, and new equations to calculate the degree of chloromethylation (DC) and cross-linking degree (CLD) were proposed. QPPO-based membrane also showed good mechanical and thermal properties. The stress of break and elongation of QPPO-based membranes was found to be above 12 MPa. Alkaline stability tests were conducted in 1 M KOH at 25 °C and 60 °C for 500 h, revealing that the primary degradation occurred to the functional group rather than the backbone, with a 57 % loss of IEC. QPPO (2.2 mmol g^{-1}) was employed as membranes and ionomers in electrolyser tests, displaying good electrolysis performance. The area-specific resistance for MPPO-IPPO electrolysers was as low as 104 mΩ cm^{-2} at 40 °C and in 0.1 M NaOH solution, and the current density was 814 mA cm^{-2} when the potential was 2.0 V. QPPO shows promising potential as AEMWE membrane offering lower ASR and SR and consequently lower energy loss and stability towards membrane mechanical failure.

M_{LDPE}-I_{SEBS} gave the best performance among 4 studied combinations of membranes and ionomers of LDPE and SEBS. The combination of PPO membrane and SEBS ionomer resulted in the highest seen charge transfer resistance of M_{PPO}-I_{SEBS} of 1.71 Ωcm^{-2}. Besides, the temperature and alkaline concentration significantly affect the performance. Higher temperature and alkaline concentration are beneficial for

performance mainly due to improved OER activity instead of OH- conductivity. QPPO showed good stability over 18 h of testing with an increase in ASR by 18 %. Most of the performance loss was seen within the first 2 h of operation. Significant effects of electrolyte flow and flow distribution in a cell were seen on current density and possibly stability which should be studied in future studies.

Chapter 6. Degradation of PPO-based membrane

The chemical stability of the membrane has a significant effect on the durability of the electrochemical cell, e.g., electrolyser. AEM is exposed to considerable alkaline and oxidative stresses due to the attack of ions and radicals, which lead to the chain scission and loss of functional groups [164]. Due to chemical degradation, the membrane will become thinner and eventually be broken, failing to function as a gas and electrical separator. A lot of literature has studied the alkaline stability of various types of AEM in alkaline solutions. The primary degradation mechanism of the AEM TMA head group in alkaline media is explained clearly, as summarised in chapter 2, whereas oxidative media is still unclear. Oxidative stability is a vital factor in the durability of AEMs in a suitable water electrolyser environment. The chemical resistance of AEMs in the literature mainly focused on alkaline stability tests in N_2 saturated high temperature/high alkaline environment, which is not directly relevant to the electrolyser anode working environment. The practical working condition of AEMs is oxygen (and hydrogen) rich, nearly neutral-pH condition if deionised water is fed. According to the literature, there are several ways to evaluate the oxidative stability of polymers. However, the conditions are not consistent or standardised. Typically, oxidative stability can be assessed in air or oxygen-saturated DI-water, H_2O_2, or Fenton's solution. The primary methodology is to immerse the membrane in the oxidative media for a certain period. Then characteristic parameters are measured, such as the membranes molecular weight, tensile strength, weight, conductivity, or IEC losses.

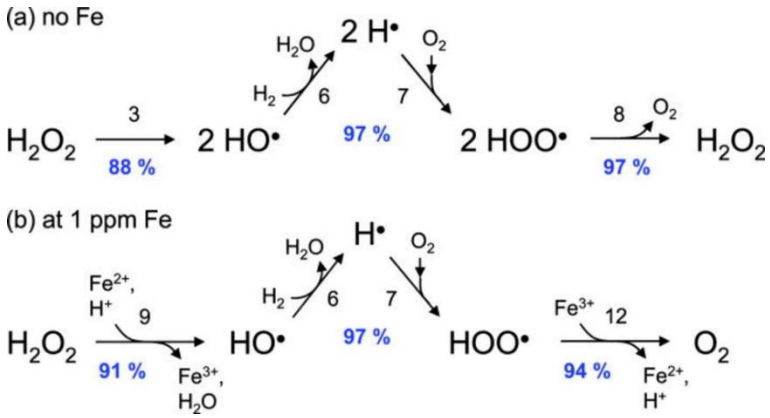

Figure 6.1 The main reaction pathways starting from H_2O_2. Reproduced with permission from [164]. Copyright (2011), The electrochemical society.

Both $HO^{\bullet}$ and $HO_2^{\bullet}$ are reactive oxygen species (ROS) with polymers and contribute to their degradation [166, 224]. The Fenton reaction is an effective oxidant of various organic substrates and can produce oxygen radicals. Fenton's solution (3 wt% H_2O_2 with 2 ppm Fe^{2+}) is prepared by adding Fe^{2+} into the H_2O_2 solution. The primary processes for radical generation are shown in Figure 6.1 [164]. However, radicals' lifetime, reactivity, and generation reaction rates are temperature-dependent. Unfortunately, even when using Fenton reagents for AEM oxidative stability study, these were done for different durations and temperatures, making the comparison difficult.

Table 6.1 The different testing methods of oxidative stability.

Membrane type	IEC (mmol g^{-1})	Ionic conductivity (mS cm^{-1})	Oxidative stability	Testing method
poly(ether ether ketone) (PEEK)[94]	1.15	14.63 (30 ^{o}C)	6.56 % loss in OH^- conductivity	in Fenton reagents at 80 ^{o}C for 1 h
poly(ether sulfone) PES [66]	1.54	30 (80 ^{o}C)	13 % loss in weight, the IEC decreasing from 1.54 to 0.93 mmol g^{-1}	in Fenton reagents at room temperature for 200 h.
poly (aryl ether ketone) (PAEK) [225]	1.35	12.3 (80 ^{o}C)	5 % loss in weight	in Fenton reagent at 80 ^{o}C for 3 days
poly(VBC-co-BMA-co-HFMA) (AQPVBH) [226]	0.232	10.9 (65 °C)	10 % weight loss	in Fenton reagent at 60 ^{o}C for 170 h
poly(vinylbenzyl chloride)-based composite membrane [22]	0.44	10 (60 °C)	7 % weight loss	In Fenton reagent at 60 ^{o}C for 25 h
	1.22	38.1 (60 °C)	53 % weight loss	In Fenton reagent at 60 ^{o}C for 25 h

*Fenton reagent in the literature here is 4×10^{-6} $molL^{-1}$ $FeSO_4$ in 3 wt % H_2O_2.

Apart from the methods shown in Table 6.1, other strategies were adopted to evaluate oxidative stability e.g., a visual approach to membrane integrity. Zhu and co-workers synthesised highly conductive and alkaline-stable AEMs-based on midblock-quaternised triblock copolystyrenes [21]. They tested the oxidation stability by immersing the membranes in the Fenton solution and observing the time when membranes broke into pieces and dissolved drastically. Liu and co-workers prepared a series of AEMs-based on chloromethylated polysulfone incorporated with quaternised graphenes [227]. The pristine membranes were soaked into a hot Fenton solution at 80 ^{o}C under stirring to examine the oxidative stability. The used Fenton reagent was refreshed every 4 hours. The deformation of the membranes was observed, such as changes to colour and physical shape. Xiong and co-workers synthesised quaternised cardo polyetherketone AEM [92]. The oxidative stability was

measured by measuring the weight loss at given time intervals after immersing the samples in a 3 wt% H_2O_2 solution at 60 ^oC. After 168 h, the weight loss of the pristine and quaternised membranes was 3 % and 2.1 %, respectively. Maurya and co-workers prepared vinylbenzyl chloride (VBC)-based AEM crosslinked by divinylbenzene (DVB) using polyethylene (PE) substrate with different functional groups for vanadium redox flow battery [22]. They incorporated different functional groups with the same anion exchange composite membranes, such as ammonium, diammonium, and phosphonium types. Richard et al. studied the oxidative stability of LDPE-based AEMs with vinylbenzyl chloride (VBC) grafts. They found the loss of the functional group and the VBC group [152].

Fu et al. prepared a PPO-based blend of proton exchange membranes by mixing n-propylamine ($PrNH_2$)-neutralized SPPO. They studied the oxidative stability of pure PPO and blended membranes. The pure PPO experienced 2 % weight loss after 1 day in the Fenton solution at 50 ^oC. The weight loss was over 40 % after 1 week. The blend membranes fared much better in this regard. The weight loss after 1 week was 9% for PPO-10 and 5 % for PPO-30.

In this chapter, oxidative stability tests were conducted. The degradation mechanism of PPO-based membranes was studied and discussed. The insights gained provide a better understanding of the degradation process of PPO-based membranes in a neutral environment and guidelines for structural design and modification of AEMs to improve the stability against radical-induced ageing. The change of weight and IEC were recorded. The membranes were tested in different solutions for oxidative stability, including H_2O_2 solution, Fenton solution, and DI water.

To study the effect of the environment on the degradation of AEMs, the oxidative stability will be tested in three different conditions by immersing the membranes in N_2 purged H_2O_2 solution and Fenton reagents (4×10^{-6} mol L^{-1} $FeSO_4$ in 3 % H_2O_2) and air-saturated DI water, separately. The samples were sealed in plastic test bottles to minimize exposure to atmospheric CO_2, which can react with OH^-counterion to produce carbonate/bicarbonate. Because oxidative degradation is affected partly by OH^- conversion to OH radical, it is essential to keep OH^- counter-ion concentration as constant as possible during the test to reduce its effect on the degradation rate. QPPO-6 (DC_2 29.5 %, CLD 4.7 %) was utilised to test oxidative stability.

6.1 Oxidation stability of AEM backbone

Several in-house and commercial polymer membranes and their functionalised chloromethylated and quaternised (headgroup) were immersed in a Fenton solution at 60 ^{o}C for 25 h. The loss of weight is shown in table 6.2.

Table 6.2 The properties of different membranes in Fenton solution at 60 ^{o}C for 25 h.

Membrane	Initial weight (mg)	Final weight (mg)	Weight loss (%)
FAA-3-30 (1.45mmol g^{-1})[a]	110.3	91.5	17.0
FAA[a]	238.1	217.1	8.8
SEBS[b]	246.3	245.5	0.3
PPO[c]	252.3	245.3	2.8
ClPPO (This work)	191.4	188.3	1.6
LDPE[b]	172.9	177.9	0.73
QPPO (1.3 mmol g^{-1}, this work)	151.6	106.4	29.8

[a] The commercial membranes
[b] The pristine membrane
[C] The membrane prepared by the pristine PPO polymer

The pristine polymers (backbone), such as FAA, SEBS, PPO, and LDPE, showed very slight weight loss after 25 h. This means they exhibit good oxidation stability. It is worth mentioning. However, that pristine PPO had slightly higher weight loss than LDPE and SEBS. Interestingly, adding the functional cholormethylated group to PPO didn't increase its oxidation stability but improved it, possibly due to the addition of chlorine. Chlorinated polyethetylene polymers have superior oxidation resistance and chemical resistance toward ozone. However, after quaternisation (head group addition), FAA-3-30 (1.5 mmol g^{-1}) and QPPO (1.3 mmol g^{-1}) showed significant weight loss and reduction in their oxidative stability. The weight loss seen cannot be explained by the loss of the head group alone. Notably, the membranes were broken into small pieces suggesting significant damage to the backbone and chain session. The degradation mechanism will be studied further below.

6.2 The effect of IEC on the degradation in H_2O_2 solution

Table 6.3 The comparison of PPO-based membrane with different IEC after degradation test

Sample	H_2O_2 Concentration (wt%)	Temperature (^{o}C)	Initial IEC[a] (mmol g^{-1})	Degradation Time (h)	IEC loss (%)	Weight loss (%)
QPPO-5	0.5	60	1.7	1	5%	9%
QPPO-6	0.5	60	1.3	1	6%	4%

[a] Error range: ±0.1

The effect of the IEC on degradation was studied. As shown in table 6.3, PPO-based membranes with different IEC of 1.7 and 1.3 mmol/g at the fixed crosslinking degree of 5 % were immersed in 0.5 wt% H_2O_2 solutions. After 1 hour, QPPO-5 and QPPO-5 lost the same level of IEC of ca. 6 %. For mass loss, QPPO-5 lost nearly twice as much mass as QPPO-6. If the lost mass is only caused by headgroup loss, then the estimated loss in QPPO-5 should be a factor of 1.3 of that of QPPO-6. The significantly higher factor of 2 suggests that backbone loss might also occur. Notably, an increase in IEC promotes oxidative degradation. This could be due to a more significant swelling ratio/water uptake and consequently improved mass transport of ROS in water channels to attack sites or the negative effect of charge distribution in on AEM backbone stability from the addition of a positive headgroup or headgroup catalytic/ mediator role in the acceleration of ROS attack of vulnerable AEM sites.

6.3 The effect of H_2O_2 concentration on QPPO AEM degradation

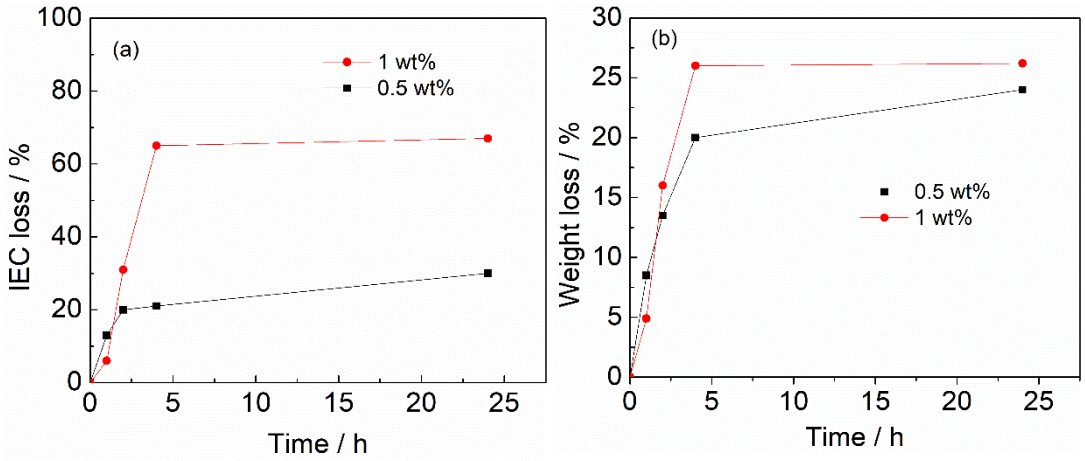

Figure 6.2 (a) IEC loss and weight loss of QPPO-based membrane in 0.5 wt%, 1 wt% H_2O_2 concentration at 60 °C.

Apart from different IEC, the effect of H_2O_2 concentration on the degradation was also investigated. The initial IEC of the PPO-based membrane is 1.6 mmol $g^{-1,}$ and the average initial weight was between 110 to 120 mg.

Figure 6.2(a) illustrates the IEC loss of QPPO-based membrane during degradation in 1 wt % and 0.5 wt% H_2O_2 solutions. Given that the studied reaction temperature was 60°C where the rate of H_2O_2 decomposition can be rapid, it can only be assumed that H_2O_2 concentration in solution remained constant for short periods below 5 h. The change of H_2O_2 concentration due to reaction with AEM polymer can be neglected due

to the small mass of membrane sample used. It can be seen from Fig 6.2(b) that the rate of mass loss or backbone degradation wasn't affected significantly despite doubling H_2O_2 concentration with mass loss of ca. 25 % after 4 h. Given the observation above on backbone/mass loss rate increase with an increase in IEC, this suggests that the headgroup controls the rate-limiting step. In other words, the reaction can be catalysed by the headgroup or by other polymer locations activated on the headgroup introduction. It could also suggest that there are two parallel degradation mechanisms. One involves oxidation of the head group. The other requires weight loss, which is not due to oxidation but due to polymer fragmentation and dissolution, as discussed in detail further below in section 5.2. On the other hand, Figure 6.2(a) shows a strong correlation between the degradation rate of IEC and H_2O_2 concentration. Reaction order above 1 was seen.

After 4 hours, there were remarkable IEC loss differences by a factor of >3 (20 % vs 65 %), close to that of second-order reaction when the QPPO-based membrane degraded in 1 wt% H_2O_2 than in 0.5 wt% H_2O_2. This can be since H_2O_2 decompose into 2 OH radicles which in turn carry out the degradation reaction, possibly attacking two headgroup locations.

The rapid loss of head groups of ca. 68 % after 4h in 1% H_2O_2 shows the vulnerability of benzyl or aryl trimethylammonium to oxidative attacks. Previously, it has been demonstrated that the benzylic carbon linking the tethered head group is a vulnerable point. From the results, it can be concluded that the slower degradation of the backbone is most likely caused by the negative effect of charge distribution on AEM backbone stability from adding a positive headgroup.

The larger swelling ratio/water uptake and consequently improved mass transport of ROS in water channels can be excluded as higher H_2O_2 concentration didn't increase the mass loss rate. Similarly, the headgroup catalytic/ mediator role in accelerating ROS attack of vulnerable AEM sites is unlikely to be the cause. Otherwise, effect of headgroup loss of ca. 68% should have been seen on the rate of mass loss after 4h unless the effect continues to take effect in solution if headgroup is lost as the whole aryl trimethylammonium as has seen detected in radiation grafted LDPE AEMs [20].

6.4 Comparison between QPPO and LDPE-based membrane

A membrane with excellent oxidation resistance will increase the lifetime of AEMWE. LDPE-g-VBC-TMA, previous AEMs synthesised by our groups, were used as the benchmark. LDPE-g-VBC-TMA showed a high ion conductivity (101 mS cm^{-1} at 60 ^oC) at high IEC (ca. 2.8 mmol g^{-1}). At the same time, the OH^- conductivity of SEBS was

140 mS cm^{-1} at 50 °C when its IEC was 1.9 mmol g^{-1}. As stated above, chemical stability is vital for membranes to guarantee the lifetime of a water electrolyser, especially oxidative resistance.

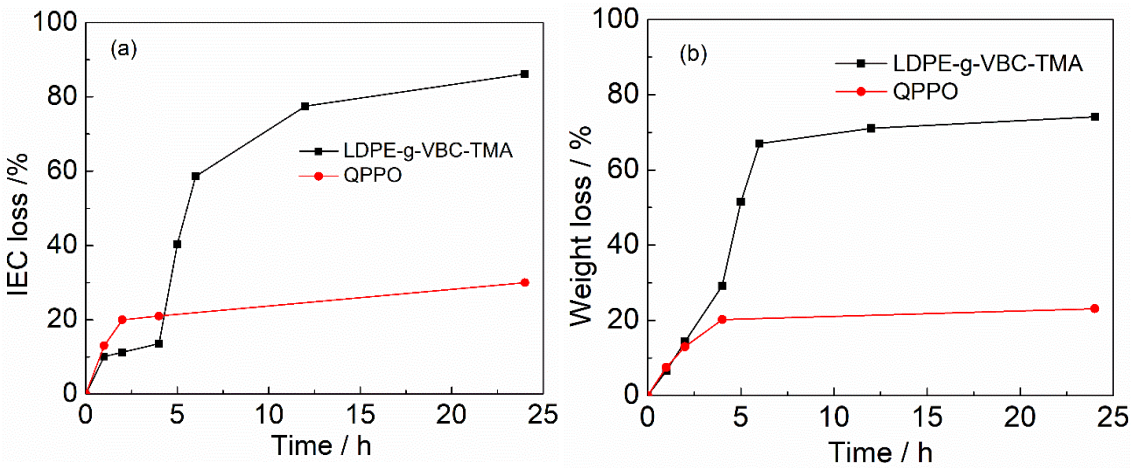

Figure 6.3 IEC (a) and weight loss (b) of LDPE-g-VBC-TMA and QPPO-based membrane in 0.5 wt% H_2O_2 at 60 °C.

Figure 6.3 shows the IEC and weight loss of LDPE-g-VBC-TMA and QPPO in 0.5 wt% H_2O_2 for a different time at 60 °C. Initially, the IEC loss of LDPE-g-VBC-TMA increased slowly. Then there was a sharp decrease within 12 h at the beginning. After 24 h, the IEC became 0.36 mmol g^{-1} and lost almost 85 % of the initial [152]. However, QPPO showed a slower rate of IEC. It only lost around 4 % after 2 h and remained ca. 85 % after 24 h. This observation suggests that the QPPO structure might be more oxidative stable than VBC-TMA due to a lack of benzylic carbon, resulting in a chain session of the VBC-TMA head group. Another factor contributing to a higher IEC loss rate in LDPE-VBC-TMA AEM is that the membrane is radiation grafted. Hence, depending on graft length, there will be a significant loss of head group per ROS attack compared to QPPO AEM. LDPE-VBC-TMA has higher IEC, which results in higher IEC rate loss, as seen and discussed above.

The weight loss of both studied AEMs had a similar trend as the IEC loss. The weight loss of LDPE-g-VBC-TMA was rapid in the first 6 h, reaching 68 %. After 24 h, only 25 % of the membrane's initial weight remained. The weight loss for PPO was approximately half that of LDPE-g-VBC-TMA with 35 % weight loss after 24 h. This can be explained by the higher oxidative stability of aromatic QPPO-based AEM. As discussed above, the stability of the backbone will be altered on functionalisation; however, QPPO remains more oxidation resistant than LDPE-VBC-based AEM.

6.5 Long-term oxidative stability test in DI water

To further test the oxidative stability in a neutral environment for the long term, QPPO-14-based membranes were immersed in DI water at 60 ^{o}C for 10 months. The morphological changes in the membranes are shown in Figure 6.4. Figure 6.4(a) shows the original transparent QPPO-based membrane. (b) and (c) reveal the membrane immersed in 1 M KOH solution, which broke into small pieces, while (d) and (e) show the membrane immersed in DI water which became water-soluble and fully dissolved in DI water after 10 months. It is common for Ion exchange polymers to lose some mass with time when immersed in water. This is because of the highly hydrophilic nature of the head group. Even commercial perfluorinated polymers with a low IEC of 0.91 mmol g^{-1} (Nafion or SPEEK) undergo weight loss due to water solubility with time, especially at elevated temperatures. As discussed, the solubility can be reduced by reducing IEC and increasing cross-linking. Both samples underwent a colour change (brown) from yellow, suggesting an ageing process [228]. The result illustrated that the backbone of PPO in DI water suffered a more severe fracture than in just the functional group. It wasn't possible to carry on other tests, for example, change in IEC, as the membranes became too brittle after the degradation test and broke into pieces.

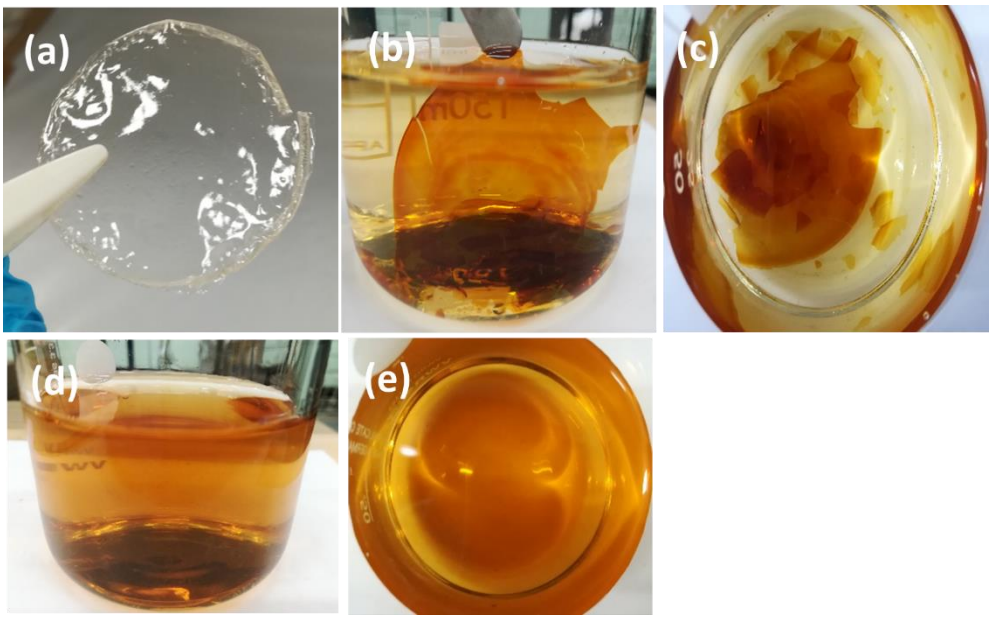

Figure 6.4 Morphological comparison of original QPPO (a), QPPO after degradation test in 1 M KOH solution (c and d) and DI (c and d) at 60 ^{o}C for 10 months.

To understand the degradation mechanism further, structure characterisation was conducted, including FTIR and NMR.

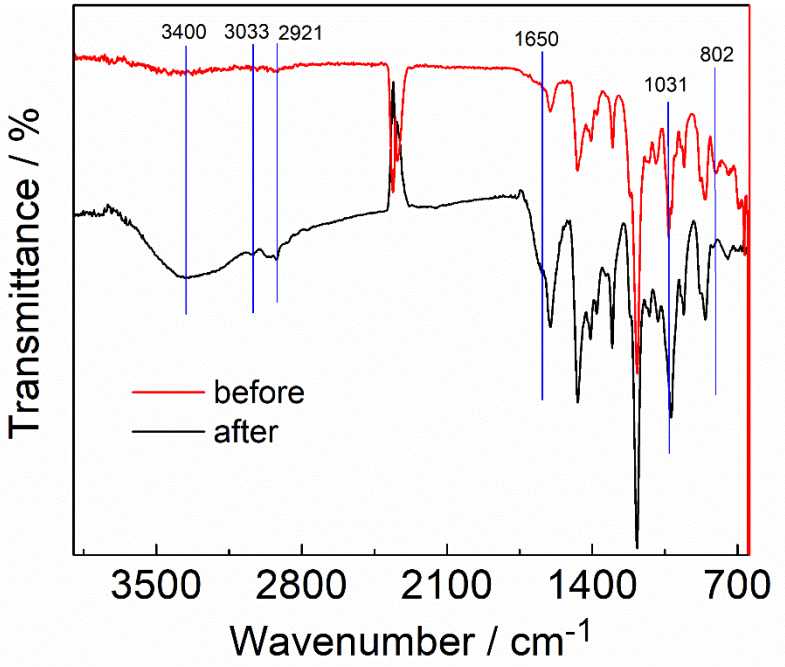

Figure 6.5 FTIR of the QPPO-based membrane before and after the chemical stability test in DI water for 10 months.

As is shown in Figure 6.5, QPPO-based membrane before and after the chemical stability test in DI water for 10 months was characterised by FTIR. The peak at 802 cm^{-1} is the C-H bending of benzene ring. The peak at 1031 cm^{-1} is the C-O stretching vibration of the ether group [229]. The new broad peak round 3102-3423 cm^{-1} is assigned to hydroxyl groups (O-H), and the new peak at 1650 cm^{-1} is the C=O of the carbonyl group [230, 231]. The carboxyl group might be obtained from the oxidation of PPO-based membrane after the ylide rearrangement. Apart from the FTIR, NMR was also adopted to characterise the degradation process. The evidence of CH2-C=O can also confirm it in C NMR at 23 ppm, which can be found in the following discussion section. The structure of QPPO is shown in Figure 6.6(a). After the degradation test, the degraded sample was characterised by solid-state ^{13}C NMR (SSNMR). As is shown in Figure 6.6(b), these two spectra almost entirely overlap. One new peak was observed at 160 ppm after degradation, designated to carbonyl (C=O). The small peak around 40 ppm aromatic-CH_2-Cl, which is a small amount of the polymer that TMA couldn't reach. It is relatively large, showing a considerable amount of chloromethylated group was not quaternised. This can explain why IEC is lower than theoretical values. There is a new peak at around 45 ppm, which should also be similar to C-aromatic. The small hump peak around 30 ppm corresponds to Ph-CH_2-Ph of crosslinking.

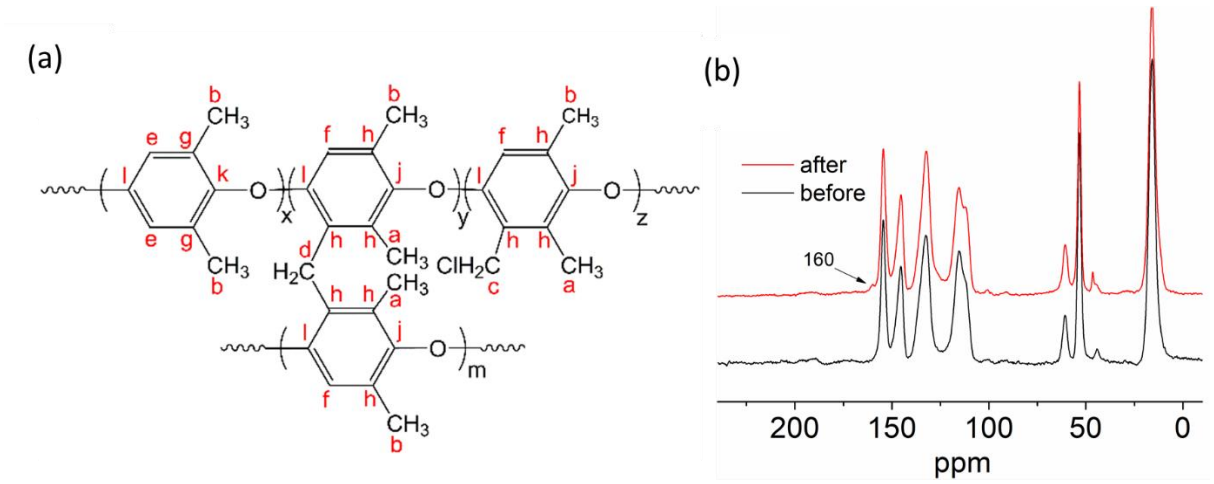

Figure 6.6 (a) The structure of QPPO and corresponding carbon shift (b)The solid-state NMR of QPPO-based membrane before and after degradation test.

To further analyse the changes in aged samples, more characterisations were conducted. Figure 6.7(a) shows the ^{13}C NMR of QPPO dissolved in DMSO-d_6 before the degradation test, which has almost the same peaks as those seen in ^{13}C solid-state NMR (Figure 6.6(b)). As is shown in Figure 6.7(a), the signal between 116 ppm to 155 ppm corresponds to the aromatic carbon in the benzyl ring. The signal at 61 ppm was assigned to the benzylic carbon of head group C-N [232].

The signal at 40 ppm is that of Ar-CH_2-Cl, suggesting despite immersion in TMA solution, not all the chloromethylated group could be reached, reacted and quaternised, which explains the lower IEC measured compared to the estimated theoretical value as seen in section 5.3.

The signal at 53 ppm corresponded to the C-N of methyl groups of TMA. After the degradation test, the remaining broken solids of the membrane were extracted/filtered and dissolved in DMSO-d_6 and characterised by ^{13}C NMR. Figure 6.7(b) that of the remaining degraded AEM sample after dissolving in DMSO-d_6, and Figure 6.7(c) shows ^{13}C NMR of the H_2O solution used for the degradation study containing soluble degradation products and compared with Figure 6.7(a), newly peaks around 173&181 ppm appear in the dissolved degradation products, corresponding to carboxylic carbon C=O carboxylic acid and aldehyde, respectively. The signal at 23 ppm is due to H_2C-C=O aliphatic carbon adjacent to the carbonyl carbon. Interestingly, the signal at 40 ppm corresponding to the chloromethyl group has disappeared, while the quaternary ammonium group at 55 and 61 remained. This suggests that part of the QPPO polymer is water-soluble or becomes water-soluble and dissolved in solution with the headgroup. In addition, there is a soluble oxidation product producing a carboxylic acid group detected. The solid fraction remaining of AEM after the degradation test seems

to be the same as that of unaged QPPO with an unreacted chloromethylated group (40 ppm). This suggests that QPPO contains two segments. One has higher quaternisation of chloromethylated group and hence highly charged and hydrophilic, resulting in water solubility with time at higher temperatures. The other section contains a higher fraction of unquaternised chloromethyl group, which remained solid. The loss of a soluble segment of QPPO results in membrane breakage in smaller pieces containing the water-insoluble fraction with lower quaternisation.

It can be concluded that there are two degradation processes involving weight loss due to fragmentation of QPPO where fragments with higher quaternisation (amination of introduced chloromethylated groups) and higher hydrophilicity become water-soluble leaving behind fragments with lower quaternisation with a higher proportion of un-aminated chloromethylated PPO. The other degradation mechanism involves IEC loss. This involves the established yield formation in addition to $OH^{\cdot}$ radicals' formation. As shown in Figure 6.8, the ylide formation proceeds for Stevenson rearrangements to produce N,N-dimethyl-phenylethylamine resulting in seen loss of IEC. The ethylamine group contains vulnerable beta carbon (ethyl group), which can undergo oxidation to form a carbonyl group (aldehyde), which can oxidise further to form a carboxylic group which was observed. The 1H NMR of the residual degradation solution was also tested. The signals were not clear due to the influence of the DI water. The hump signal around 2.1 ppm is expected to be C-H of amine.

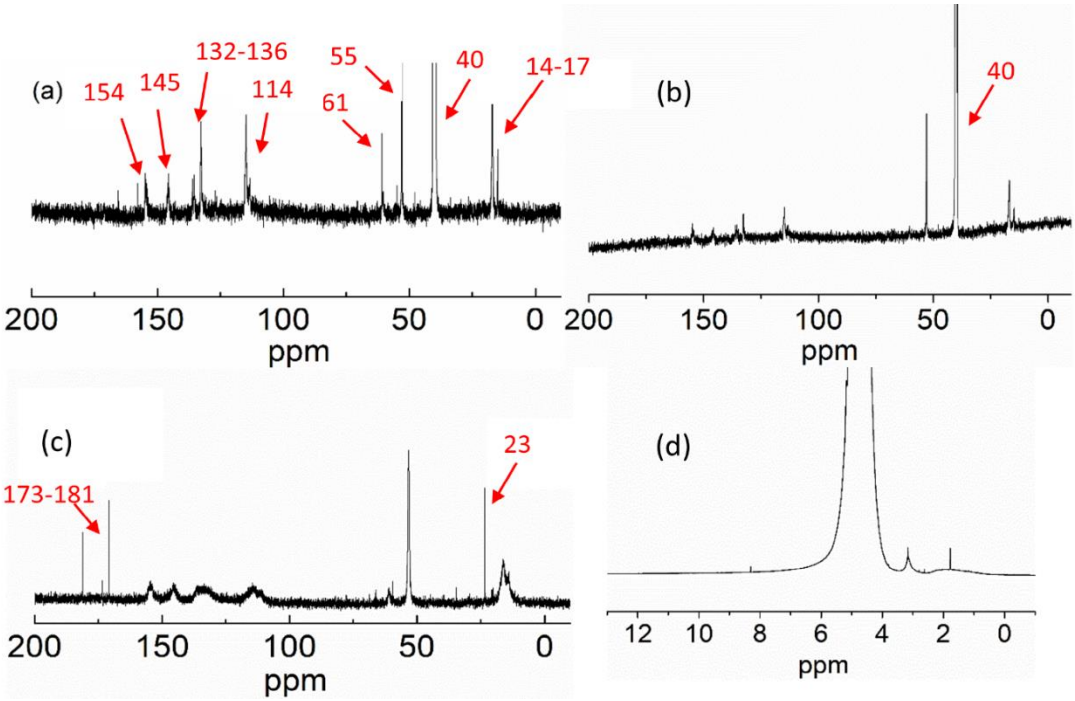

Figure 6.7 ^{13}CNMR of (a) QPPO before degradation test, (b) extracted sample after degradation test (c) the residual degradation solution and (d) the ^{1}H NMR of the residual degradation solution.

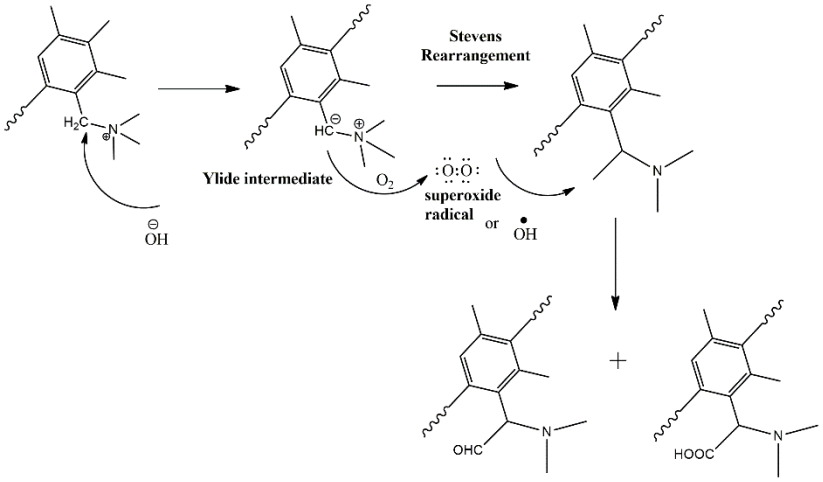

Figure 6.8 The degradation mechanism of QPPO-based membrane [152, 160].

The oxygen or OH radical attacks the methyl group on the rearranged ylide and forms aldehyde or carboxyl attached to the CH2 group, explaining the NMR signatures.

Chapter summary

Despite extensive studies on the alkaline stability of AEMs, the degradation mechanism of AEMs in oxidative media is neglected. This chapter tested the oxidative stability of different membranes in a Fenton solution at 60 ºC at room temperature for 25 h. The pristine LDPE, PPO and ClPPO showed good oxidative stability (weight loss of less than 2 %). After functionalisation, the QPPO-based membrane suffered ca. 29 % mass loss. The oxidative stability was tested in H_2O_2, Fenton solution and DI water. The effect of IEC and H_2O_2 concentration on QPPO AEM degradation were studied. More considerable swelling ratio/water uptake and consequently improved mass transport of ROS in water channels to attack sites, or adverse effect of charge distribution on AEM backbone stability from the addition of positive headgroup, or headgroup catalytic/ mediator role in the acceleration of ROS attack of vulnerable AEM sites. Compared with LDPE-based membrane, QPPO-based membrane shows better oxidative stability. The degradation mechanism of PPO-based membrane under DI water conditions was studied. The residual degradation solution and extracted sample after the degradation test were characterised by NMR. The possible degradation mechanism is that oxygen or OH radicals attack the methyl group on the rearranged ylide, forming aldehyde or carboxyl attached to the CH_2 group.

Chapter 7. Preparation and characterisation of QPPO/PTFE composite membrane

As one of the vital roles in anion exchange membrane water electrolysers (AEMWE), anion exchange membranes work as the barrier between evolved oxygen and hydrogen gases to avoid their direct mixing and provide an ionic conduction path to transport OH^- from cathode to anode. AEMs are expected to demonstrate good comprehensive properties, including high ionic conductivity, durable mechanical strength, and good chemical resistance. However, it is difficult for the stand-alone homogenous anion exchange membrane to simultaneously meet all these requirements and long-term operation. Therefore, modification strategies to AEMs were taken into consideration to meet these requirements. These include composite membrane structures, such as sandwich and pore-filled structures [233-235]. There are several methods to prepare the composite membrane, including the physical blending method, sol-gel method, infiltration method, in situ polymerization method, interfacial polymerization method, etc. among which, physical blending method attracts most of the attention due to the wide availability [236]. In this method, the filler and substrate were prepared separately. The filler was physically dispersed into the polymer substrate by melting or solution blending. Then the composite membrane was obtained after polymer solidification. According to the substance introduced, the composite membrane can be divided into organic, inorganic and hybrid enhancement. Yang et al. prepared a solution casting method poly(vinyl alcohol)/3-(trimethyl ammonium) propyl-functionalised silica (designated as QPVA/Q-SiO_2) composite polymer membrane. Wu et al. reinforced the polytetrafluoroethylene-based membrane by using PTFE. The ionic conductivity of the composite membrane was not as good as the pristine polymethacrylate membrane (25 S cm^{-1} VS 0.018 S cm^{-1} at 20 ^oC).

Different methods are reported to enhance the mechanical properties of PPO-based composite membranes. Rathod et al. prepared functionalised boron nitride/PPO-based composite AEM for water desalination, exhibiting excellent thermal and mechanical stability. With ionic conductivity of 6.3×10^{-3} S cm^{-1} at IEC 1.92 mmol g^{-1}. The stress for 5 wt% composite membranes is 37.14 MPa, 28% higher than 28.90 MPa exhibited by virgin QPPO membrane [237]. To improve the comprehensive properties of the AEMs, Chen et al. prepared the sandwich structure of the composite membrane. They introduced the 1,2-dimetylimidazolium-modified silica (ImSiO_2) to triple-ammonium side-chain PPO-based (TA-PPO) membrane. The Im-SiO_2/TA-PPO composite

membrane exhibits higher hydroxide conductivity and good dimensional stability. The maximum hydroxide conductivity reached 0.1 S cm^{-1} at 80 ^{o}C, and the swelling ratio is 8.2 % [238]. For the composite membrane, the effective conductivity of the porous membrane can be obtained via the Bruggeman relationship, which

To enforce a PPO-based membrane, polytetrafluoroethylene (PTFE, thickness 50 μm, 68% porosity, pore size 0.5 μm) was utilised as the matrix in this study. QPPO-14 (DC_2 49 %, CLD 1.9 %) was chosen to prepare the QPPO/PTFE-based composite membrane due to its good ionic conductivity.

Results and discussion

7.1 QPPO/PTFE composite membrane

0.5 g ClPPO (ClPPO-14) was dissolved in THF to prepare the impregnation solution (14 wt%). The PTFE porous membrane (pore size 0.5 μm) was immersed into the impregnation solution under ultrasonic vibration for 2 min to ensure the even distribution of the solution in the pores of the PTFE membrane substrate. As is shown in table 7.1, the weight of PTFE increased from 98 mg to 113 mg, and the thickness increased from 70 μm to 76 μm after immersion in impregnation solution and drying off the solvent. The density of the ClPPO is ca. 1.1 mg cm^{-3}. The area of PTFE is 6.5 cm^2.

Table 7.1 Parameter of PTFE and PPO/PTFE composite membrane.

	PTFE	QPPO/PTFE composite membrane
Weight (mg)	98	113
Thickness (μm)	70	76

This means there is a total of ca. 6 μm layer of ClPPO covering the PTFE membrane surface divided between the two faces of the PTFE membrane. This layer is not homogeneously covering the entire PTFE surface, as shown in Figures 7.1 (c) & (d) where some of the PTFE pores in some sections of the membrane remain visible. The remaining ClPPO also partially fill the available pores in the PTFE. The percentage of pores filled is equivalent to 31.4 % volume of the available pores considering the manufacturer's reported porosity of 68%. This means that the volume fraction of ClPPO in the composite membrane is around 21.4 %.

Tortuosity (τ) describes the sinuosity of the pore space and influences flux transport in porous media [183, 239]. In porous membranes, high tortuosity normally reflects a long transport path. The tortuosity factor can be obtained via the reciprocal of porosity, 1.5 in this case [240-242]. For the composite membrane, the composite membrane's

anticipated conductivity compared to that of homogenous PPO-based AEM would be a factor of 0.1 ($0.21^{1.5}$), which can be obtained from the porosity to the power of tortuosity [239, 243, 244].

Future work should focus on the impregnation and fabrication process to achieve higher filling values by using a higher impregnation solution.

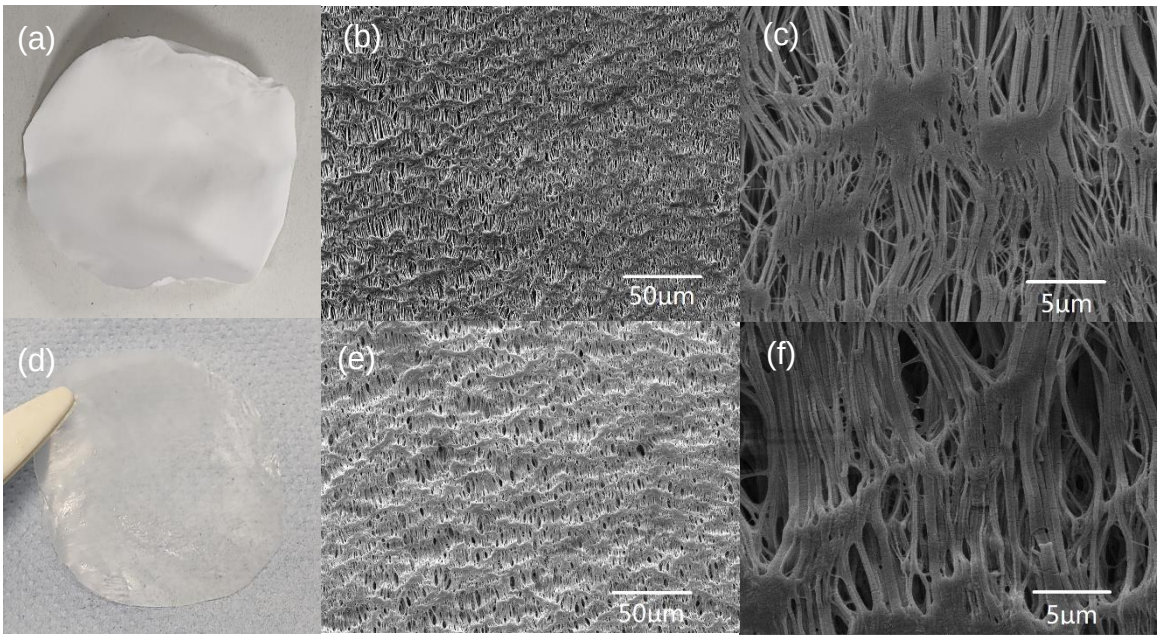

Figure 7.1 (a) unfilled PTFE and its the SEM surface morphology of pure PTFE membrane (b) 1kx, (c)10kx. (d) the ClPPO impregnated PTFE membrane and the SEM surface morphology of pure PTFE membrane (c)1kx, (d)10kx.

The pure PTFE is hydrophobic, while the QPPO/PTFE composite membrane becomes hydrophilic due to the high hydrophobic property of QPPO. As is shown in Figure 7.1, the fibres of PTFE are apparent and separated from each other. The threads seem to congregate together upon ClPPO impregnation, where ClPPO acts as the binder. The PTFE is the continuous phase, and the QPPO is the disperse phase.

7.2 Thermal stability

Figure 7.2 shows the TGA studying the stability of the composite QPPO/PTFE membrane. QPPO/PTFE composite membrane exhibited good thermal properties. QPPO than the PTFE support limited the thermal stability as anticipated. The apparent decomposition seen at 350 °C in PPO is due to the degradation of the head group [202]. Finally, the second stage of weight loss at around 480 °C can be assigned to the backbone chain decomposition of QPPO. The rapid decomposition >500 °C is that of PTFE and QPPO. Because of the lower wt% of QPPO in the composite membrane of 13 wt%, the weight loss caused by QPPO decompaction is much lower than that of

pristine QPPO. This explains that at temperatures below 500°C, the weight loss of composite membrane was below 10 % compared to 60 % for QPPO 14. in other words, the anticipated loss in composite membrane would have been only 13 % of the 60%, which is under 8 %.

There is a slight mass loss (<5 %) below the temperature of 150 °C, which is attributed to inner water loss from the polymer [201]. As discussed earlier, the components of PPO in the composite membrane show good water uptake. Before the thermal stability tests, the membranes were thoroughly dried in a vacuum oven at 60 °C. The PPO materials rapidly absorbed water from the air during sample transfer to the TGA instrument.

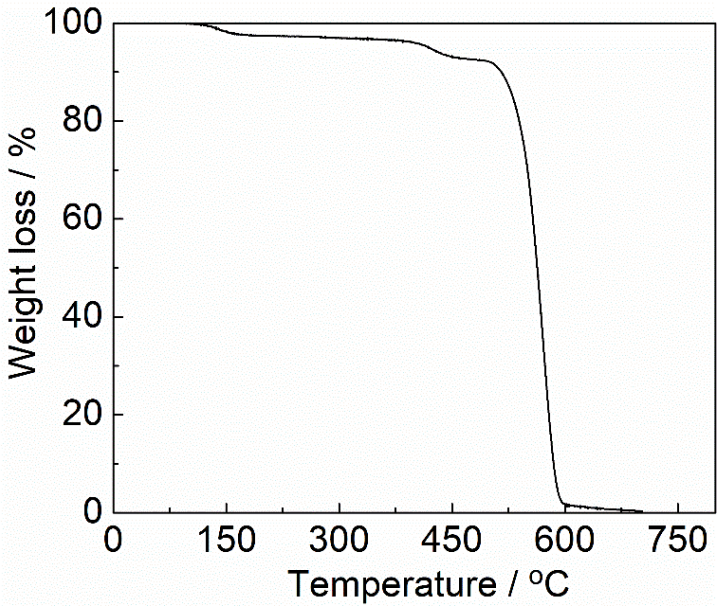

Figure 7.2 TGA of QPPO/PTFE-based membrane

7.3 Mechanical properties

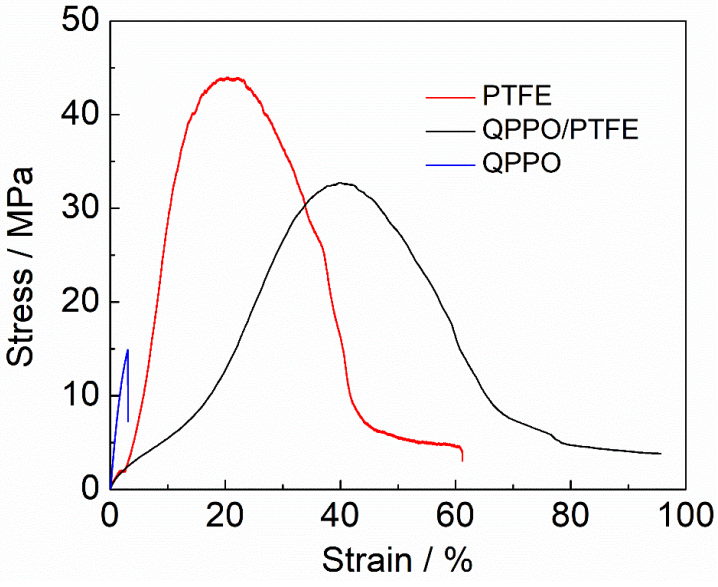

Figure 7.3 mechanical properties of QPPO (wet), PTFE (dry), and QPPO/PTFE (wet)-based membranes as dry samples.

The mechanical property of the QPPO/PTFE composite membrane was tested and compared with pristine PPO and porous PTFE membranes. As is shown in Figure 7.3, the tensile strength of PPO/PTFE-based composite membranes was significantly higher than that of homogenous PPO. Tensile strength increased from 14 MPa for Q-PPO AEM to 33 MPa for Q-PPO/PTFE AEM. The pristine porous PTFE-based membrane showed excellent mechanical strength and good elongation at break of 43 MPa and 60 %, respectively. The pristine PTFE membrane is hydrophobic, and the PTFE membrane used to test mechanical properties was dry. For the QPPO/ PTFE composite membrane, the membrane becomes hydrophilic in the presence of QPPO. The water inside the composite membrane among PTFE fibre chains can act as lubricants, improving membrane flexibility (elongation at break increased to 96 % from 60 % for PTFE alone) but resulting in a reduction in tensile strength from that of PTFE of 43 to 33 MPa for composite membrane. Good flexibility keeps the membrane from breaking under mechanical stresses, especially in the presence of electrolyser clamping force. The enhancement of tensile strength over pristine QPPO should result in more extended durability under mechanical stresses and, consequently, a longer lifetime of the electrolyser.

7.4 Ionic conductivity

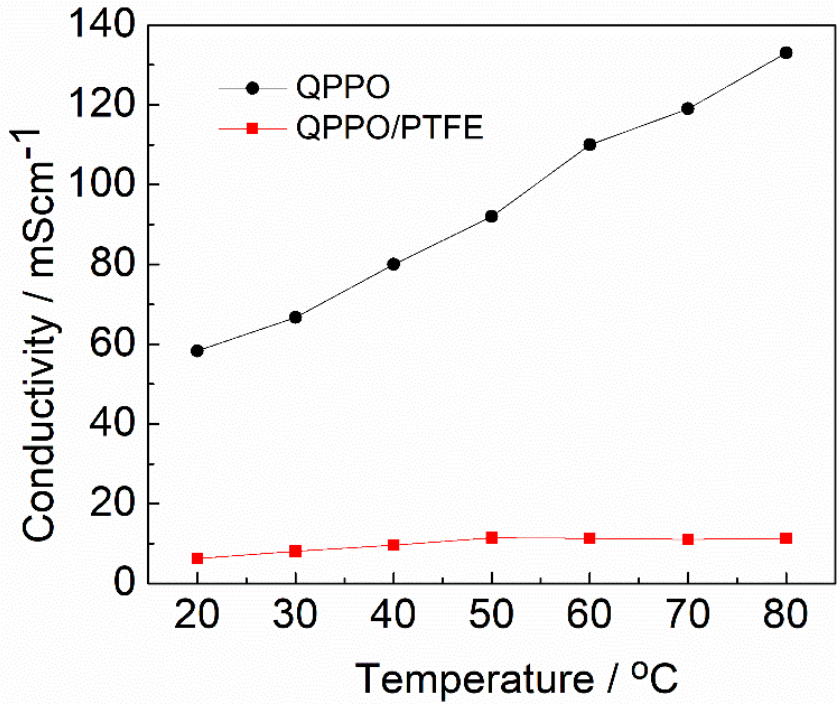

Figure 7.4 Ionic conductivity of QPPO/PTFE and QPPO-based membranes.

The ionic conductivity of the composite membrane was tested from 20 °C to 80 °C under an N_2 atmosphere. As is shown in Figure 7.4, the conductivity of the QPPO/PFTE composite membrane-based membrane is, as expected, lower than the PPO-based membrane. At 20 °C, the conductivity of the PPO/PTFE-based membrane is 6.25 mS cm^{-1}, much lower than the 58.30 mS cm^{-1} of the PPO-based membrane. That means the conductivity of composite membranes is only 11% of that of pristine QPPO. Considering the impregnated volume fraction of QPPO and PTFE tortuosity, the expected conductivity is significantly higher at 28%. The additional loss of conductivity can be attributed to lower water uptake. Impregnation of QPPO in PTFE pores will restrict QPPO swelling. Due to the hydrophobic nature of PTFE repelling water away, membrane water uptake will be limited further. Evidence of this can be seen by a lack of conductivity increase due to lower water uptake or dehydration in the composite membrane at temperatures above 50 °C. Besides, the conductivity of the composite membrane did not increase at elevated temperatures after 50 °C. This may be because the content of PPO in the composite membrane is too low, and continuous phases were not formed in the composite membrane, which significantly affects the formation of the water transport channel. The ratio of PPO in the composite membrane should be increased in future work.

7.5 Dynamic gravimetric vapour sorption (DVS)

Water sorption is used to characterise the adsorption ability of AEM towards water molecules. Adsorption isotherm models can depict the interaction mechanisms between the adsorbent and the adsorbate at a constant temperature,-based on the test's equilibrium data and the adsorbent's adsorption properties [245]. Dynamic gravimetric vapour sorption (DVS) was tested to study the water sorption and diffusion coefficient.

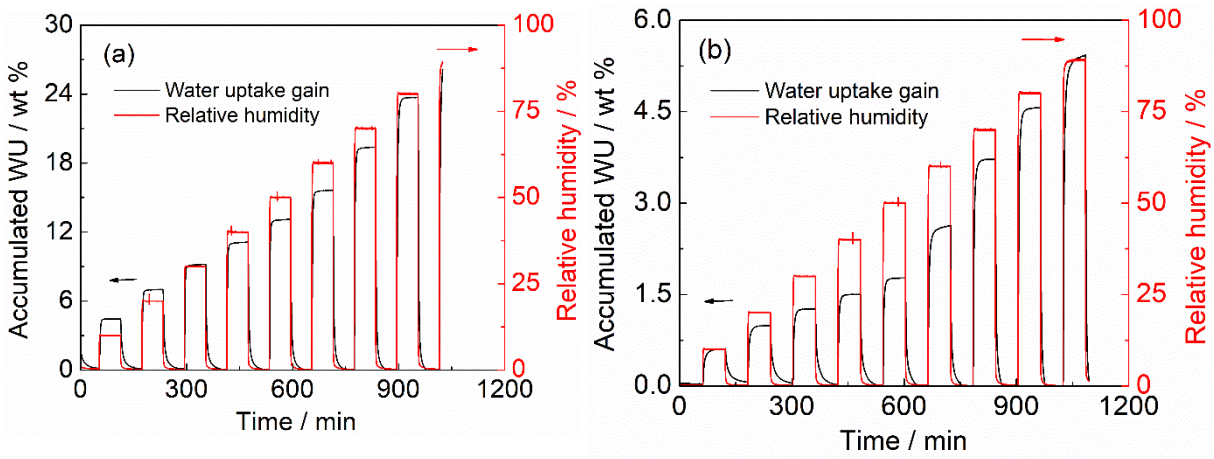

Figure 7. 5 Experimental sorption data (weight change and relative humidity change) of PPO (a) and QPPO/PTFE (b)-based membrane at 60 °C.

The experimental sorption data for PPO and PPO/PTFE-based membranes are shown in Figure 7.5. Weight change and relative humidity were obtained as the function of time. The membrane dried and absorbed the water vapour under relative humidity. QPPO membrane absorbed water to reach a saturation level faster (54 min) than PPO/PTFE composite membrane (72 min) despite the higher level of water uptake in pristine QPPO AEM. This means water diffusion is faster (more significant diffusion coefficient) in QPPO than in Q-PPO/PTFE. This can be explained by the inhomogeneous composition of QPPO/PTFE, where more significant hydrophilic regions were larger water clusters (slower to diffuse), and hydrophobic regions (PTFE). To illustrate the water uptake equilibrium more clearly, the water vapour sorption isotherm data (the equilibrium water content) were plotted against the target RH in Figure 7.5(b).

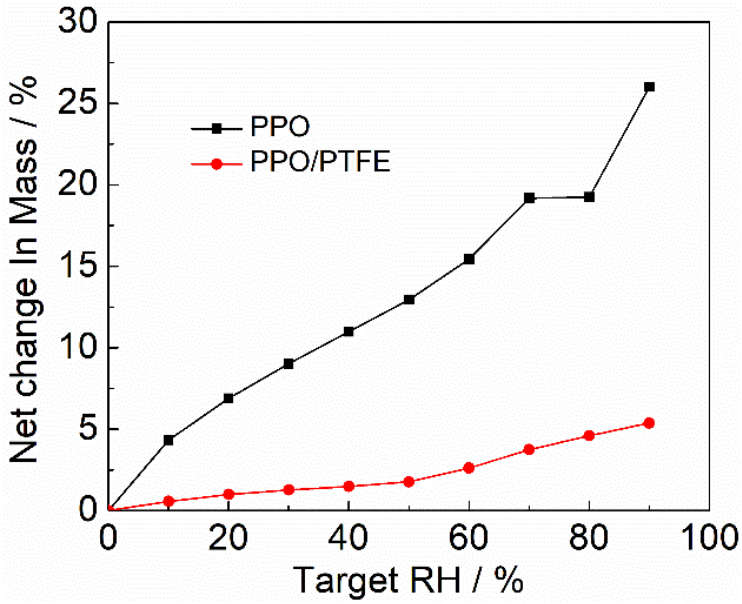

Figure 7.6 Water vapour sorption isotherms of PPO and QPPO-PTFE-based membranes at 60 °C.

As is shown in Figure 7.6, PPO-based membrane has higher water sorption/uptake than PPO/PTFE composite membranes. At 40 % RH, the net change mass is 10.98 %, while for the composite membrane, this is 1.59 %. The sorption isotherm of PPO and QPPO/PTFE-based membrane exhibited a concurrent increase in the mass change value with the increase in the target RH. Similarly, at 90 % RH, water uptake of QPPO was 28 %, while for QPPO-PTFE, it was only 5.3 %. It is worth pointing out that water uptake of PPO/PTFE of 5.3 % at 90 % RH can increase to 40 % if the data are

normalised by the 13 wt% of QPPO in QPPO/PTFE. This assumes water is only trapped or sorped by QPPO. However, the reality is that water can also fill through capillary action the unfilled pores of PTFE. As discussed above, 31.4 % of the PTFE pores or 29% of the total membrane volume remain unfilled. Considering a density of 1 g cm^{-3} for the polymer and water, this means that a significant fraction of the 13 % water sorped can be caused by trapped water in unfilled PTFE pores, which doesn't contribute to conductivity.

It is crucial to study the gas-solid adsorption isotherms in the DVS process. In general, there are five curves according to the categorisation of isotherm characteristics [245]. The isotherm of type I describes the adsorption on the microporous adsorbent. Type II and III describe adsorption for macroporous adsorbents with solid and weak adsorbate-adsorbent interactions. Types IV and V represent mono-and multilayer adsorption plus capillary condensation [246, 247]. PPO and QPPO/PTFE composite membranes show the Type II isotherms (concave upward) curve, which typically describes adsorption on mesoporous monolayer materials (usually disperse solids with > 50 nm pore diameter) at low pressure and on mesoporous multilayer material at high pressure near saturation with no hysteresis.

7.6 Long-term tests

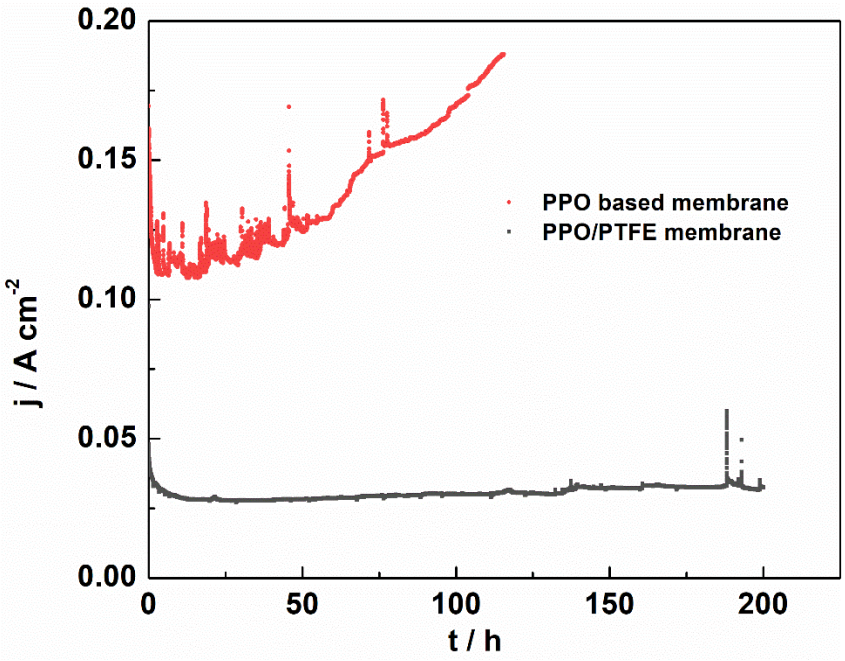

Figure 7.7 Comparison of long-term tests of PPO-based and PPO/PTFE membranes at 1.7 V in 0.1 NaOH at 40 °C.

Figure 7.7 shows the current density of water electrolyser using PPO-based AEM and QPPO/PTFE composite AEM at 1.7 V in 0.1 NaOH at 40 ^{o}C. The PPO-based membrane water electrolyser operated for 111 h before having a catastrophic failure/short circuit. With time, the softening of the membrane results in the penetration of the mesh anode into the membrane and eventually causes a short circuit with the cathode. This can be seen by a gradual increase in current density after 50h. QPPO/PTFE AEM water electrolyser operated for 200 h at stable performance until the experiment was terminated with no short-circuiting. Besides, the peaks or scatters in the curve might be caused by the bubbles attached on the surface of catalysts. During the operation of the water electrolyser, hydrogen and oxygen were generated continuously, and they tended to block the active sites by the attachment on the catalyst surface. The adsorption and detachment of bubbles from their surface will cause the unstable performance of the electrolyser [248].

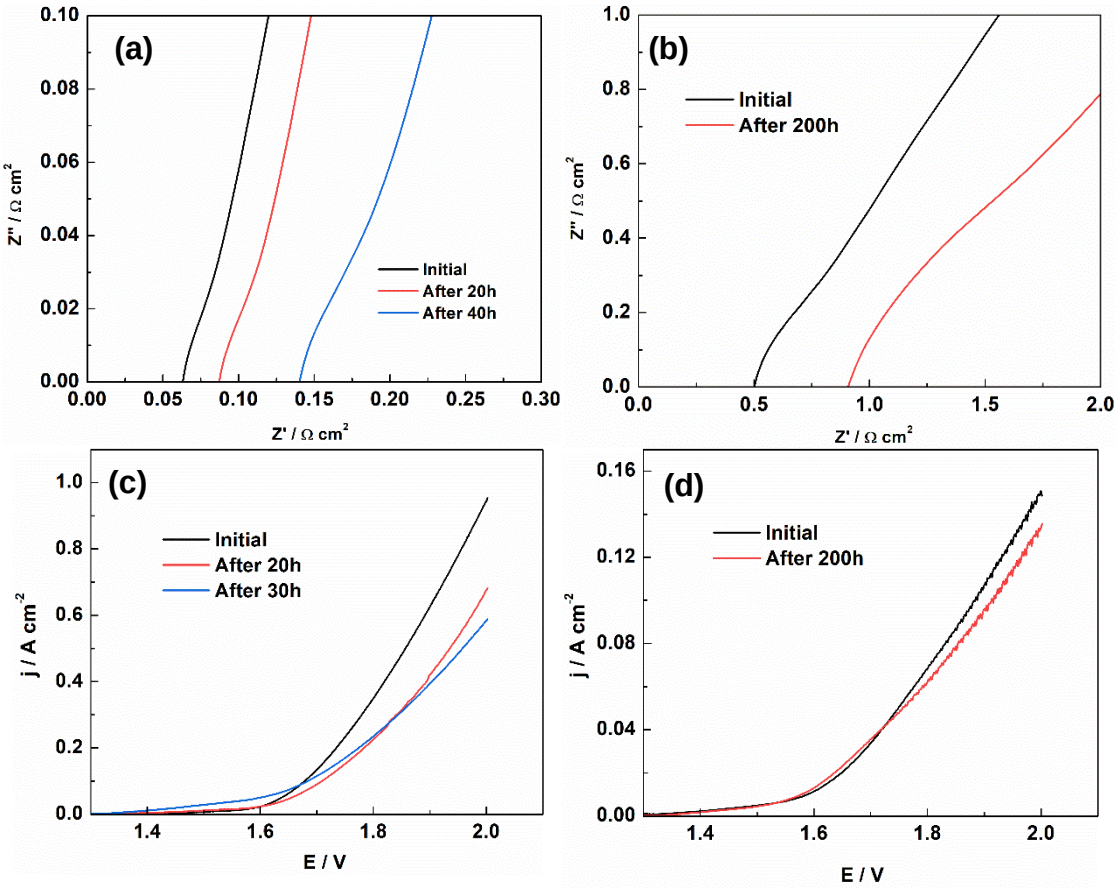

Figure 7.8 (a) EIS of PPO-based membrane before and after the long-term test. (b) EIS of PPO/PTFE composite membrane before and after the long-term test. (c) Polarisation curves of QPPO-based membrane before and after the long-term test. (d) Polarisation curves of QPPO/PTFE-based membrane before and after long-term.

Figure 7.8 shows the EIS and polarisation curves of the PPO-based membrane (110 μm) and QPPO/PTFE composite membrane (76 μm) before and after long-term tests. As shown in Figure 7.8(a), the initial area-specific resistance (ASR) of the PPO-based membrane was 0.063 Ω cm^{-2}, much lower than that of the QPPO/PTFE composite membrane of 0.5 Ω cm^{-2}. After 20 h and 40 h, the PPO-based membrane impedance increased to 0.088 and 0.14 Ω cm^{-2}, respectively. The doubling of ASR after 40h can be explained by the possible loss of IEC due to the use of 0.1 M supporting electrolytes. It should be noted that using supporting electrolytes mitigates losses from catalytic activity due to ionomer degradation. Given PPO's high operating current density, the increase in ASR results in a significant increase in IR losses and hence electrolyser voltage to maintain the same current density at 20 and 30 h. For QPPO/PTFE composite membrane, after 200 h, the ASR also almost doubled from 0.5 Ωcm^{-2} to 0.9 Ω cm^{-2}, as is shown in Figure 7.8(b). However, given the lower operating current density, the increase in IR losses has a limited effect on the polarisation curve. PPO-based membrane current at 2 V decreased from 0.95 A cm^{-2} to 0.68 A cm^{-2} and 0.59 A cm^{-2} after 20 h and 40 h, respectively. For QPPO/PTFE composite membrane, the current density decreased from 0.15 A cm^{-2} to 0.135 A cm^{-2} after 40 h, (Figure 7.8 (c) and (d)).

Chapter Summary

In this chapter, PPO was reinforced by PTFE. The PPO/PTFE composite membrane was obtained and showed good mechanical and thermal properties. The mechanical stress increases significantly from 14 MPa to 33 MPa. The conductivity of the composite membrane is still relatively low, 11.3 mS cm^{-1} and 2.6 %, respectively, due to the poor PPO impregnation in PTFE pores, with only 31.4 % of pores were filled. The PPO-based membrane has higher water sorption than QPPO/PTFE composite membranes, resulting in additional conductivity losses in the composite membrane. At 40 % RH, the net change mass is 10.98 %, while the composite membrane is 1.59 %. The durability was also tested in a water electrolyser. Compared with the PPO-based membrane, the ASR of the composite membrane was high of 0.5 Ω cm^{-2}. Notably, the reinforcement strategy of AEM using PTFE composite demonstrated success with failure-free 200 h of operation, compared to 50 h for pristine PPO. For future work, the PPO impregnation needs to be improved, which can be achieved by increasing the concentration of doping solution and immersion time.

Chapter 8. Conclusion and future work

8.1 Conclusion

Quaternised Poly(2,6-dimethyl-1,4-phenylene oxide) (QPPO)-based anion exchange membranes were prepared successfully via Friedel-Crafts reaction using $SnCl_4$ as catalyst and 1,3,5-trioxane and chlorotrimethylsilane as 'environmentally friendly' chloromethylating reagents. The overlooked cross-linking side reaction during the chloromethylation process was analysed, and new equations to calculate the degree of chloromethylation (DC) and cross-linking degree (CLD) were proposed. To ensure the solubility in NMP during quaternisation process, ClPPO polymers with DC_2 higher than 29.5 % and CLD lower than 4.8 % were found to be suitable for quaternisation and membrane processing. When DC is too low, i.e., <29.5 %, it is difficult for the chloromethylated polymer to dissolve, then membrane fabrication is impossible. The QPPO-based membrane also showed good mechanical and thermal properties. The stress of break and elongation of QPPO-based membranes was found to be around 14 MPa. Alkaline stability tests were conducted in 1 M KOH at 25 °C and 60 °C for 500 h, revealing that the primary degradation occurred to the functional group rather than the backbone with a 6% loss of IEC. QPPO (2.2 mmol g^{-1}) was employed as both membranes and ionomers in electrolyser tests, displaying good electrolysis performance. The area-specific resistance for M_{PPO}-I_{PPO} electrolysers was as low as 104 mΩ cm^{-2} at 40 °C and in 0.1 M NaOH solution, and the current density was 814 $mAcm^{-2}$ when the potential was 2.0 V. QPPO shows promising potential as AEMWE membrane offering lower ASR and SR and consequently lower energy loss and stability towards membrane mechanical failure. M_{LDPE}-I_{SEBS} gave the best performance. It also displays that the PPO membrane and SEBS ionomer saw the highest charge transfer resistance of M_{PPO}-I_{SEBS} of 1.71 Ωcm^{-2}. Besides, the temperature and alkaline concentration significantly affect the performance. Higher temperatures and higher alkaline concentrations are beneficial for performance. It is also necessary to point out that in DI water, the performance might be worse when the temperature increases from 40 °C to 60 °C due to the low dimension stability of the ionomer at a high temperature. There are two possible degradation paths for PPO-based membranes in oxidative conditions. One is to lose the functional groups, and the other is to generate the quinone methides in the residual solution.

PPO backbone is stable to oxidation, which was the aim of the study. However, headgroup oxidation and oxidation after rearrangements of the ethyl group limit

oxidative stability. Besides, to increase the mechanical property and reduce the water uptake, the PPO/PTFE composite membrane was fabricated and showed good mechanical and thermal properties. The mechanical stress rises significantly from 14 MPa to 33 MPa of stress. The conductivity and water sorption of the composite membrane are still relatively low, 11.3 mS cm^{-1} and 2.6 %, respectively, which might be due to the low PPO loading, only equivalent to 21.4 % volume of PTFE less than the 68 % porosity. Compared with the PPO-based membrane, the composite membrane showed a high area impedance (0.5 Ω cm^{-2}). The durability was also tested in water electrolyser. The composite membrane electrolyser was able to operate for 200 h,

8.2 Future Work

- The exact substituted sites on aromatic rings remain unclear for the AEM preparation process. The number and order of substitution positions reported in the literature are contradictory, potentially influencing the degree of chloromethylation. More investigation needs to be conducted on the chloromethylation position. Besides, the amination process needs to be investigated in-depth, especially the heterogeneous amination. Besides, even homogeneous amination doesn't provide uniformity if the amount of TMA is controlled so that not all chlotomethylated groups are aminated. Future work can study using a micro reactor to improve homogeneity.
- For AEM design, more chemically stable structures need to be developed, including a new type of backbone and the functional group. More membrane structures should be designed without the heteroatom linkages in the polymer main chains.
- Besides, more investigation on AEM degradation under neutral conditions should be conducted as the electrolysers are supposed to operate in a close to neutral (de-ionised water) environment. Most AEM studies on degradation are conducted under highly alkaline conditions. In addition, the oxidative process of AEMs and the degradation mechanism of head group loss under pH-neutral conditions.
- Only limited studies investigated AEMWE testing using AEMs prepared via the FC route. Thus, future studies should focus more on measuring these AEMs performances and durability under actual operating conditions.

- More non-experimental methods, including molecular dynamics, orbital simulation techniques, neural networks, etc., should be employed in the membrane preparation field. Those methods can supplement the experimental approaches to acquire better AEM structure and performance knowledge.
- The PPO impregnation in the PTFE substrate needs to be improved to achieve close to 100% filling of available pores. This can be achieved by increasing the concentration of doping solution and immersion time and exploring other substrates.

Reference

[1] D.W. Sintayehu, Ecosystem Health and Sustainability, 4 (2018) 225-239.
[2] M. Shen, S. Ye, G. Zeng, Y. Zhang, L. Xing, W. Tang, X. Wen, S. Liu, Mar Pollut Bull, 150 (2020) 110712.
[3] M. Mamlouk, M. Manolova, Chapter 6. Alkaline Anionic Exchange Membrane Water Electrolysers, in: Electrochemical Methods for Hydrogen Production, 2019, pp. 180-252.
[4] F. Yilmaz, M.T. Balta, R. Selbaş, Renew. Sust. Energ., 56 (2016) 171-178.
[5] G. Das, B.J. Park, J. Kim, D. Kang, H.H. Yoon, Sci Rep, 9 (2019) 9572.
[6] N.D. Charisiou, C. Italiano, L. Pino, V. Sebastian, A. Vita, M.A. Goula, Renew. Energy, 162 (2020) 908-925.
[7] U. Caudillo-Flores, I. Barba-Nieto, M.J. Muñoz-Batista, D. Motta Meira, M. Fernández-García, A. Kubacka, Chemical Engineering Journal, 425 (2021).
[8] M. Wang, Z. Wang, X. Gong, Z. Guo, Renewable and Sustainable Energy Reviews, 29 (2014) 573-588.
[9] H.A. Miller, K. Bouzek, J. Hnat, S. Loos, C.I. Bernäcker, T. Weißgärber, L. Röntzsch, J. Meier-Haack, Sustain. Energ. Fuels, 4 (2020) 2114-2133.
[10] S.J. Peighambardoust, S. Rowshanzamir, M. Amjadi, Int. J. Hydrog. Energy, 35 (2010) 9349-9384.
[11] E.J. Park, S. Maurya, M.R. Hibbs, C.H. Fujimoto, K.-D. Kreuer, Y.S. Kim, Macromolecules, 52 (2019) 5419-5428.
[12] Y. Zhao, X. Li, W. Li, Z. Wang, S. Wang, X. Xie, V. Ramani, J. Power Sources, 444 (2019) 227250-227258.
[13] D. Henkensmeier, M. Najibah, C. Harms, J. Žitka, J. Hnát, K. Bouzek, J. Electrochem. Energy Convers. Storage, 18 (2021).
[14] M. Mamlouk, (2021).
[15] R. Vinodh, A. Ilakkiya, S. Elamathi, D. Sangeetha, Materials Science and Engineering B-Advanced Functional Solid-State Materials, 167 (2010) 43-50.
[16] Q. Duan, S. Ge, C.-Y. Wang, J. Power Sources, 243 (2013) 773-778.
[17] P. Knauth, H. Hou, E. Bloch, E. Sgreccia, M.L. Di Vona, Journal of Analytical and Applied Pyrolysis, 92 (2011) 361-365.
[18] T.H. Jinli Qiao, Tatsuhiro Okada, polymer, 46 (2005) 10809-10816.
[19] M.W. Takeshi Ueki, Micromolecules, 41 (2008) 3739-3749.
[20] R. Espiritu, B.T. Golding, K. Scott, M. Mamlouk, Journal of Materials Chemistry A, 5 (2017) 1248-1267.
[21] M. Zhu, M. Zhang, Q. Chen, Y. Su, Z. Zhang, L. Liu, Y. Wang, L. An, N. Li, Polym. Chem., 8 (2017) 2074-2086.
[22] S. Maurya, S.-H. Shin, M.-K. Kim, S.-H. Yun, S.-H. Moon, J. Membr. Sci., 443 (2013) 28-35.
[23] S. Siracusano, V. Baglio, N. Van Dijk, L. Merlo, A.S. Aricò, Applied Energy, 192 (2017) 477-489.
[24] C.H. Lee, H.B. Park, Y.M. Lee, R.D. Lee, Ind. Eng. Chem. Res., 44 (2005) 7617-7626.
[25] D. Li, E.J. Park, W. Zhu, Q. Shi, Y. Zhou, H. Tian, Y. Lin, A. Serov, B. Zulevi, E.D. Baca, C. Fujimoto, H.T. Chung, Y.S. Kim, Nature Energy, 5 (2020) 378-385.
[26] X. Chu, Y. Shi, L. Liu, Y. Huang, N. Li, J. Mater. Chem. A, 7 (2019) 7717-7727.
[27] S. Maurya, S.-H. Shin, Y. Kim, S.-H. Moon, RSC Adv., 5 (2015) 37206-37230.
[28] W. You, K.J.T. Noonan, G.W. Coates, Progress in Polymer Science, 100 (2020) 101177.

[29] K.L. Lim, C.Y. Wong, W.Y. Wong, K.S. Loh, S. Selambakkannu, N.A.F. Othman, H. Yang, Membranes (Basel), 11 (2021).
[30] M. Mandal, ChemElectroChem, 8 (2020) 36-45.
[31] J.L. Yan, H.D. Moore, M.R. Hibbs, M.A. Hickner, Journal of Polymer Science Part B-Polymer Physics, 51 (2013) 1790-1798.
[32] R.A. Becerra-Arciniegas, R. Narducci, G. Ercolani, S. Antonaroli, E. Sgreccia, L. Pasquini, P. Knauth, M.L. Di Vona, Polymer, 185 (2019) 121931-121941.
[33] Y. Hu, D.W. Gu, F. Li, X.C. Qi, K.H. Yang, X.D. Liu, H. Li, Y.M. Zhang, Journal of Materials Science, 51 (2016) 5834-5842.
[34] S. Hou, M. Meng, D. Liu, P. Zhang, ChemSusChem, 14 (2021) 3059-3063.
[35] G.G. Wang, Y.M. Weng, D. Chu, R.R. Chen, D. Xie, J. Membr. Sci., 332 (2009) 63-68.
[36] J.Y. Jeon, S. Park, J. Han, S. Maurya, A.D. Mohanty, D. Tian, N. Saikia, M.A. Hickner, C.Y. Ryu, M.E. Tuckerman, S.J. Paddison, Y.S. Kim, C. Bae, Macromolecules, 52 (2019) 2139-2147.
[37] P. Khomein, W. Ketelaars, T. Lap, G. Liu, Renew. Sust. Energ., 137 (2021).
[38] K. Vanherck, G. Koeckelberghs, I.F.J. Vankelecom, Progress in Polymer Science, 38 (2013) 874-896.
[39] C. Wang, B. Mo, Z. He, Q. Shao, D. Pan, E. Wujick, J. Guo, X. Xie, X. Xie, Z. Guo, J. Membr. Sci., 556 (2018) 118-125.
[40] R. Espiritu, B.T. Golding, K. Scott, M. Mamlouk, J. Power Sources, 375 (2017) 373-386.
[41] N. Yokota, M. Shimada, H. Ono, R. Akiyama, E. Nishino, K. Asazawa, J. Miyake, M. Watanabe, K. Miyatake, Macromolecules, 47 (2014) 8238-8246.
[42] S. Moulay, Designed Monomers and Polymers, 14 (2012) 179-220.
[43] Y. Zhao, X. Li, S. Wang, W. Li, X. Wang, S. Chen, J. Chen, X. Xie, Int. J. Hydrog. Energy, 42 (2017) 30013-30028.
[44] M. Tanaka, K. Fukasawa, E. Nishino, S. Yamaguchi, K. Yamada, H. Tanaka, B. Bae, K. Miyatake, M. Watanabe, J. Am. Chem. Soc., 133 (2011) 10646-10654.
[45] J.Y. Chu, K.H. Lee, A.R. Kim, D.J. Yoo, Polymers, 10 (2018).
[46] J. Cheng, G. He, F. Zhang, Int. J. Hydrog. Energy, 40 (2015) 7348-7360.
[47] J.H. Wang, S.H. Li, S.B. Zhang, Macromolecules, 43 (2010) 3890-3896.
[48] C.G. Arges, J. Parrondo, G. Johnson, A. Nadhan, V. Ramani, J. Mater. Chem., 22 (2012).
[49] O.I. Deavin, S. Murphy, A.L. Ong, S.D. Poynton, R. Zeng, H. Herman, J.R. Varcoe, ENERG ENVIRON SCI, 5 (2012).
[50] T.T. Li, X.M. Yan, J.F. Liu, X.M. Wu, X. Gong, D.X. Zhen, S.L. Sun, W.T. Chen, G.H. He, J. Membr. Sci., 573 (2019) 157-166.
[51] D. Shin, A.F. Nugraha, F. Wijaya, S. Lee, E. Kim, J. Choi, H.J. Kim, B. Bae, RSC Adv., 9 (2019) 21106-21115.
[52] Y. Liu, J.Y. Wang, J. Membr. Sci., 596 (2020).
[53] M.A. Hossain, Y. Lim, S. Lee, H. Jang, S. Choi, T. Hong, L. Jin, W.G. Kim, React. Funct. Polym., 73 (2013) 1299-1305.
[54] G.G. Wang, Y.M. Weng, J. Zhao, R.R. Chen, D. Xie, J. Appl, 112 (2009) 721-727.
[55] V. Yadav, A. Rajput, P.P. Sharma, P.K. Jha, V. Kulshrestha, Colloids and Surfaces a-Physicochemical and Engineering Aspects, 588 (2020).
[56] D.V. Golubenko, B. Van der Bruggen, A.B. Yaroslavtsev, J. Appl, 137 (2020).
[57] L.D. Wang, Y. Liu, J.Y. Wang, J. Appl, 136 (2019).
[58] W.T. Lu, Z.G. Shao, G. Zhang, J. Li, Y. Zhao, B.L. Yi, Solid State Ionics, 245 (2013) 8-18.
[59] L. Xiong, Y.F. Hu, Z.G. Zheng, Z.L. Xie, D.Y. Chen, Chinese Journal of Polymer Science, 38 (2020) 278-287.

[60] H. Jang, M.A. Hossain, S. Lee, J. Ha, J. Yoo, K. Kim, W. Kim, J. Nanosci. Nanotechnol., 15 (2015) 8842-8848.
[61] X.M. Yan, X.M. Wu, G.H. He, S. Gu, X. Gong, J. Benziger, J. Appl, 132 (2015).
[62] M. Iravaninia, S. Rowshanzamir, Fuel Cells, 16 (2016) 135-149.
[63] X.Q. Wang, C.X. Lin, Q.G. Zhang, A.M. Zhu, Q.L. Liu, Int. J. Hydrog. Energy, 42 (2017) 19044-19055.
[64] M. Ciftci, M.A. Tasdelen, Journal of Polymer Science, 58 (2020) 412-416.
[65] P. Liu, Y.Q. Zheng, S.M. Lin, Q. Yang, Y.Z. Hong, Q.G. Zhang, Q.L. Liu, J. Power Sources, 452 (2020).
[66] W. Lu, Z.-G. Shao, G. Zhang, Y. Zhao, J. Li, B. Yi, Int. J. Hydrog. Energy, 38 (2013) 9285-9296.
[67] K.H. Gopi, S.G. Peera, S.D. Bhat, P. Sridhar, S. Pitchumani, Int. J. Hydrog. Energy, 39 (2014) 2659-2668.
[68] M.A. Hossain, H. Jang, S.C. Sutradhar, J. Ha, J. Yoo, C. Lee, S. Lee, W. Kim, Int. J. Hydrog. Energy, 41 (2016) 10458-10465.
[69] T. Huang, G. He, J. Xue, O. Otoo, X. He, H. Jiang, J. Zhang, Y. Yin, Z. Jiang, J.C. Douglin, D.R. Dekel, M.D. Guiver, J. Membr. Sci., 597 (2020) 117769.
[70] S.S. Koilpillai, S. Dharmalingam, International Journal of Energy Research, 39 (2015) 317-325.
[71] M.T. Perez-Prior, A. Varez, B. Levenfeld, J. Polym. Sci. Pol. Chem., 53 (2015) 2363-2373.
[72] G.C. Abuin, P. Nonjola, E.A. Franceschini, F.H. Izraelevitch, M.K. Mathe, H.R. Corti, Int. J. Hydrog. Energy, 35 (2010) 5849-5854.
[73] H. Zarrin, J. Wu, M. Fowler, Z.W. Chen, J. Membr. Sci., 394 (2012) 193-201.
[74] M.L. Di Vona, R. Narducci, L. Pasquini, K. Pelzer, P. Knauth, Int. J. Hydrog. Energy, 39 (2014) 14039-14049.
[75] M. Manohar, A.K. Thakur, R.P. Pandey, V.K. Shahi, J. Membr. Sci., 496 (2015) 250-258.
[76] X. Duan, C. Wang, T. Wang, X. Xie, X. Zhou, Y. Ye, J. Membr. Sci., 552 (2018) 86-94.
[77] S. Velu, K. Rambabu, Journal of Engineering Science and Technology, 10 (2015) 1162-1179.
[78] L. Sun, T. Okada, Journal of memmbrane science, 183 (2001) 213-221.
[79] R. Espiritu, B.T. Golding, K. Scott, M. Mamlouk, Journal of Power Sources, 375 (2018) 373-386.
[80] M. Tanaka, M. Koike, K. Miyatake, M. Watanabe, Polymer Chemistry, 2 (2011) 99-106.
[81] X.M. Yan, G.H. He, S. Gu, X.M. Wu, L.G. Du, Y.D. Wang, Int. J. Hydrog. Energy, 37 (2012) 5216-5224.
[82] C.G. Arges, L. Wang, M.s. Jung, V. Ramani, J. Electrochem. Soc., 162 (2015) F686-F693.
[83] E. Kim, S. Lee, S. Woo, S.H. Park, S.D. Yim, D. Shin, B. Bae, J. Power Sources, 359 (2017) 568-576.
[84] Z.A. Yi, Y.Y. Xu, L.P. Zhu, H.B. Dong, B.K. Zhu, Chinese Journal of Polymer Science, 27 (2009) 695-702.
[85] M. Moghadasi, H.R. Mortaheb, J. Appl, 134 (2017).
[86] J.F. Zhou, M. Unlu, J.A. Vega, P.A. Kohl, J. Power Sources, 190 (2009) 285-292.
[87] M. Iravaninia, S. Azizi, S. Rowshanzamir, Int. J. Hydrog. Energy, 42 (2017) 17229-17241.
[88] L. Pasquini, M.L. Di Vona, P. Knauth, New Journal of Chemistry, 40 (2016) 3671-3676.
[89] V. Yadav, S.K. Raj, N.H. Rathod, V. Kulshrestha, J. Membr. Sci., 611 (2020).

[90] A. Carbone, R. Pedicini, I. Gatto, A. Sacca, A. Patti, G. Bella, M. Cordaro, Polymers, 12 (2020).
[91] X.M. Yan, G.H. He, S. Gu, X.M. Wu, L.G. Du, H.Y. Zhang, J. Membr. Sci., 375 (2011) 204-211.
[92] Y. Xiong, Q.L. Liu, Q.H. Zeng, J. Power Sources, 193 (2009) 541-546.
[93] E. Mahendiravarman, D. Sangeetha, Int. J. Hydrog. Energy, 38 (2013) 2471-2479.
[94] A. Jasti, S. Prakash, V.K. Shahi, J. Membr. Sci., 428 (2013) 470-479.
[95] X.M. Yan, S. Gu, G.H. He, X.M. Wu, J. Benziger, J. Power Sources, 250 (2014) 90-97.
[96] T.T. Li, X.M. Wu, W.T. Chen, X.M. Yan, D.X. Zhen, X. Gong, J.F. Liu, S.F. Zhang, G.H. He, Chin. J. Chem. Eng, 26 (2018) 2130-2138.
[97] X.H. Li, Q.F. Liu, Y.F. Yu, Y.Z. Meng, J. Mater. Chem. A, 1 (2013) 4324-4335.
[98] X.M. Yan, L. Gao, W.J. Zheng, X.H. Ruan, C.M. Zhang, X.M. Wu, G.H. He, Int. J. Hydrog. Energy, 41 (2016) 14982-14990.
[99] X.M. Wu, W.T. Chen, X.M. Yan, G.H. He, J.J. Wang, Y. Zhang, X.P. Zhu, J. Mater. Chem. A, 2 (2014) 12222-12231.
[100] X.M. Yan, R.L. Deng, Y. Pan, X.W. Xu, I. El Hamouti, X.H. Ruan, X.M. Wu, C. Hao, G.H. He, J. Membr. Sci., 533 (2017) 121-129.
[101] D.Y. Chen, M.A. Hickner, ACS Appl. Mater. Interfaces, 4 (2012) 5775-5781.
[102] X.Y. He, M.Y. Gang, Z. Li, G.W. He, Y.H. Yin, L. Cao, B. Zhang, H. Wu, Z.Y. Jiang, Science Bulletin, 62 (2017) 266-276.
[103] Q. Gao, X.T. Pan, P.I. Buregeya, Y. Lu, X.L. Zhang, X.B. Yan, Z.X. Hu, S.W. Chen, J. Appl, 135 (2018).
[104] M. Ozawa, T. Kimura, R. Akiyama, J. Miyake, J. Inukai, K. Miyatake, Bulletin of the Chemical Society of Japan, 90 (2017) 1088-1094.
[105] R. Ren, S. Zhang, H.A. Miller, F. Vizza, J.R. Varcoe, Q. He, J. Membr. Sci., 591 (2019).
[106] X.H. Li, Q.F. Liu, Y.F. Yu, Y.Z. Meng, J. Membr. Sci., 467 (2014) 1-12.
[107] X.H. Li, Y.F. Yu, Q.F. Liu, Y.Z. Meng, J. Membr. Sci., 436 (2013) 202-212.
[108] X.H. Li, Y.F. Yu, Q.F. Liu, Y.Z. Meng, ACS Appl. Mater. Interfaces, 4 (2012) 3627-3635.
[109] W.H. Mei, Z. Wang, Chem. Res. Chin. Univ., 31 (2015) 1056-1061.
[110] N. Yokota, H. Ono, J. Miyake, E. Nishino, K. Asazawa, M. Watanabe, K. Miyatake, ACS Appl. Mater. Interfaces, 6 (2014) 17044-17052.
[111] D.W. Seo, M.A. Hossain, D.H. Lee, Y.D. Lim, S.H. Lee, H.C. Lee, T.W. Hong, W.G. Kim, Electrochimica Acta, 86 (2012) 360-365.
[112] M.A. Hossain, Y. Lim, S. Lee, H. Jang, S. Choi, Y. Jeon, S. Lee, H. Ju, W.G. Kim, Solid State Ionics, 262 (2014) 754-760.
[113] H. Fang, M.A. Hossain, S.C. Sutradhar, F. Ahmed, K. Choi, T. Ryu, K. Kim, W. Kim, Int. J. Hydrog. Energy, 42 (2017) 12759-12767.
[114] M. Shimada, S. Shimada, J. Miyake, M. Uchida, K. Miyatake, J. Polym. Sci. Pol. Chem., 54 (2016) 935-944.
[115] M.A. Hossain, Y.D. Lim, H.H. Jang, Y.T. Jeon, J.S. Lim, S.H. Lee, W.G. Kim, H.S. Jeon, Electron. Mater. Lett., 9 (2013) 797-799.
[116] D.W. Seo, Y.D. Lim, M.A. Hossain, S.H. Lee, H.C. Lee, H.H. Jang, S.Y. Choi, W.G. Kim, Int. J. Hydrog. Energy, 38 (2013) 579-587.
[117] N. Manjula, R. Balaji, K. Ramya, N. Rajalakshmi, Int. J. Hydrog. Energy, 45 (2020) 10304-10312.
[118] M. Manohar, A.K. Das, V.K. Shahi, Desalination, 413 (2017) 101-108.
[119] K.H. Gopi, S.G. Peera, S.D. Bhat, P. Sridhar, S. Pitchumani, Bulletin of Materials Science, 37 (2014) 877-881.

[120] P.F. Msomi, P. Nonjola, P.G. Ndungu, J. Ramonjta, J. Appl, 135 (2018) 45959-45967.
[121] K.H. Gopi, S.D. Bhat, A.K. Sahu, P. Sridhar, J. Appl, 133 (2016) 43693-43703.
[122] B. Lee, H. Lim, J.E. Chae, H.-J. Kim, T.-H. Kim, J. Membr. Sci., 574 (2019) 33-43.
[123] S. Gu, J. Skovgard, Y.S. Yan, ChemSusChem, 5 (2012) 843-848.
[124] Z. Feng, P.O. Esteban, G. Gupta, D.A. Fulton, M. Mamlouk, Int. J. Hydrog. Energy, 46 (2021) 37137-37151.
[125] B.H. Oh, A.R. Kim, D.J. Yoo, Int. J. Hydrog. Energy, 44 (2019) 4281-4292.
[126] G.G. Wang, Y.M. Weng, D. Chu, D. Xie, R.R. Chen, J. Membr. Sci., 326 (2009) 4-8.
[127] H. Jang, S. Lee, J. Ha, K. Choi, T. Ryu, K. Kim, H.S. Jeon, W. Kim, Energies, 9 (2016).
[128] M.A. Hossain, H. Ring, S. Lee, T. Hong, L. Jin, F. Tan, D. Kim, W. Kim, Int. J. Hydrog. Energy, 40 (2015) 1324-1332.
[129] H. Ono, J. Miyake, K. Miyatake, J. Polym. Sci. Pol. Chem., 55 (2017) 1442-1450.
[130] G.H. Wang, Y.M. Weng, J. Zhao, D. Chu, D. Xie, R.R. Chen, Polym. Adv. Technol., 21 (2010) 554-560.
[131] D. Valade, F. Boschet, B. Ameduri, J. Polym. Sci. Pol. Chem., 48 (2010) 5801-5811.
[132] Z. Zhao, F. Gong, S. Zhang, S. Li, J. Power Sources, 218 (2012) 368-374.
[133] D.R. Dekel, J. Power Sources, (2017).
[134] J. Schauer, J. Zitka, Z. Pientka, J. Krivcik, J. Hnat, K. Bouzek, J. Appl, 132 (2015).
[135] N. Chen, C. Hu, H.H. Wang, S.P. Kim, H.M. Kim, W.H. Lee, J.Y. Bae, J.H. Park, Y.M. Lee, Angew Chem Int Ed Engl, 60 (2021) 7710-7718.
[136] P. Fortin, T. Khoza, X. Cao, S.Y. Martinsen, A. Oyarce Barnett, S. Holdcroft, J. Power Sources, 451 (2020).
[137] W.E. Mustain, M. Chatenet, M. Page, Y.S. Kim, ENERG ENVIRON SCI, 13 (2020) 2805-2838.
[138] Z. Sun, B. Lin, F. Yan, ChemSusChem, 11 (2018) 58-70.
[139] N. Ziv, A.N. Mondal, T. Weissbach, S. Holdcroft, D.R. Dekel, J. Membr. Sci., 586 (2019) 140-150.
[140] N. Ziv, D.R. Dekel, Electrochemistry Communications, 88 (2018) 109-113.
[141] J.S. Park, S.H. Park, S.D. Yim, Y.G. Yoon, W.Y. Lee, C.S. Kim, J. Power Sources, 178 (2008) 620-626.
[142] S. Li, H.B. Zhang, K.Q. Wang, F. Yang, Y.T. Han, Y.R. Sun, J.H. Pang, Z.H. Jiang, Polymer Chemistry, 11 (2020) 2399-2407.
[143] S. Gu, G. He, X. Wu, C. Li, H. Liu, C. Lin, X. Li, J. Membr. Sci., 281 (2006) 121-129.
[144] S. Gu, R. Cai, T. Luo, Z. Chen, M. Sun, Y. Liu, G. He, Y. Yan, Angew Chem Int Ed Engl, 48 (2009) 6499-6502.
[145] L. Wu, T. Xu, W. Yang, J. Membr. Sci., 286 (2006) 185-192.
[146] T. Xu, Z. Liu, W. Yang, J. Membr. Sci., 249 (2005) 183-191.
[147] T. Xu, D. Wu, L. Wu, Progress in Polymer Science, 33 (2008) 894-915.
[148] J.S. Park, G.G. Park, S.H. Park, Y.G. Yoon, C.S. Kim, W.Y. Lee, Macromol. Symp., 249 (2007) 174-182.
[149] C.X. Lin, Y.Z. Zhuo, E.N. Hu, Q.G. Zhang, A.M. Zhu, Q.L. Liu, J. Membr. Sci., 539 (2017) 24-33.
[150] J. Parrondo, M.-s.J. Jung, Z. Wang, C.G. Arges, V. Ramani, J. Electrochem. Soc., 162 (2015) F1236-F1242.
[151] D.R. Dekel, S. Willdorf, U. Ash, M. Amar, S. Pusara, S. Dhara, S. Srebnik, C.E. Diesendruck, J. Power Sources, 375 (2018) 351-360.

[152] R. Espiritu, B.T. Golding, K. Scott, M. Mamlouk, J. Mater. Chem. A, 5 (2017) 1248-1267.
[153] J. Muller, A. Zhegur, U. Krewer, J.R. Varcoe, D.R. Dekel, ACS Mater Lett, 2 (2020) 168-173.
[154] K.-D. Kreuer, P. Jannasch, J. Power Sources, 375 (2018) 361-366.
[155] J. Chen, C. Li, J. Wang, L. Li, Z. Wei, Journal of Materials Chemistry A, 5 (2017) 6318-6327.
[156] J. Parrondo, Z. Wang, M.S. Jung, V. Ramani, Phys Chem Chem Phys, 18 (2016) 19705-19712.
[157] J. Wang, S. Gu, R.B. Kaspar, B. Zhang, Y. Yan, ChemSusChem, 6 (2013) 2079-2082.
[158] Z. Wang, J. Parrondo, V. Ramani, J. Electrochem. Soc., 163 (2016) F824-F831.
[159] C.G. Arges, V. Ramani, Proc Natl Acad Sci U S A, 110 (2013) 2490-2495.
[160] D. Li, A.R. Motz, C. Bae, C. Fujimoto, G. Yang, F.-Y. Zhang, K.E. Ayers, Y.S. Kim, ENERG ENVIRON SCI, 14 (2021) 3393-3419.
[161] J.J. Chen, C.P. Li, J.C. Wang, L. Li, Z.D. Wei, J. Mater. Chem. A, 5 (2017) 6318-6327.
[162] S. Wierzbicki, J.C. Douglin, A. Kostuch, D.R. Dekel, K. Kruczala, J Phys Chem Lett, 11 (2020) 7630-7636.
[163] W. Lu, G. Zhang, J. Li, J. Hao, F. Wei, W. Li, J. Zhang, Z.-G. Shao, B. Yi, J. Power Sources, 296 (2015) 204-214.
[164] L. Gubler, S.M. Dockheer, W.H. Koppenol, J. Electrochem. Soc., 158 (2011).
[165] N. Ye, Y. Xu, D. Zhang, J. Yang, R. He, Polymer Degradation and Stability, 153 (2018) 298-306.
[166] S.S. Admira Bosnjakovic, The Journal of Physical Chemistry B, 108 (2004) 4332-4337.
[167] F. Bu, Y. Zhang, L. Hong, W. Zhao, D. Li, J. Li, H. Na, C. Zhao, J. Membr. Sci., 545 (2018) 167-175.
[168] J. Fan, S. Willdorf-Cohen, E.M. Schibli, Z. Paula, W. Li, T.J.G. Skalski, A.T. Sergeenko, A. Hohenadel, B.J. Frisken, E. Magliocca, W.E. Mustain, C.E. Diesendruck, D.R. Dekel, S. Holdcroft, Nat. Commun., 10 (2019) 2306.
[169] Y. Hou, B. Zhou, W. Zhou, C. Shen, Y. He, Int. J. Hydrog. Energy, 37 (2012) 11887-11893.
[170] R. Espiritu, M. Mamlouk, K. Scott, Int. J. Hydrog. Energy, 41 (2016) 1120-1133.
[171] J.Y. Chu, K.H. Lee, A.R. Kim, D.J. Yoo, J. Membr. Sci., 611 (2020).
[172] F. Fayyazi, E.A. Feijani, H. Mahdavi, Chem. Eng. Sci., 134 (2015) 549-554.
[173] R. Thimmappa, K. Scott, M. Mamlouk, Int. J. Hydrog. Energy, 45 (2020) 28303-28312.
[174] W. Tang, Y. Yang, X. Liu, J. Dong, H. Li, J. Yang, Electrochimica Acta, 391 (2021).
[175] O.D. Thomas, K.J. Soo, T.J. Peckham, M.P. Kulkarni, S. Holdcroft, J Am Chem Soc, 134 (2012) 10753-10756.
[176] S. Maurya, C.H. Fujimoto, M.R. Hibbs, C. Narvaez Villarrubia, Y.S. Kim, Chem. Mater., 30 (2018) 2188-2192.
[177] G. Gupta, K. Scott, M. Mamlouk, J. Power Sources, 375 (2017) 387-396.
[178] J. Yang, Q. Yu, F. Zhao, J. Lu, Z. Ge, Synth. Commun., 41 (2011) 3455-3461.
[179] Y. Li, T. Xu, J. Appl, 114 (2009) 3016-3025.
[180] L. Wu, T.W. Xu, W.H. Yang, J. Membr. Sci., 286 (2006) 185-192.
[181] T.W. Xu, W.H. Yang, J. Membr. Sci., 238 (2004) 123-129.
[182] M.T. Kwasny, L. Zhu, M.A. Hickner, G.N. Tew, J Am Chem Soc, 140 (2018) 7961-7969.
[183] P. Knauth, L. Pasquini, R. Narducci, E. Sgreccia, R.A. Becerra-Arciniegas, M.L. Di Vona, J. Membr. Sci., 617 (2021).

[184] L. Zeng, Q. He, Y. Liao, S. Kuang, J. Wang, W. Ding, Q. Liao, Z. Wei, Research, 2020 (2020) 4794706-4794716.
[185] L. Liu, X. Chu, J. Liao, Y. Huang, Y. Li, Z. Ge, M.A. Hickner, N. Li, ENERG ENVIRON SCI, 11 (2018) 435-446.
[186] A.M. Park, R.J. Wycisk, X. Ren, F.E. Turley, P.N. Pintauro, J. Mater. Chem. A, 4 (2016) 132-141.
[187] J. Pan, J. Han, L. Zhu, M.A. Hickner, Chem. Mater., 29 (2017) 5321-5330.
[188] A.K. Mohanty, Y.E. Song, B. Jung, J.R. Kim, N. Kim, H.-j. Paik, Int. J. Hydrog. Energy, 45 (2020) 27346-27358.
[189] Q. Liu, Z. Wang, A. Yu, J. Li, H. Shen, H. Wang, K. Yang, H. Zhang, Int. J. Hydrog. Energy, 46 (2021) 24328-24338.
[190] N. Pantamas, C. Khonkeng, Am. J. Appl. Sci., 9 (2012) 1577-1582.
[191] V. Galvan, B. Shrimant, C. Bae, G.K.S. Prakash, ACS Applied Energy Materials, 4 (2021) 5858-5867.
[192] Y. Wu, C. Wu, J.R. Varcoe, S.D. Poynton, T. Xu, Y. Fu, J. Power Sources, 195 (2010) 3069-3076.
[193] Acta Chim. Sin., 78 (2020) 69-75.
[194] K.H. Gopi, S.G. Peera, S.D. Bhat, P. Sridhar, S. Pitchumani, Bull. Mater. Sci, 37 (2014) 877-881.
[195] G.D. JONES, Ind. Eng. Chem. Res., 44 (1952) 2686-2693.
[196] A.M. James, S. Harding, T. Robshaw, N. Bramall, M.D. Ogden, R. Dawson, ACS Appl Mater Interfaces, 11 (2019) 22464-22473.
[197] N.M. Al Andis, J. Chem., 2013 (2013) 1-4.
[198] M.H. Feng Wang, Yu Seung Kim, Thomas A. Zawodzinski, James E. McGrath, J. Membr. Sci., 197 231-242.
[199] G.P.R. Yan Gao, Michael D. Guiver, Xigao Jian, J POLYM SCI POL CHEM, 41 (2003) 497-507.
[200] P. Yu Xu, K. Zhou, G. Lu Han, Q. Gen Zhang, A. Mei Zhu, Q. Lin Liu, J. Membr. Sci., 457 (2014) 29-38.
[201] X. Lin, J.R. Varcoe, S.D. Poynton, X. Liang, A.L. Ong, J. Ran, Y. Li, T. Xu, J. Mater. Chem. A, 1 (2013) 7262-7269.
[202] C. Xiao Lin, X. Qin Wang, E. Ning Hu, Q. Yang, Q. Gen Zhang, A. Mei Zhu, Q. Lin Liu, J. Membr. Sci., 541 (2017) 358-366.
[203] T.A. Sherazi, S. Zahoor, R. Raza, A.J. Shaikh, S.A.R. Naqvi, G. Abbas, Y. Khan, S. Li, Int. J. Hydrog. Energy, 40 (2015) 786-796.
[204] B.P. Tripathi, T. Chakrabarty, V.K. Shahi, J. Mater. Chem., 20 (2010) 8036-8044.
[205] L. Ma, N.A. Qaisrani, M. Hussain, L. Li, Y. Jia, S. Ma, R. Zhou, L. Bai, G. He, F. Zhang, J. Membr. Sci., 607 (2020).
[206] Z. Yang, M. Zhang, Y. Xiao, X. Zhang, M. Fan, Macromolecular Materials and Engineering, 306 (2020).
[207] T.P. Pandey, H.N. Sarode, Y. Yang, Y. Yang, K. Vezzù, V.D. Noto, S. Seifert, D.M. Knauss, M.W. Liberatore, A.M. Herring, J. Electrochem. Soc., 163 (2016) H513-H520.
[208] G. Shukla, V.K. Shahi, Int. J. Hydrog. Energy, 43 (2018) 21742-21749.
[209] X.L. Gao, L.X. Sun, H.Y. Wu, Z.Y. Zhu, N. Xiao, J.H. Chen, Q. Yang, Q.G. Zhang, A.M. Zhu, Q.L. Liu, J. Mater. Chem. A, 8 (2020) 13065-13076.
[210] Y. Bai, Y. Yuan, L. Miao, C. Lü, J. Membr. Sci., 570-571 (2019) 481-493.
[211] A. Ouadah, H. Xu, T. Luo, S. Gao, X. Wang, Z. Fang, C. Jing, C. Zhu, J. Power Sources, 371 (2017) 77-85.
[212] J. Li, S. Wang, F. Liu, X. Wang, H. Chen, T. Mao, Z. Wang, J. Membr. Sci., 581 (2019) 303-311.

[213] M. Bhushan, M. Mani, A.K. Singh, A.B. Panda, V.K. Shahi, J. Mater. Chem. A, (2020).
[214] J. Dong, H. Li, X. Ren, X. Che, J. Yang, D. Aili, Int. J. Hydrog. Energy, 44 (2019) 22137-22145.
[215] B. Shen, B. Sana, H. Pu, J. Membr. Sci., 615 (2020).
[216] C. Yang, S. Wang, W. Ma, L. Jiang, G. Sun, J. Membr. Sci., 487 (2015) 12-18.
[217] X. Yan, X. Yang, X. Su, L. Gao, J. Zhao, L. Hu, M. Di, T. Li, X. Ruan, G. He, J. Power Sources, 480 (2020).
[218] C. Cheng, X. He, S. Huang, F. Zhang, Y. Guo, Y. Wen, B. Wu, D. Chen, Int. J. Hydrog. Energy, 45 (2020) 19676-19690.
[219] B. Shen, H. Pu, Polymer, 207 (2020).
[220] M. Mamlouk, J.A. Horsfall, C. Williams, K. Scott, Int. J. Hydrog. Energy, 37 (2012) 11912-11920.
[221] G. Gupta, K. Scott, M. Mamlouk, Fuel Cells, 18 (2018) 137-147.
[222] M. Mamlouk, K. Scott, J. Power Sources, 286 (2015) 290-298.
[223] V. Antonucci, A. Di Blasi, V. Baglio, R. Ornelas, F. Matteucci, J. Ledesma-Garcia, L.G. Arriaga, A.S. Aricò, Electrochimica Acta, 53 (2008) 7350-7356.
[224] Q. Li, L. Liu, S. Liang, Q. Li, B. Jin, R. Bai, Polymer Chemistry, 5 (2014).
[225] K. Shen, J. Pang, S. Feng, Y. Wang, Z. Jiang, J. Membr. Sci., 440 (2013) 20-28.
[226] Y. Zhang, J. Fang, Y. Wu, H. Xu, X. Chi, W. Li, Y. Yang, G. Yan, Y. Zhuang, J Colloid Interface Sci, 381 (2012) 59-66.
[227] L. Liu, C. Tong, Y. He, Y. Zhao, C. Lü, J. Membr. Sci., 487 (2015) 99-108.
[228] H. Kaczmarek.
[229] C. Xu, Y. Xu, M. Chen, Y. Zhang, J. Li, Q. Gao, S.Q. Shi, Chemical Engineering Journal, 390 (2020).
[230] A.G. Fahmi, Z. Abidin, C. Kusmana, D. Kharisma, V. Prajaputra, W.R. Rahmawati, IOP Conference Series: Earth and Environmental Science, 399 (2019).
[231] E. Fumoto, S. Sato, T. Takanohashi, Energy & Fuels, 34 (2020) 5231-5235.
[232] T.R. Heyong He, Anton Lerf, Jacek Klinowski, The Journal of Physical Chemistry A, 100 (1996) 19954-19958.
[233] Y. Yao, Y. Luo, H. Lu, B. Wang, Composite Structures, 192 (2018) 507-515.
[234] J. Liu, Y. Liu, W. Yang, Q. Ren, F. Li, Z. Huang, J. Power Sources, 396 (2018) 265-275.
[235] S. Xu, D. Lu, P. Wang, Y. Zhao, Y. Sun, J. Qi, J. Ma, J. Membr. Sci., 601 (2020).
[236] Y. Li, G. He, S. Wang, S. Yu, F. Pan, H. Wu, Z. Jiang, J. Mater. Chem. A, 1 (2013).
[237] N.H. Rathod, V. Yadav, A. Rajput, J. Sharma, D.K. Shukla, V. Kulshrestha, Colloid and Interface Science Communications, 36 (2020).
[238] N. Chen, C. Long, Y. Li, D. Wang, H. Zhu, Electrochimica Acta, 268 (2018) 295-303.
[239] M.T.Q.S. da Silva, M. do Rocio Cardoso, C.M.P. Veronese, W. Mazer, Materials Today: Proceedings, 58 (2022) 1344-1349.
[240] S. Adnan, M. Hoang, H. Wang, Z. Xie, Desalination, 284 (2012) 297-308.
[241] B. Tjaden, S.J. Cooper, D.J.L. Brett, D. Kramer, P.R. Shearing, Current Opinion in Chemical Engineering, 12 (2016) 44-51.
[242] H.T. Hamad, D.W. Abbood, A.S. Mustafa, IOP Conference Series: Materials Science and Engineering, 454 (2018).
[243] G. Madabattula, S. Kumar, J. Electrochem. Soc., 167 (2020).
[244] S.J. Cooper, A. Bertei, P.R. Shearing, J.A. Kilner, N.P. Brandon, SoftwareX, 5 (2016) 203-210.
[245] M.A. Al-Ghouti, D.A. Da'ana, J Hazard Mater, 393 (2020) 122383.

[246] G.S. Alexandra Nistor, Carmen Racles, Maria Cazacu Mater. Plast., 48 (2011) 33-37.
[247] G.L.A. M.D. Donohue, Advances in Colloid and Interface Science, 76 (1998) 137-152.
[248] S.H. Ahn, I. Choi, H.Y. Park, S.J. Hwang, S.J. Yoo, E. Cho, H.J. Kim, D. Henkensmeier, S.W. Nam, S.K. Kim, J.H. Jang, Chem Commun (Camb), 49 (2013) 9323-9325.